Development and Calibration of a Heat Flux Microsensor

by

Jonathan M. Hager

Thesis submitted to the Faculty of the

Virginia Polytechnic Institute and State University

in partial fulfillment of the requirements for the degree of

Master of Science

in

Mechanical Engineering

APPROVED:

Thomas E. Diller, Chairman

Shinzo Onishi

Wing F. Ng

February 3, 1989

Blacksburg, Virginia

Development and Calibration of a Heat Flux Microsensor

by

Jonathan M. Hager

Thomas E. Diller, Chairman

Mechanical Engineering

(ABSTRACT)

The concept, design, fabrication, and calibration of a new type of layered heat flux gage is described. Using thin-film microfabrication techniques the gage design is able to combine many of the desireable characteristics of other previous gage designs to produce a gage that has a very small size, high frequency response, and the ability to measure very high heat flux rates. The heat flux microsensor incorporates a differential thermopile, a set of 100 differential thermocouple pairs connected in series across a thin thermal resistance layer. The gage is fabricated on a model surface without the need for additional adhesives. The design configuration allows the thermal insulating layer to remain very thin, while still retaining the high output typical of much thicker gages. The small overall thickness of the gage, less than 2 μm, gives it a fast time response with the capability of measuring heat transfer in transient flow conditions. The combination of small thickness and small surface dimensions, 1 mm by 1 cm, gives the microsensor negligible flow and thermal disruption.

The performance of a prototype microsensor deposited on Corning 7059 glass was measured. Steady-state calibrations were done using a convection calibration apparatus. The measured sensitivity (before amplification) was 0.164 mV per watt/cm^2. The output was linear over the range tested from 800 to 9000 watts/m^2. The unsteady response was tested using a continuous laser beam directed through a variable speed chopper wheel onto the gage surface. Results showed a frequency response of at least 1 kHz.

Acknowledgements

I would like to extend my deepest gratitude to Dr. Thomas E. Diller, who displayed great patience, care, and insight during his supervision of this thesis. I would also like to thank he and Dr. Shinzo Onishi for giving me the opportunity to work on developing their invention, and of Vatell Corp. for his constant encouragement and support. Furthermore, I thank Shinzo for his constant guidance, teaching, and never-ending patience during the development of this work.

This material is based upon work supported by the Vatell Corporation, the Virginia Center for Innovative Technology, and the National Science Foundation under Grant No. CBT-8814364. The government has certain rights in this material.

I would like to thank my family, especially my parents, for their support, encouragement and most of all patience throughout my college years.

I express thanks, most of all, to all my friends, both old and new, whose friendships have helped me endure. Special thanks to and

Table of Contents

List of Illustrations

List of Tables

Nomenclature

D	jet diameter, cm
E	Gardon gage output, mV
E_m	microsensor output, mV
f	Gardon gage sensitivity, mV/(W/m^2)
h_i	heat transfer coefficient based on isothermal gage surface assumption, W/(m^2-K)
h_c	corrected heat transfer coefficient over the center plate, W/(m^2-K)
K_2	thermocouple sensitivity for copper constantan = 0.042 mV/°C
k	thermal conductivity, W/m-K
n	number of thermocouple pairs
Nu	Nusselt number = $\frac{hD}{k}$, dimensionless
q_c	convection heat flux, W/m^2
q_m	convection heat flux of microsensor, W/m^2
Re	jet Reynolds number, dimensionless
S	sensitivity of microsensor, mV/(W/cm^2)
S_T	thermocouple sensitivity for copper nickel, μV/°C
t	time response
T_1	temperature of upper gage surface, °C

T_2	temperature of lower gage surface, °C
T_3	temperature of model surface, °C
T_a	temperature of air jet, °C
T_m	temperature of microsensor surface, °C
T_p	temperature of the plate, °C
T_∞	temperature of the surroundings, °C
α	material thermal diffusivity, m^2/s
δ	gage thickness, μm
ε	Gardon gage surface emissivity, dimensionless
σ	Stephan-Boltzman constant = $5.67x10^{-8}$ $W/(m^2\text{-}K^4)$

Introduction

Throughout the research and testing community, there is growing concern for monitoring the heat transfer between a surface and the fluid flowing over it. The applications range from the electronics industry to the aerospace industry. The reason for the increased concern is due to a greater demand for specialty materials, more extreme environment applications, and much higher efficiency standards. Though temperature measurement techniques are available for many of these applications, the measurement of both steady and unsteady heat transfer has not been well developed. Problems have been encountered in calibration, measurement of high heat flux rates, and measurement at elevated temperatures.

There are a variety of gages available to detect heat flux, falling in four general categories. These include measurement of the electric power dissipated by a heater at steady state, the temperature difference across a known thermal resistance in a surface, the time rate of change of thermal energy in a surface, and the spatial temperature gradient in the fluid normal to the surface(Diller, 1988). The concept used for the research involving the heat flux microsensor is that of the second category. This method uses a differential thermocouple as its primary element, one thermocouple acting as a cold junction on one side of a planar thermal resistance and another on the other side acting as a hot junction. The heat flux that passes through the gage sets up a temperature difference across the gage, generating an output signal approximately proportional to the heat flux. Other available

gages based on the second category include Gardon gages(Gardon, 1953), RdF Microfoil gages(Ortolano et al., 1983), thin-film gradient fluxmeters(Godefroy et al., 1986), and Schmidt-Boelter gages(Kidd, 1981). Gages that are based on similar principle, yet incorporate resistance thermometers instead of thermocouples include sandwich type gages(Epstein, 1986;Hayashi et al.,1986). Each of these sensors has advantages over the next for particular heat flux ranges and specific applications. One of their disadvantages is that some are limited to low heat flux application and cannot withstand high temperature environments. None are optimum for accurate high heat flux and high speed flow measurement due to both thermal and momentum boundary layer disruption. Thermal disruption can be caused by a gage whose fabrication material is much different than the model material, a large surface area gage resulting in a thermal gradient across the surface of the gage, or a very thick gage whose upper surface temperature becomes different from the surrounding model surface. Physical boundary layer disruption can be caused by a thick gage whose surface is not flush with the surrounding model surface, such as those attached to the surface with adhesive or some other mechanical means. Additionally, few can respond rapidly enough to measure unsteady heat transfer fluctuations without compensation.

A heat flux sensor has been developed that can gather the best qualities of each of the available gages, yet surpass them in available measurement range, high temperature application, high speed flow capability, and unsteady heat transfer application. Photolithography, a basic technique of microelectronics, enables very fine circuit patterns to be created with resolutions of several micrometers. Using these techniques allows for the construction of many tiny interconnected thermocouple pairs in a very small area. Because the sensitivity is created by the many thermocouples in the thermopile instead of by large temperature gradients, the gage can be very thin. By this design and the ability to fabricate the gage on a model surface, the problems with influencing the thermal boundary condition and the disruption of the fluid flow past the surface can be eliminated. High vacuum sputtering techniques allow thin films to be created that are only a few angstroms thick and are capable of withstanding service temperatures up close to the lowest melting point of the materials used. Because the measured voltage output is linear with surface heat flux

and the time response is so fast, the microsensor is ideal for measuring transient or unsteady heat flux.

A gage that can satisfy these requirements has been developed by the author using thin-film fabrication techniques in the Hybrid Microelectronics Lab at VPI&SU. The original concept was devised through collaboration between Dr. Thomas Diller of the Mechanical Engineering Department and Dr. Shinzo Onishi of the Electrical Engineering Department. This gage has been tested and calibrated to prove its worthiness. For a gage fabricated out of pure copper and nickel metals, along with ceramic films of aluminum oxide, aluminum nitride, and silicon monoxide, the temperature measurement range should be well above 600 °C. The heat flux range that has been accurately measured is from 800 to 9000 watts/m^2. The gages can be presently made on Corning 7059 glass substrates, with overall gage dimensions of 1.0 cm x 1.0 mm x 2.0 μm. The time response for this prototype gage has been shown to be better than 1.0 ms, possibly fast enough to measure unsteady heat transfer fluctuations. The following pages display these results and how they enable this gage to surpass the others available.

Literature Review

There are basically four methods to measure heat flux, as mentioned in the introduction, and within these there are a variety of different designs. The heat flux microsensor design uses one of these methods, measuring heat flux by monitoring a temperature difference across a finite thermal resistance. The output signal from this type of gage is generated due to the temperature difference set up by the conduction of incident heat flux through the gage layers. The temperature difference is measured by thin layers of temperature sensors on either side of the thermal resistance. The output is found to be proportional to the temperature gradient through this thermal barrier (Figure 1 on page 5). This can be shown by the simple heat conduction equation:

$$q'' = \frac{k}{\delta} \Delta T \qquad (1)$$

where k is the thermal conductivity of the thermal resistance and δ is the thickness of this layer. The designs of closest comparison to this research include either single or multiple combinations of differential temperature sensing elements. These sensing elements are found in two categories, either in the form of resistance thermometers or thermocouples. The sensing elements are incorporated with a range of different dielectric and thermal resistance films to form the heat flux gages available.

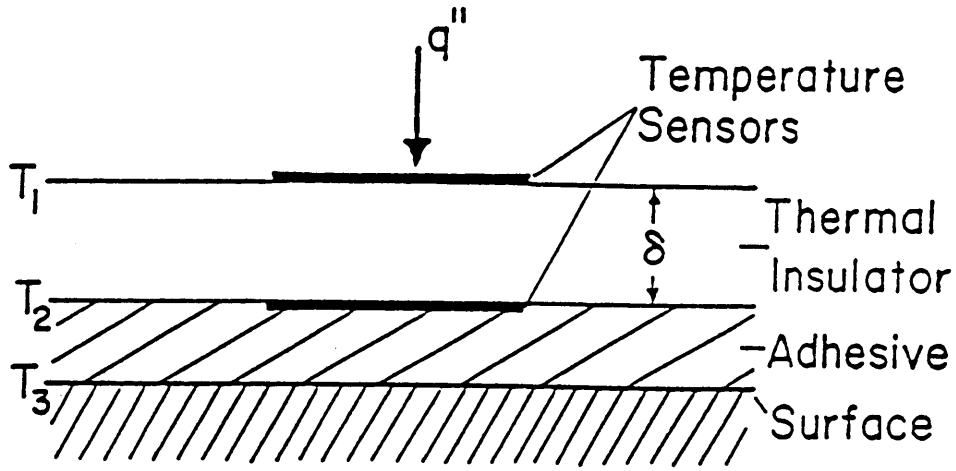

Figure 1. Schematic Cross Section of a Layered Heat Flux Gage

There are many important goals to achieve when designing this type of heat flux sensor. These are 1) to create a very small very thin sensor, 2) to have the physical properties of the gage be able to withstand a wide range of temperatures, and 3) to have a high frequency response and still generate a measureable, reliable signal. Included in producing a reliable signal, the sensor must have low heat capacity so as not to offset the output signal over time. Increasing the signal many times requires a thicker gage which then reduces the measureable frequency range. A thicker gage also restricts the application to low speed flow due to boundary layer disruption if the sensor is not flush with the surface. Most of the gage designs use thin-film microelectronic techniques to construct a multilayer electronic circuit less than 50 μm thick. The advantages of these techniques allow the fabrication of very small, high resolution gages whose presence on a test model goes relatively unnoticed. Withstanding higher temperatures many times requires more exotic materials to avoid gage characteristic variation. This may reduce the signal output. These are some of the trade-offs encountered in creating a heat flux gage for a particular measurement application.

Resistance Sensors

The first category of gages to be discussed will be those incorporating resistance thermometry. Resistance thermometers are based on the principle that the electrical resistance of metals varies with temperature. For pure thin films, this variation was found to be very close to linear (Epstein et al., 1985). The temperature is monitored by recording the resistance using a bridge circuit and converting the signal to temperature by a previous calibration coefficient. A high sensitivity can be achieved with this method. When used for a layered gage, the resistance films are deposited on each side of a thermal resistance. The output of the gage, a result of the temperature difference set up by the incident heat flux, is then a resistance value which converts to a temperature difference.

A thin-film heat flux gage developed at MIT by Epstein et al.(1985), uses 0.13 μm nickel resistance films deposited using photolithography techniques along with DC sputtering vapor deposition

(Figure 2 on page 8). The resistance elements are fabricated on each side of a Polymide (Kapton) substrate acting as a 25 μm thermal resistance layer. By using long thin films of high volume resistivity and temperature coefficient, a maximum service temperature of 327 °C can be reached, while still maintaining good accuracy. The advantages of this design include: a measurement frequency range from DC to 100 kHz, fabrication and testing is independent of the test article, since the substrate is a component of the gage, and heat flux measurement is independent of the test article material. There are also disadvantages of this design. The direct relation between the temperature difference and the heat flux is valid only up to a certain frequency due to the thermal resistance layer thickness. For a 25 μm layer this frequency is about 20 Hz. For the range of 20-1500 Hz, the response is constructed through numerical signal processing, and above this range the assumption that the temperature transient response of the upper resistance thermometer is used to determine the heat flux. This presents considerable mathematical manipulation. Another problem with the design is its thickness. The thickness may be relatively small, but since the gage is separate from the model, it must be attached by adhesive, 5.0 μm thick bringing the total gage thickness to about 33 μm. In high heat flux applications this may cause the upper film temperature to be considerably different from the test article surface, therefore influencing the thermal boundary condition. The thickness may also trip the boundary layer in many high speed flow applications. Finally, a problem due to the resistance elements is that the necessary excitation voltage results in a small amount of heat dissipation which may offset the gage temperature.

Another version of the MIT-style gage was developed in Japan by Hayashi et al.(1986). For this version the resistance thermometers were deposited with a thermal resistance layer between them directly on the substrate by the sputtering process (Figure 3 on page 9). This eliminates the need for adhesive, yet the gages are fabricated on probes which present different advantages and disadvantages. The heat resistance film is silicon monoxide (SiO) whose deposited thickness is around 17.1 μm, about half that of Epstein's design. The sensing elements are long, straight, and thin instead of the serpentine pattern of Epstein's gage, increasing spatial resolution a little to about 1mm. The gage is protected both electrically and mechanically on both sides by thin films of SiO. The

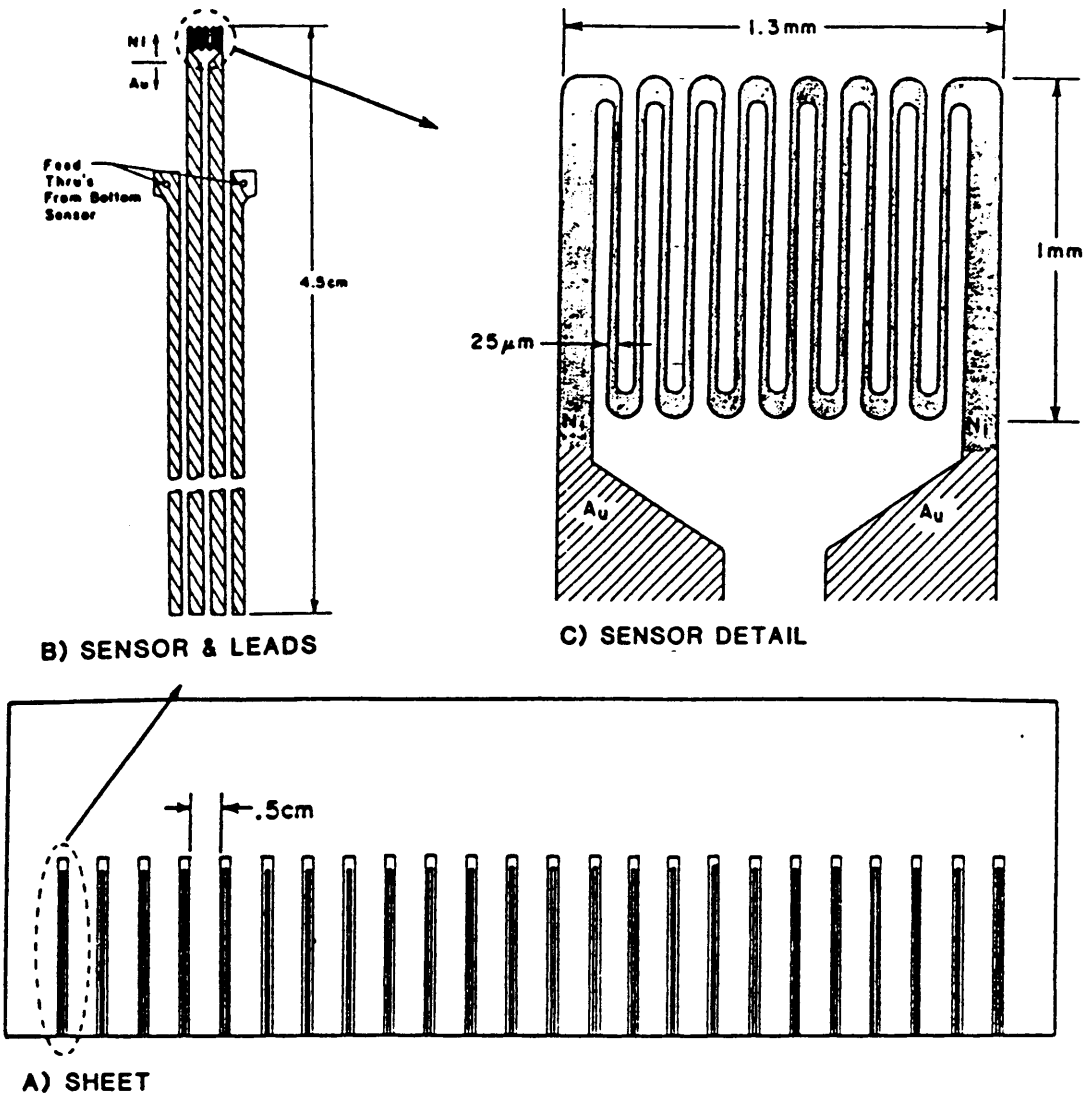

Figure 2. High Frequency Gage (Epstein et al., 1985)

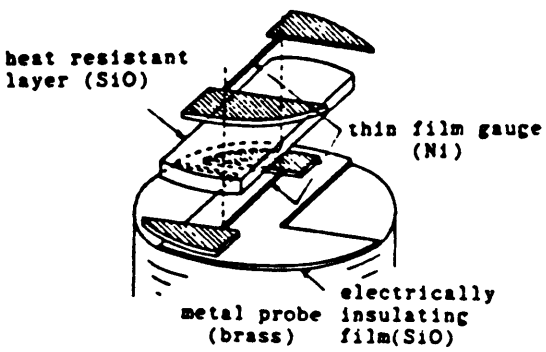

Figure 3. Multi-layered Gage (Hayashi et al., 1986)

reduction in the thermal resistance layer thickness and its greater thermal conductivity, reduced the sensitivity to 0.021 mV per watt/cm^2. One would expect the reduced thickness to increase the frequency response, but only a measurement range up to 600 Hz has been achieved. The reason may be that the added thermal resistance of the protection layers hampers the response time and accuracy since the measurement is based on the assumption of a 1-D steady state conduction analysis. Though the overall thickness of the gage is smaller than the previous design, the possible decrease in both thermal and geometrical disruption are seemingly negated by the use of a probe. The probe then leads to accuracy problems in high speed flows. The advantage of the probe is that heat flux measurements can be taken in various regions of the flow away from the model surface.

Thermocouple Sensors

The second category of layered temperature difference heat flux gages incorporate thermocouples as the temperature sensing elements. Thermocouples are based on the principle of the Seebeck coefficient which states that when two dissimilar metals form two junctions at different temperatures a current is produced around the loop. The emf measured across one of these junctions depends on the sum of the respective Seebeck coefficients of the metals. There are a variety of metal combinations which can be used, but there are only a few well documented pairs. The decision to use a certain metal combination can rely on many factors, some of which are: service temperature, deposition characteristics, corrosion characteristics, and output signal. One of the advantages of a thermocouple over a resistance thermometer is that it has a self-generating signal only requiring a temperature difference. The problem with using a thermocouple is that its sensitivity is very small, low in the μV/°C range. In using a thermocouple as a component of a heat flux gage, it is connected in series with another junction on the other side of a thermal resistance whose temperature is a little different to form a differential thermocouple. For this situation the two small signals are subtracted from each other to give an extremely small, almost immeasurable signal unless the ΔT is large. To generate a sufficient signal, while still keeping the gage thin and thus the ΔT low, a

number of differential pairs can be connected in series to add up the voltage differences. This results in a differential thermopile which can have a greater output than resistance thermometers. One design consideration is to achieve the maximum number of differential pairs while still keeping the gage surface area small.

One of the present leading manufacturers of this type of gage is the RdF corporation ,(Ortolano et al., 1983). They use the idea of a series connection of differential thermocouple pairs on either side of a thermal resistance(Figure 4 on page 12). The thermal barrier used is a piece of Kapton ranging in thickness from 50 μm to about 250 μm. The thermocouple junctions, chromel-alumel, are etched patterns from a previously clad piece of Kapton. Thin layers of Kapton protect each thermoelement surface. This brings the overall gage thickness to between 76 μm and 330 μm, resulting in a range of sensitivities from low to very high; 0.064 to 35.0 mV per watt/cm^2. The advantages of this design are that the gages are extremely durable and can be used for a wide variety of low heat flux applications since there are a range of sizes and mounting methods available. Choosing the K-type thermocouple pair along with a large thermal barrier thickness helps to give the high output but this limits the maximum operating temperature to 260 °C and the time response to about 2 Hz. The fastest time response, 50 Hz, is obtained using the thinnest gage, but is still too low for measurement of many unsteady heat transfer phenomena. This design, much like Epstein's MIT-style gage, is fabricated independent of the test article and must be applied with adhesive or some other mechanical means. To prevent surface disruption by the gage, it is either mounted in a recessed portion on the model surface or the model surface is built up. The thickness of the gage requires such a deep recess that the the surface temperature distribution of the model is sure to be disrupted. This will also reduce the accuracy of the 1-D heat flow assumption. Finally, resolution is poor as compared to other designs with the smallest gage size in excess of 0.96 cm^2.

A heat flux gage developed in France (Godefroy et al., 1986) uses sputtering techniques along with metal masks, instead of etching, to produce a much higher service temperature sensor. The gradient fluxmeter, as it is called, incorporates Pt-Pt 10% Rh metal combinations (type S) for the single differential thermocouple used(Figure 5 on page 13). Depositing these films using RF cathodic

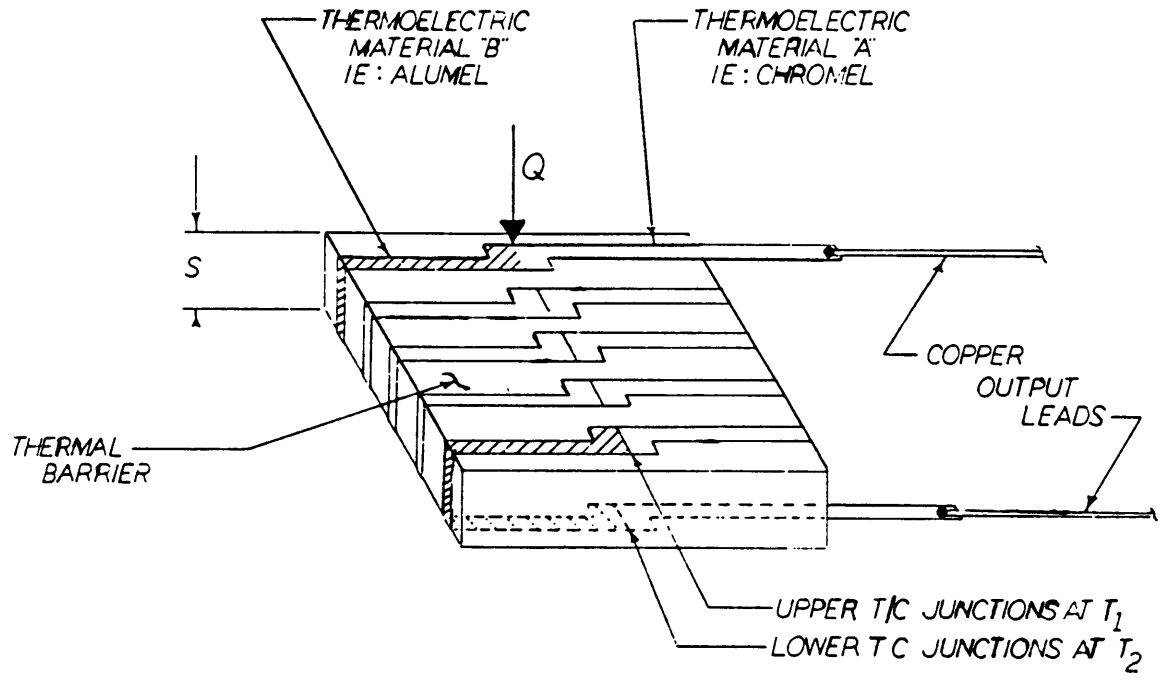

Figure 4. RdF Micro-Foil Sensor (Ortolano et al., 1983)

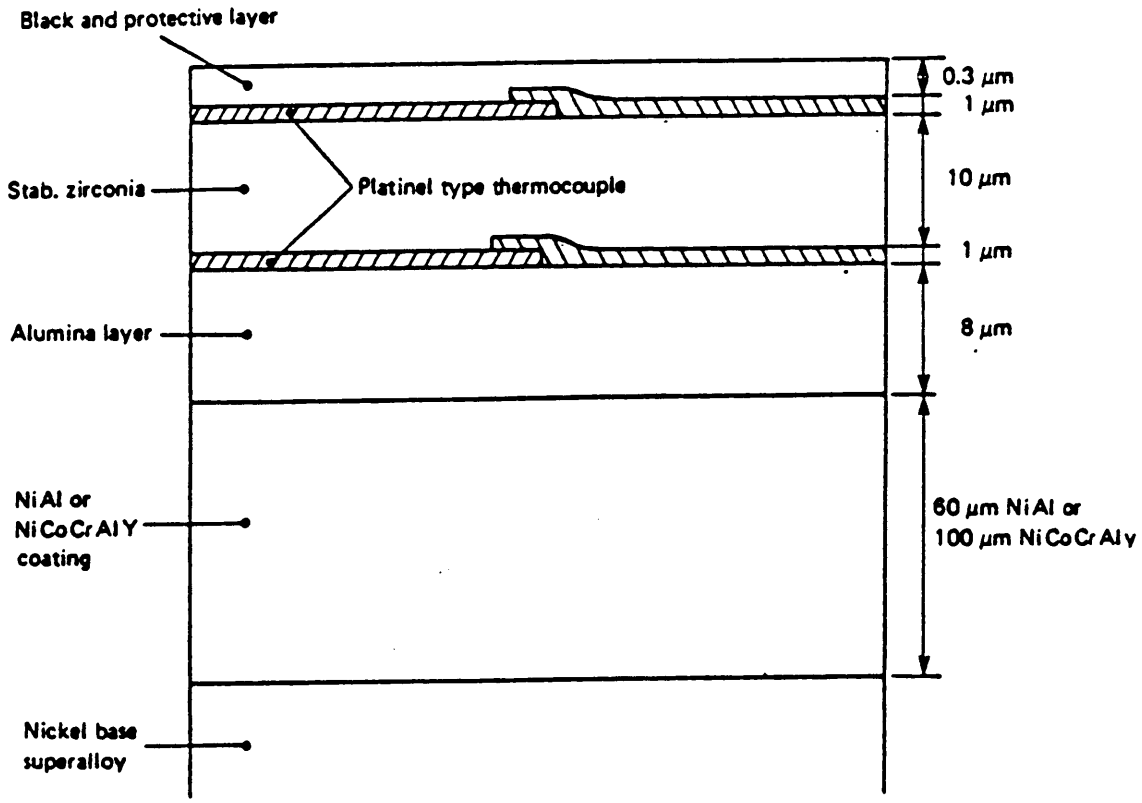

Figure 5. French Fluxmeter (Godefroy et al., 1986)

sputtering alone is not sufficient to maintain good adhesion up to the maximum service temperature of 1100 °C. To aide in adhesion, superalloy substrates were used, coated with a 5 component alloy of NiCoCrAlY or a 2 component alloy of NiAl. This interface layer has been found to achieve good adhesion to both the substrate and sensor materials. This base layer is deposited by a CVD vapor phase process with a thickness ranging from 60 to 100 μm. On top of this layer an 8 μm layer of Al_2O_3 is sputtered for both electrical insulation and for a diffusion barrier. A single thermocouple, 1 μm thick, is sputtered through a metal mask, and a thermal resistance layer of zirconium, 10 μm thick, is deposited between this thermocouple and another one above it. The top protective layer is a 0.5 μm blackened layer of Al_2O_3, whose color aids in radiative absorption. The general design is very effective , yet there are problems with electrical conductivity in zirconia at elevated temperatures. Also since only one differential thermocouple pair is used, a very low sensitivity is achieved, 0.002 mV per watt/cm^2. The work reported by Godefroy was very preliminary, but the direct fabrication of a multiple layer thin-film sensor is very similar to the microsensor design. With an overall thickness of better than 80 μm (20 μm excluding the interface layer), the accuracy is limited to low speed flows. No frequency data was available, but due to the thickness it is expected to be poor.

The third gage version using thermocouples as a component, is the Schmidt-Boelter gage used by Calspan (Kidd, 1981). Again the sensors are used as a direct measurement instrument based on an axial temperature gradient since the gage is mounted on the end of a cylindrical heat sink, which is the same principle as the other designs (Figure 6 on page 16). In the design process a 2-D heat conduction analysis using finite element techniques helped to predict performance characteristics. This was found to be more accurate than standard exact solution models. The design consists of 2 mil constantan wire wound about 35 turns around a 0.635 mm thick rectangular aluminum wafer. One half of the constantan wire, along a longer side, is electroplated with copper forming a series connection of differential thermocouples on either side of the thermal resistance wafer. Anodizing the aluminum wafer electrically insulates the gage. The sensor is then mounted in a recessed area on the end of a 0.635 cm(¼") diameter anodized aluminum rod, acting as a heat sink, by a thin

layer of epoxy. The top sensor surface is also covered by a thin layer of epoxy for protection. The total gage thickness ranges from about 762 μm-1.016 mm, but this does not include the heat sink to which it is mounted. These gages are found to have excellent durability, yet can only achieve a maximum service temperature of 316 °C. The gage surface is semi-contourable, if the wafer is molded to the model shape before construction. As other gages of this type, the calibration coefficient is independent of the gage temperature, thus the output is proportional to the incident heat flux. The sensitivity is quite high for this design, 1.3-3.1 mV per watt/cm^2, and is proportional to the number of turns of constantan wire(N), or essentially the number of thermocouple junctions used.

$$\frac{\Delta E_o}{\dot{q}_0} = l \cdot \delta \cdot \frac{N}{K_l} \qquad (2)$$

ΔE_o represents the potential drop, l represents the wafer thickness, δ represents the thermoelectric sensitivity of the thermocouple pair, and K_l represents the thermal conductivity of the aluminum wafer. With the high sensitivity, the response time is limited to approximately 1 second. This restricts the measurement application to steady heat transfer. The other disadvantages of the design are based on the thickness of the gage, the use of adhesives, and the heat sink used. Recessing the gage helps to minimize surface boundary layer disruption but introduces error through 2-D conduction since the recess must be very deep. The use of adhesives, though thin layers, will add more thermal resistance and thus hamper performance. Finally, if all are to be mounted on a rod and then mounted in a model of different material, the thermal characteristics of the model will change and therefore errors will result due to the change in the thermal boundary condition.

Each of the different gage designs propose a variety of good qualities necessary for the particular test situation it was designed for. The problem in this research field is that there is no gage available that includes all of the qualities necessary to be a universal heat flux sensor. This is summarized by Kidd(1981) in his description of an ideal transducer.

> "An ideal transducer for aerodynamic heat transfer measurement applications in continuous wind tunnels would have an output signal directly proportional to the heat flux incident on the sensing surface, a heat flux sensitivity $\geq$20 mV/Btu/ft^2-sec(17.65 mV/W/cm^2), and a time response on the

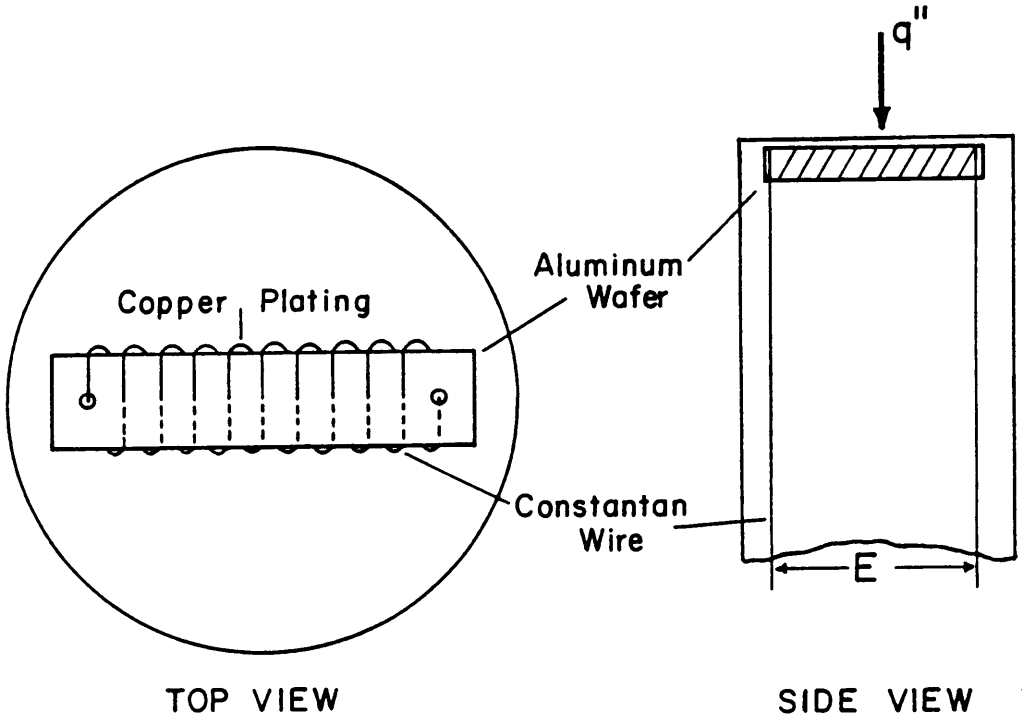

Figure 6. Schmidt-Boelter Gage Concept (Kidd, 1981)

order of 0.10 seconds. In addition, the ideal transducer would have a sensing surface temperature exactly the same as the adjacent model or test article surface, a maximum continuous service temperature of at least 1500 °F(815 °C), and a calibration scale factor completely independent of ambient gage temperature. Physical characteristics of the transducer should include small size ($\leq$0.125 in. diam. by $\leq$0.35 in.), ability to be contoured exactly to match a model surface, and ability to withstand any normal test environment with no structural damage. It may be possible to achieve one or more of these ideal performance factors with practical application of the Schmidt-Boelter concept; however, even an inexperienced gage designer would recognize that it would be virtually impossible to attain all of these performance factors in one gage. Therefore, design tradeoffs have to be made."

The objective of the heat flux microsensor is to do just that, fill the void of each gage all in one transducer without necessary tradeoffs. A table comparing the characteristics of each design with those of the heat flux microsensor follows(Table 1 on page 18).

Table 1. Comparison Table

Type	Gage Thickness	Service T(°C)	Sensitivity ($mV/W/cm^2$)	Max. Freq. Response
Epstein et al.,1985	33μm	327	N.D.	100 kHz
Hayashi et al.,1986	20μm	N.D.	0.021	600 Hz
Ortolano et al.,1983	76-330μm	260	0.0011-0.58	50 Hz
Godefroy et al.,1986	80-120μm	1100	0.002	N.D.
Kidd,1981	762μm-1.016mm	316	1.3-3.1	1 Hz
microsensor	2μm	600	0.164	> 1 kHz

Note: N.D. stands for No Data

Gage Design

The heat flux microsensor is a complex design compared to those previously discussed. Using available thin-film microelectronic techniques, however, the fabrication of such a design is possible. Combining the ideas of previous gage designs with some state-of-the-art techniques, a very small, very thin, and durable heat flux sensor has been developed.

Operational Theory

One of the major advantages of the heat flux microsensor is that it can be fabricated on many different substrate surfaces. The basic principle of the sensor is based on the Seebeck coefficient and thus thermocouples. The Seebeck effect was identified in 1821 (Jackson and Mushin, 1985). The theory states that when two dissimilar wires are twisted into a two junction loop, a current is generated about this loop. The emf produced across one of these junctions was found to vary with temperature. This emf is the measure of the temperature difference between the higher temperature junction, or hot junction, and the voltage measuring device acting as a cold junction.

Using the principle of the Seebeck coefficient, the lower and upper layers of copper/nickel thermocouple junctions, (Figure 7 on page 22), detect temperatures in the form of emf outputs. The two are isolated from one another by the thermal insulating layer. This layer is silicon monoxide, a ceramic of low thermal conductivity, whose thickness regulates the temperature drop across the gage. A thicker layer better isolates the two temperature sensors, advantageous in steady-state performance; yet, for the rapid conduction of heat through the film necessary for a fast time response, a thinner film is required. Connecting two such thermocouple junctions across the thermal resistance adds the two opposing signals in the form of a voltage difference between two similar leads. A single pair of such thermocouples is considered a differential thermocouple whose output would be very small, especially since the temperature difference would be small, around 0.01 °C per watt/cm^2 with a very thin thermal resistance layer. Connecting many such differential thermocouples together in series much like forming a thermopile, which is a set of thermocouple junctions connected in series, would create a differential thermopile. This configuration adds each of the emf differences to produce a more measureable signal. The larger the number of the differential pairs, the thinner the thermal resistance layer can be to generate the same output. This is the reason for using thin-film fabrication techniques.

For the heat flux sensor tested, 100 differential thermocouples are connected in series in an area covering 1.0 mm x 1.0 cm and a thickness less than 2.0 μm. In order to generate a signal of 100 μV using a thermocouple with a sensitivity of 23 μV/ °C, the temperature drop necessary using a single differential thermocouple would be 4.3 °C. Using 100 such pairs, on the other hand, requires a temperature drop of only 0.043 °C. This is the reason why thermal disruption of the surface is avoided with the microsensor design, the microsensor surface temperature is essentially that of the surface it is fabricated on. The entire gage is protected by a film of aluminum nitride. This film is much thinner than the base film because it need only be a uniform coating to electrically and mechanically protect the metalized layers of the gage. The output which is measured, between the two copper terminals, is the temperature difference set up by the heat flux which conducts through all of the layers of the microsensor with negligible loss due to gage thickness. Applying the basic

theory of heat flux (equation 1), a temperature difference over a finite thermal resistance, the gage can be approximated as a 1-D transport model. Using this theory along with thin-film techniques produces a heat flux sensor of reasonable output and negligible substrate surface disruption both thermally and physically.

Layer Design

Thin film fabrication techniques allow very intricate conductor patterns to be made in a small area on a substrate. The restriction on size and intricacy depends on the facilities and fabrication methods available. For the research involving the heat flux microsensor, lithographic techniques were used. These techniques, such as the lift-off method, require image transfers using emulsions and wet processing. Stainless steel masks are a better method because they eliminate possible chemical reaction, dust particles, or other contaminants that could damage the fine patterns. Since stainless steel masks could not be used, the microsensor design was kept simple and made relatively large to try to reduce chances of contaminant particle damage. Using a differential thermopile, a series connection across multiple layers was achieved. This required the deposition of two metal layers, a thermal insulating layer, and both an electrical insulating layer and a protective barrier layer. The complete overlay of the microsensor layers is shown in Figure 8 on page 23. The individual layer patterns can be found in appendix A, Figure 23 on page 62 through Figure 29 on page 68.

The first layer, or electrical insulating layer, is used for conductive substrates to prevent electrical grounding of the microsensor to the substrate. Additionally this layer has to have high thermal conductivity so as not to reduce the frequency response or the accuracy of the gage. For the sample tested, the microsensor was fabricated on a glass substrate so this base layer was not necessary.

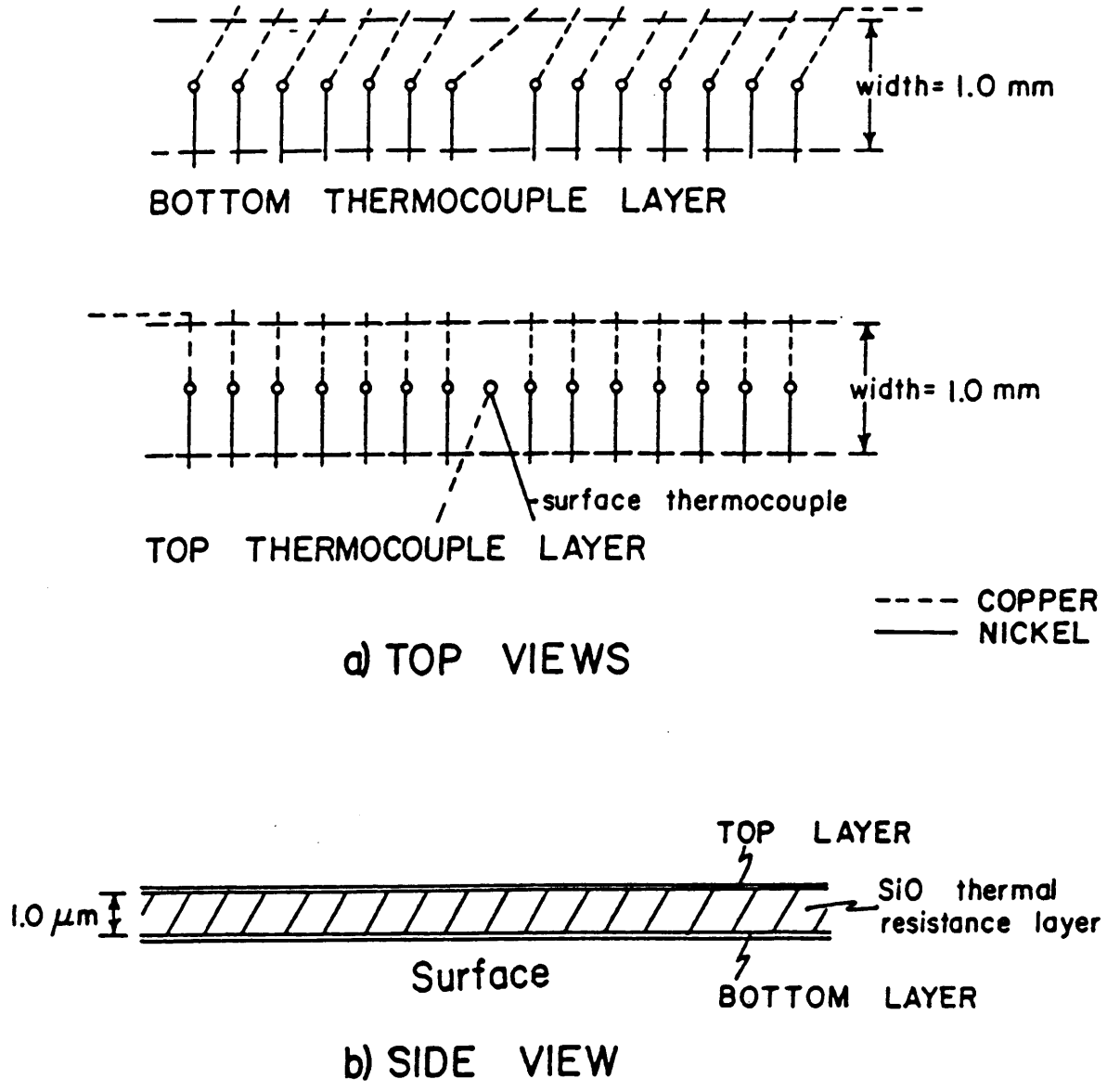

Figure 7. Microsensor Design

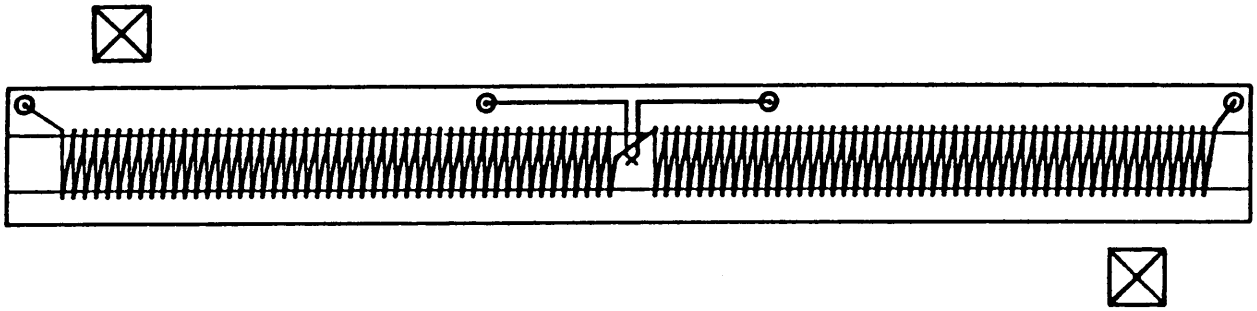

Figure 8. Heat Flux Microsensor Pattern Overlay

The second and third layers are the two metalization layers that must form the bottom layer of thermocouples. The requirement for this design is to create as many thermocouple junctions as possible in a very small area. This minimizes measurement error due to a substantial temperature variation across the surface of the gage, while still producing a relatively large signal. As mentioned earlier, restrictions would depend on laboratory conditions and techniques. Being the first prototype, the pattern was limited to 100 thermocouple junctions across a small strip 1.0 cm in length. To fit the large amount of junctions and to keep the pattern simple, straight lines were used for the thin-film junction leads, or *fingers*. Copper and nickel were chosen to form the thermocouples, because the copper-nickel thermocouple produces a reasonable signal and can attain service temperatures around 700 °C.

The thermal insulating layer is the most critical layer of the microsensor. It must be a thin film of high thermal resistance and excellent electrical insulating properties. The film covers the thermocouple junctions along the centerline and considerably beyond to limit heat flow to 1-D conduction. The thickness of the film is very important in determining the gage sensitivity. A thicker film would give a greater output because it would set up a larger ΔT across the gage. Too thick of a layer risks thermal disruption of the model surface, if the gage surface temperature becomes much greater than the model surface temperature. The thickness is also limited by the step coverage of the metalization layers deposited on top. Because high steps break the electrical continuity of the metal films, the thickness of the thermal insulating layer was kept below 1.0 μm. To achieve thermopile connection, though, the ends of the lower fingers must be left exposed. Silicon monoxide was used for this thermal insulating layer because it has an expansion coefficient on the order of metal films and its insulating characteristics were found to be more than satisfactory.

The metalization layers, fifth and sixth, are deposited on top of the thermal insulating layer. These layers consist of copper and nickel fingers forming a strip of thermocouple junctions above the lower junctions. The series connections between layers are at the portions of the fingers that protrude beyond the thermal insulating layer. A surface thermocouple was incorporated in the gage

design to monitor the gage surface temperature and is deposited along with the upper metalization layers.

The top layer of the gage is a very thin film of aluminum nitride. Not only is this top, or barrier layer, used for electrical insulation, but is also used for overall protection of the delicate microsensor. Aluminum nitride was chosen because it forms a very tough, scratch resistant film of high thermal conductivity. Consequently, it is able to protect against a majority of the test flow particles that may strike it, without hampering thermal performance. For most cases, except for very extreme environments, a very thin film on the order of 0.06 μm is sufficient.

Steady State Calibration Method

To test the performance of the heat flux microsensor and to compare its behavior to the other available sensors, a calibration was performed. Since the gage is designed to work in a multi-mode heat transfer environment, it is best to calibrate it in each of these separate modes. Standard conduction calibrations are limited to very low heat fluxes and were therefore not performed. Convection calibration was used for a range of steady-state heat fluxes, because much of the proposed application of the microsensor is in convective environments. The radiation tests performed were used to determine the time response characteristics and will be discussed in the next chapter.

Apparatus

For application in convective environments, a convective calibration is necessary to obtain a more accurate calibration factor than that achieved through the usual practice of radiative calibration. Analysis using Gardon gages (Borell and Diller, 1987) showed that in convective regimes there can be a non-linear relation between output and heat flux due to temperature variation across the gage surface. For the microsensor, this variation should be negligible. The calibration apparatus developed by Borell and Diller(1987) was redesigned for easier data acquisition (appendix F, figures

46 and 50). It was further modified to use a 1.6 cm diameter free jet impinging onto the constant temperature calibration plate to give higher heat flux. Typically, a calibration with this convection apparatus would be done with one gage, alone, mounted at the center of the calibration plate. In this case, however, a gage fabricated on Corning 7059 glass was mounted along the centerline of the calibration plate next to a calibrated Gardon gage placed at the center. A thin-film thermocouple, also fabricated on 7059 glass, was placed on the other side of the Gardon gage to determine the microsensor surface temperature (Figure 9 on page 28). With future microsensors this should not be necessary since a surface thermocouple is incorporated in the design. For the sample which was tested, the thermocouple did not work due to circuit overlap. Measurement of the gage temperature was necessary because of the added thermal resistance of the glass substrate placed on the calibration plate. This caused the glass surface to be at a different temperature than the plate surface, requiring a correction of the heat flux. For metal substrates, such a correction should not be needed. The signal leads for both the microsensor and the thermocouple were attached to the terminal pads using Dynalloy 350 solderable conductive silver paint cured by baking. This enabled electrical contact at the terminal pads of the sensors but may have almost doubled the resistance of the gage up to about 6 kΩ. Both the heat flux microsensor and the thermocouple were mounted to the calibration plate using Thermalcote, a high thermal conductivity paste. They were held in place with a thin rigid horizontal strip attached at its endpoints. This was enough to fix the gage and thermocouple in place while the jet impinged upon them.

Technique

The calibration of the heat flux microsensor was done by comparison of its output to that of a calibrated Gardon gage. This is not as accurate as the direct calibration method (Borell and Diller, 1987) covered in appendix F, but it does give a good measure of the sensor performance. The Gardon gage was connected to a Thermogage DC amplifier, through a second amplifier(IFA signal

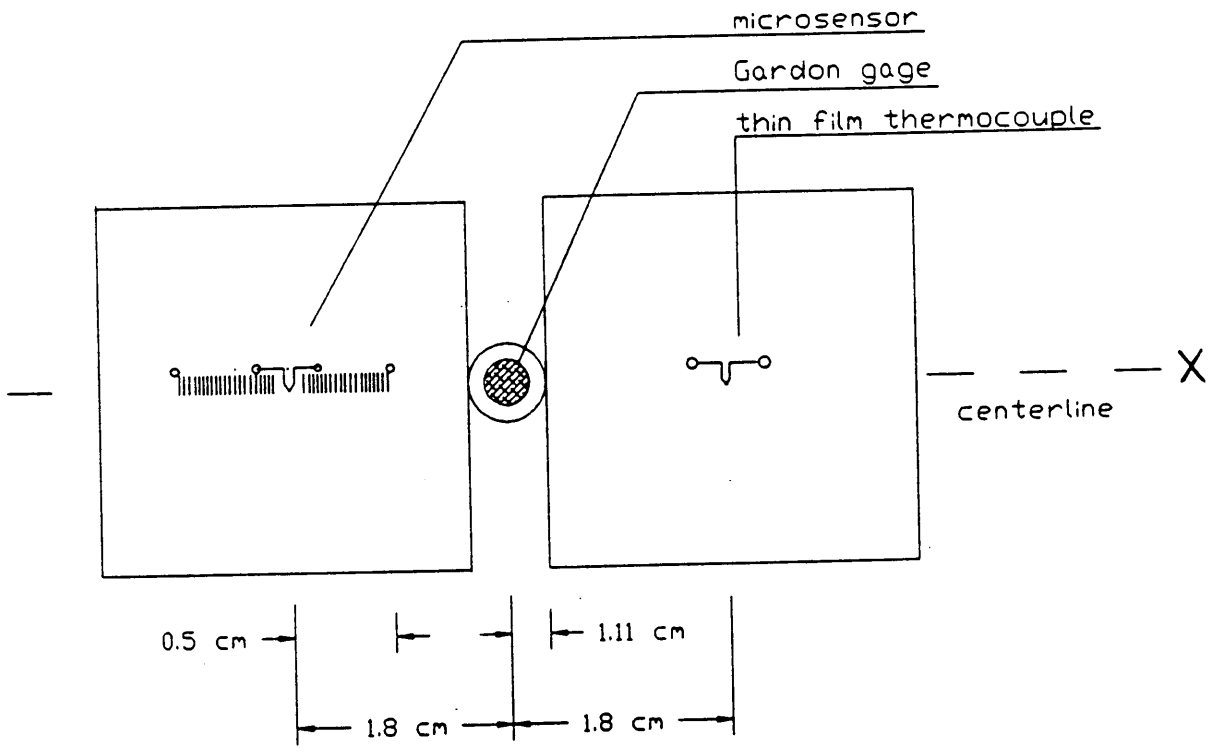

Figure 9. Measurement Sensor Orientation

conditioner) for a gain of 10,054, and then into the computer data acquisition system. The microsensor was connected to the HP 3468 multimeter which was able to read the unamplified output in microvolts and average a number of readings with the HP 41CV calculator, forming the HP data acquisition system. In the future the microsensor signal can also be input into the data acquisition system when a proper amplifier is used. This would enable the data acquisition program to quickly take multiple readings of each gage output, averaging blocks of readings separately and then tabulating the results. For the present calibration this was done on the respective measurement systems separately and then later tabulated for calculations. The copper-nickel thin-film thermocouple was referenced to 0°C with an ice bath and its output was measured with a voltmeter. The calibrated sensitivity was 23 μV/°C (Figure 10 on page 31). The measurements were taken for a full range of heat fluxes controlled by the setpoint temperatures of the 5 heated plates in the apparatus. The jet air velocity was kept constant during the calibration. The heat flux range measured by the Gardon gage varied from 1000 to 19000 watts/m^2. The local heat transfer coefficient was calculated from a Gardon gage sensitivity of f= 0.241 mV per watt/cm^2 and the method as specified by Borell and Diller(1987).

$$h_i = \frac{\frac{E}{f} - \varepsilon\sigma(T_p^4 - T_\infty^4)}{(T_p - T_a)} \tag{3}$$

$$h_c = h_i \frac{1}{1 - \frac{3}{4}\frac{fh_i}{K_2}} \tag{4}$$

$$q_c = h_c(T_p - T_a) \tag{5}$$

The microsensor heat flux was found using the temperature difference between the thin-film thermocouple, microsensor surface, and the jet air flow. Since the heat transfer coefficient is largely a function of the flow, it was assumed to be constant across the region close to the impingement point of the jet. Using an assumption of a constant heat transfer coefficient, the heat flux incident on the microsensor was calculated as

$$q_m = h_c(T_m - T_a) \qquad (6)$$

From this value of heat flux and the measured voltage output of the microsensor, E_m, the sensitivity was found for each data point.

$$S = \frac{Q_m}{E_m} = \frac{h_c(T_m - T_a)}{E_m} \qquad (7)$$

Performance Results

Since the performance of the heat flux microsensor was unknown, except for theoretical calculations, the convection calibration required some trial and error testing. Initial predictions were that the microsensor would have a very low sensitivity, 0.015 mV per watt/cm^2 (Diller and Onishi, 1988), so the microsensor was tested using the maximum heat fluxes obtainable by the convection apparatus. Additionally, the initial calculations were for a microsensor fabricated on a metal substrate, heat sink, and mounted in the plate. The microsensor calibration was performed using a gage fabricated on glass.

After a series of trials(appendix B) a reliable calibration procedure was used to produce a final data set, set 3. There was a 2.0 μV signal displayed by the multimeter for the microsensor at ambient conditions so it was taken as an offset. The signal from each gage was recorded using the HP data acquisition system. The ambient value of the thin-film thermocouple was checked and found to be equivalent to that measured by the T-type thermocouples of the calibration plate. The heat flux range was 0-19,000 W/m^2, as measured by the Gardon gage. Throughout this range, the recorded thin-film thermocouple temperatures were found to be as much as 30 °C lower than the plate temperature. The heat flux range measured by the microsensor was therefore, between 0 and 8494 W/m^2. This was calculated using equations (3) through (6), to find the corrected heat transfer co-

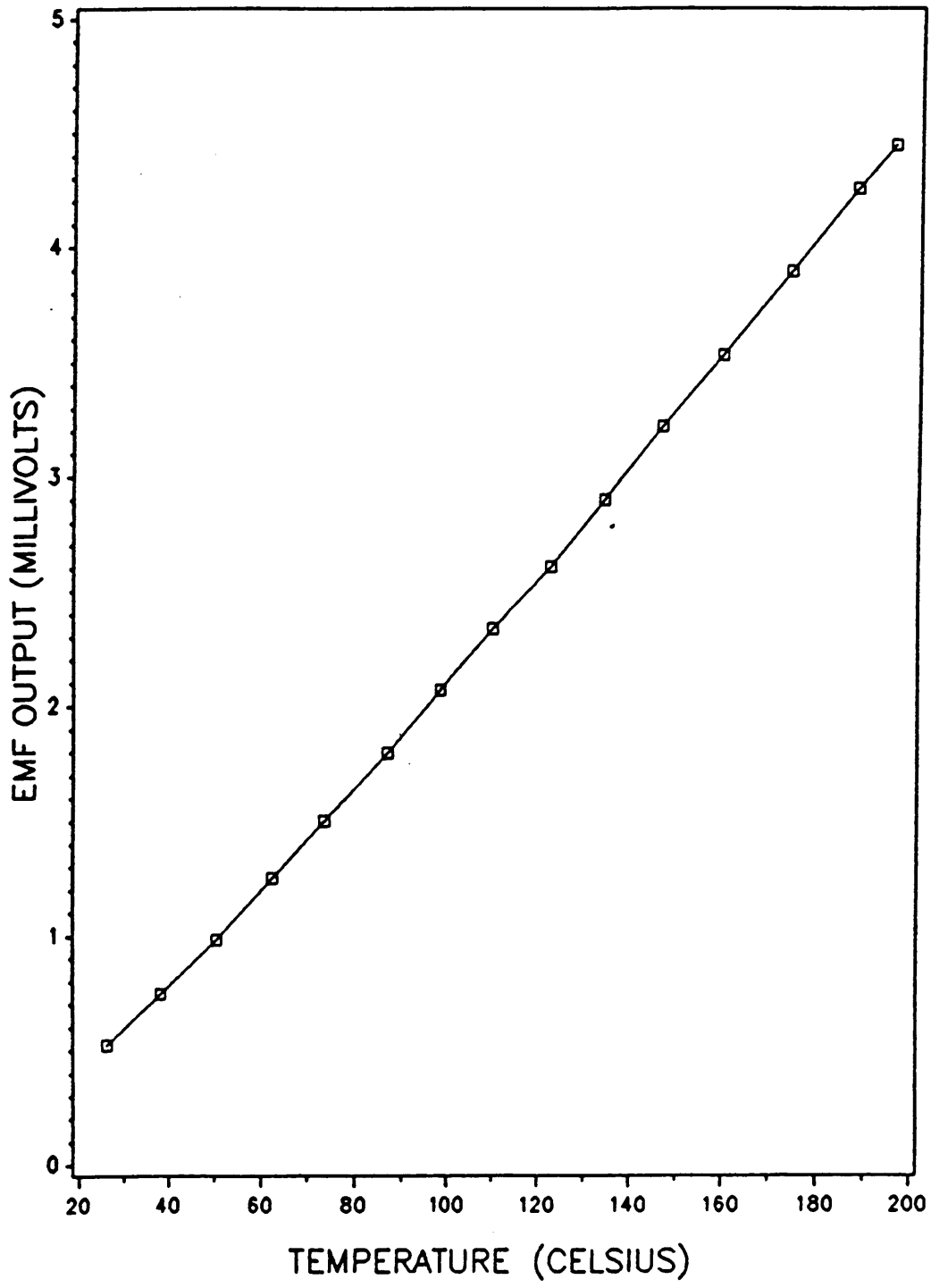

Figure 10. Copper-Nickel Thin-Film Thermocouple Calibration

efficient determined by the calibrated Gardon gage, with a sensitivity of 0.241 mV per watt/cm^2. The air jet was aimed at the Gardon gage and it was assumed that the heat transfer coefficient calculated using the Gardon gage would be the same for the microsensor and the thin-film thermocouple. The average heat transfer coefficient, of 322 W/m^{2}K, was found to be consistent throughout the calibration. The jet air speed, related by a static pressure tap and a hot wire, was measured and found to be 63 m/s. The average sensitivity of the microsensor was calculated to be 0.176 mV per watt/cm^2, using equation (7). The standard deviation was found to be $4.4x10^{-2}$ or a variation of about 25%(Table 2 on page 72). This standard deviation was very high, so the data was reanalyzed. Noting the first data point sensitivity of 0.287 was greater than 2 standard deviations from the mean, it was determined to be offseting the true results. A popular statistical test, Chauvenet's criterion, was used to analyze this data point (Schenck, 1979). This criterion states that

> ".. any reading out of a series of readings shall be rejected if the magnitude of its deviation from the true or mean value is such that the probability of the occurrence of such deviation does not exceed 1/2n."

According to this criterion if the data point was greater than 1.96 standard deviations from the mean, the point should be rejected. The first value on the table satisfied this criterion and was discarded. This resulted in an average sensitivity of 0.164 mV per watt/cm^2 and a standard deviation of $2.0x10^{-2}$ (Table 3 on page 73). This corresponds to a 95 percent confidence interval of $\pm 9\%$.

Analyzing the plot of the corrected and uncorrected data of set 3 (Figure 11 on page 34), one can see that the increase in sensitivity due to the temperature correction, shown by the slopes of the curves, is considerable. These results showed that the heat flux incident on the microsensor was up to 2.5 times less than that detected by the Gardon gage. It can also be observed on this plot that the temperature correction tends to skew the data. The temperature correction adds considerable uncertainty to the calibration results. Figure 12 on page 35 gives the comparison between the outputs of the microsensor and the Gardon gage. The sensitivity of the microsensor is about 21% less than that of the Gardon gage, which is still very good considering the size difference. However, a plot of the heat flux distribution for the orifice (Figure 13 on page 36) was acquired and the ap-

proximate gage positions were marked. Even though all three gages are in the impingement region of the jet, the Gardon gage experienced a higher heat transfer coefficient than the microsensor. Consequently, the uniform heat transfer coefficient assumption provides a conservative estimate of the microsensor sensitivity. The results that were obtained were remarkably good and provide encouragement for future prototypes.

The results of the gage calibration can also be used to estimate the thermal conductivity of the silicon monoxide layer. The voltage output which is measured between the copper terminals is proportional to the temperature difference set up by the heat flux which is conducted through the microsensor. Assuming one-dimensional heat transfer through the thermal resistance of the gage results in the following equations.

$$q_m = \frac{k}{\delta}(T_1 - T_2) \tag{8}$$

$$E_m = nS_T(T_1 - T_2) \tag{9}$$

Based on a value of $\delta = 0.7$ μm for the thermal resistance layer thickness and a value of $S_T = 23$ μV/°C for the thermocouple sensitivity, gives an estimate of $k = 0.10$ W/m K for the thermal conductivity of the silicon monoxide. This is an order of magnitude lower than the expected value 1.4 W/m K, based on the bulk properties of silicon monoxide(Hayashi et al., 1986).

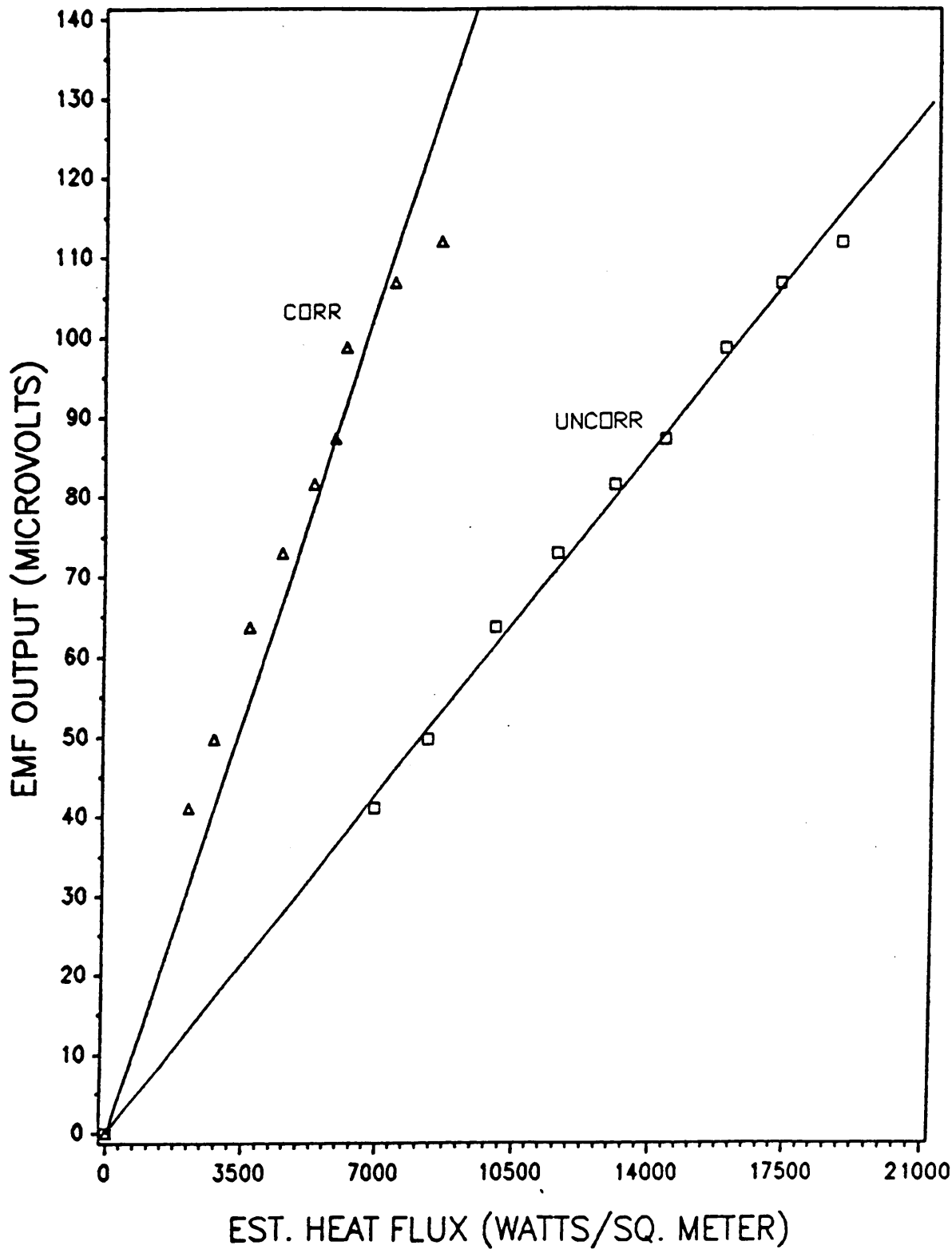

Figure 11. Steady State Plot Set 3 (corr vs. uncorr)

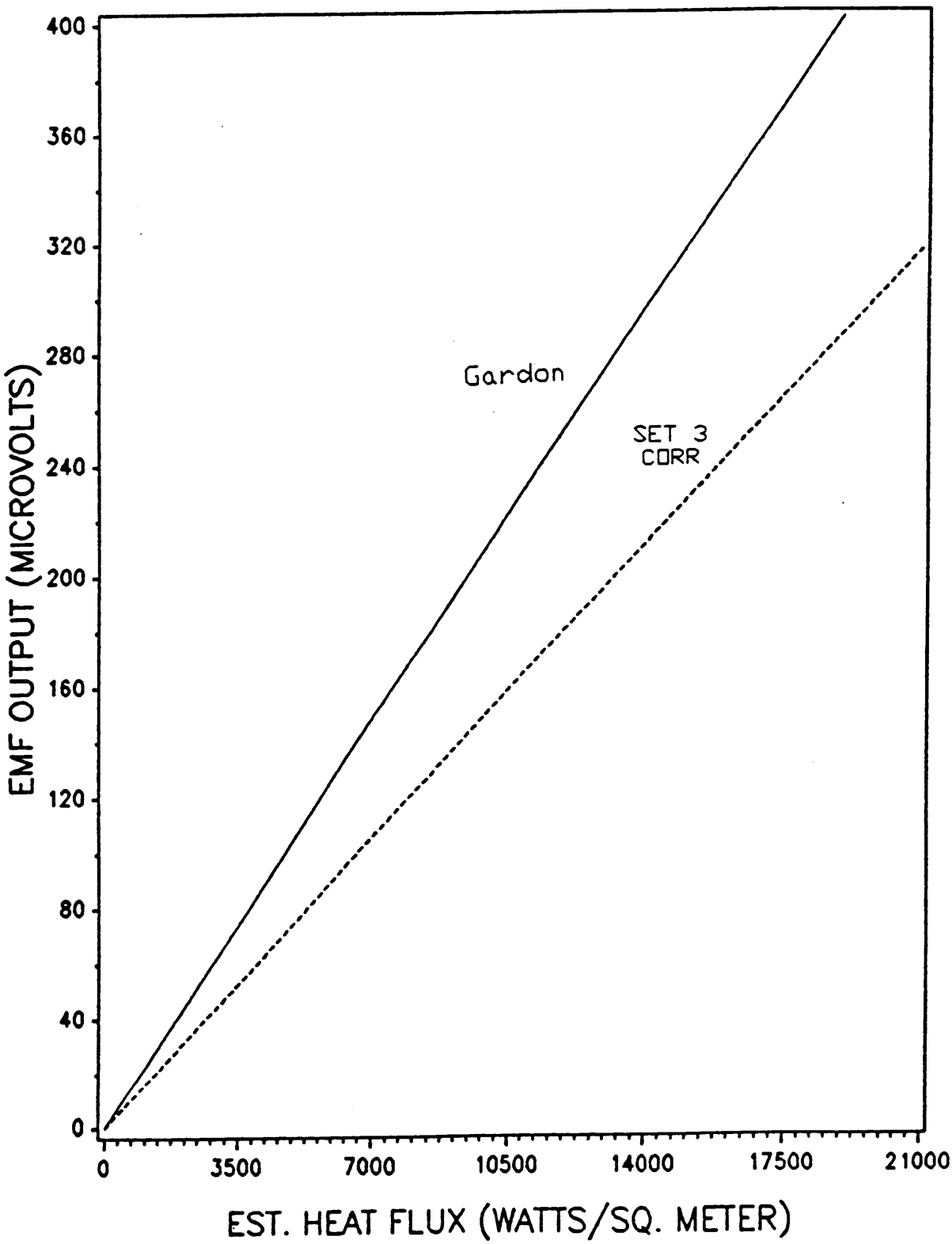

Figure 12. Steady State Plot Set 3 (Gardon vs. corr)

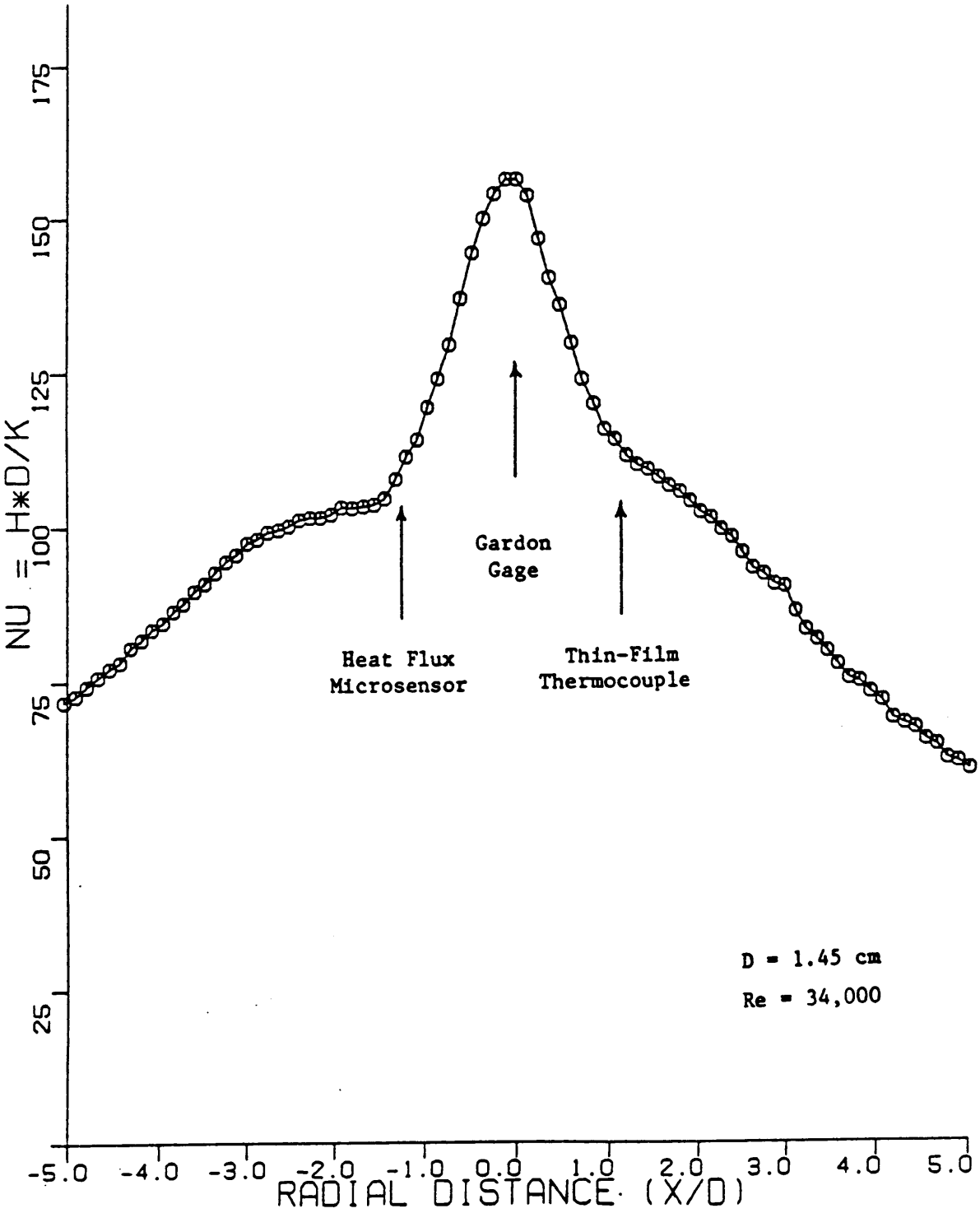

Figure 13. Jet Heat Transfer Distribution

Radiation Frequency Response

The steady state performance results of the heat flux microsensor showed a greater output than anticipated, proving that the very thin design was indeed viable. Another major advantage of the microsensor is that since the thermal resistance layer is so thin, about 0.7 μm, the response time to unsteady heat flux should be quite small. According to an equation developed by Hager(1965), the resulting time response to 98% of the final temperature distribution can be calculated for a layered gage from

$$t = 1.5\frac{\delta^2}{\alpha} \qquad (10)$$

Using a value for α of $5x10^{-7}m^2/s$, which is representative of typical insulating materials, gives a time response of about 4 μs for this design. A powerful chopped radiation source was used to directly measure the time and frequency response of the gage.

Apparatus

The radiation source was a 5 watt Argon-ion continuous laser. The laser beam was directed through a chopper wheel(Figure 14 on page 39). The 8″ chopper wheel was driven by a variable

speed motor so that the chopping frequency could be adjusted from 0 to 125 Hz. The chopper wheel consists of 2 windows, each 25% of the arc of the wheel, so that there was sufficient difference between the beam size and the window size to assure complete beam chopping. An EG&G photovoltaic photodiode was used to produce a record of the time varying characteristics of the input signal. A beam splitter was used along with a series of mirrors to direct a small portion of the beam toward the photodiode, while still keeping the majority of the radiative flux incident on the microsensor surface. This gave a record of the input signal that could be compared to the output signal of the microsensor. The ideal input waveform would be a square wave. Although the chopper wheel approximated this, the finite size of the laser beam caused the change in flux level to be less than instantaneous. A pulse laser would have resulted in a better representation but one was not available. The microsensor was mounted on a small stand bolted to the test table and a blackened cylindrical shroud was placed around it to try to limit possible room reflections of the beam and also to block the beam in between tests.

The unamplified AC signal included line noise and its harmonics. In order to reduce this noise, as before, the gage was connected by a twisted-shielded pair to a Dynamics differential amplifier which reduced the noise to between 10 and 20 μV peak to peak. Without the amplifier, even with its unreliability, the signal to noise ratio would have been less than 1. The 20 μV noise could be reduced no further due to the present exposed terminal connections. The output signal was connected to channel 2 of a Nicolet digital oscilloscope. Channel 1 was for the photodiode input. The direct input signal from the photodiode was not used because the signal showed an extreme amount of high frequency, > 1 kHz., ringing due to an RC component of the diode(Figure 33 on page 87). To eliminate the ringing and overshoot, a 2 kHz low pass filter, part of an IFA signal conditioner, was initially used. This reduced the ringing,(Figure 34 on page 88) but a 1 kHz low pass filter eliminated it, only allowing for a small overshoot (Figure 35 on page 89). Now the signal was connected to channel 1 of the oscilloscope. The scope enabled the input on channel 1 to be viewed simultaneously with the output channel 2, both triggering off of channel 1. Time records of input and output were recorded for various chop frequencies.

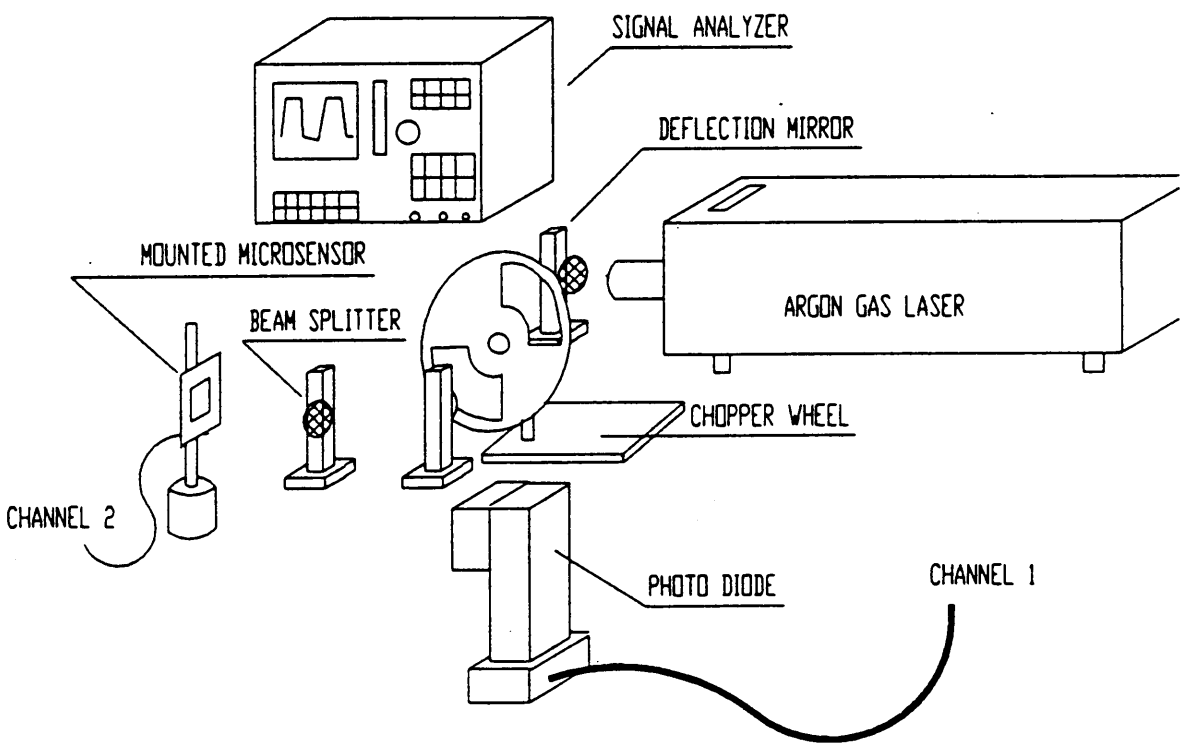

Figure 14. Frequency Response Apparatus

The time records were useful to get an idea of the visual characteristics of the input and output signals, such as waveform shape and noise content. These traces were not sufficient to actually determine the time response of the heat flux microsensor with respect to the input flux. The best way to relate this information is to form a frequency response function or a Bode plot. This was produced through an HP FFT signal analyzer with the input signal in channel 1 and the output signal in channel 2. Power spectrum plots for each signal and frequency response plots were also acquired.

Technique

To obtain the time records the laser was set for 1 watt output, which was found to be sufficient for the microsensor response and was the most that could be used with the present photodiode, to prevent saturation. The records were taken for various frequency settings of the chopper wheel beginning with the lowest frequency of 26 Hz followed by 47 Hz, 84 Hz, and the maximum frequency of 110 Hz. The Nicolet oscilloscope was used to store time records of at least one full cycle for each waveform.

The frequency response function was necessary to determine specific characteristics about the microsensor response. The measurements were done at the same 1 watt power level. The microsensor and photodiode signals were sampled simultaneously. Continuous peak mode averaging with 80% overlap was used for a frequency span of 0 to 50 Hz(Figure 15 on page 42). The reason for the 50 Hz limit was largely due to previous chopper wheel damage at the higher frequencies. The sampling was started with the chopper wheel off. While the averaging continued, the speed of the chopper wheel was slowly increased sweeping the chopper frequencies very slowly. Higher harmonics, above the chopper frequency, are replaced due to the larger magnitude of the fundamental frequency. If the voltage is adjusted slowly enough, a continuous frequency domain representation is produced, where the frequency response plot represents the ratio of the output to the

input. Any skipped frequencies show up as peaks and any large slopes are a result of passing through the frequency range too quickly.

Performance Results

The results shown in the time records display both some expected and unexpected waveforms. Running the photodiode signal through the low pass filter produced an approximate square wave input. The on and off points of the laser are identified at the upper and lower corners of the waveform(Figure 16 on page 45). The decay and growth of the photodiode signal at the chopping point regions is due to the chopper wheel cutting a finite beam and possibly the nonideal time response of the photodiode system itself. This limits the accuracy of the comparison between the signals. There are also some characteristics of the microsensor signal that should be noted. A low signal to noise ratio can be measured on the plots which could be reduced further if a more efficient differential amplifier is used to lower the common mode noise. The other alternative is to increase the signal by increasing the heat flux incident on the microsensor. This is of course limited by the photo diode. Additionally, a waveform disturbance of almost twice the chopping frequency and about half the amplitude can be seen following the output signal on all 4 plots (Figure 16 on page 45 to Figure 19 on page 48). This waveform shows up as peaks on the time records or tends to cause the the waveform to look as if the DC signal is increasing during the time there is constant flux incident on the microsensor surface. This would be opposite of what would be explained as heating effects as a result of using a glass substrate which may build up heat on the lower surface of the gage instead of drawing it away as a heat sink. This type of heating effect would be displayed as a decrease in signal output because the ΔT across the microsensor would be decreasing. This may be explained as an effect due to the presence of the higher frequency waveform. Additional uncertainty lies in the problem that the gage made on glass is mostly transparent to the laser. Consequently, there may be some reflected energy from the back surface of the glass. With the combination of the uncertainty of the cut-off in the input signal and the output signal distortion,

Linear Resolution

MEASURE:	CHAN 1 Freq Resp		CHAN 2 Freq Resp	
WINDOW:	CHAN 1 Hanning		CHAN 2 Hanning	
AVERAGE:	TYPE Cont Peak	# AVGS 10	OVERLAP 80%	TIME AVG Off
FREQ:	CENTER 25 Hz		SPAN 50.0 Hz	BW 93.7mHz
	REC LGTH 16.0 S	Δt 7.81mS		
TRIGGER:	TYPE Freerun	LEVEL 0.0 Vpk	SLOPE Pos	PREVIEW Off
INPUT: CH 1 CH 2	RANGE AutoRng↑ AutoRng↑	ENG UNITS 1.0 V/EU 1.0 V/EU	COUPLING AC (Flt) AC (Gnd)	DELAY 0.0 S 0.0 S
SOURCE:	TYPE Rndm Noise		LEVEL 0.0 Vpk	OFFSET 0.0 Vpk

Figure 15. Signal Analyzer Sampling Setup

it is difficult to determine the actual microsensor response. It can be said that the response is very close to that of the input across the frequencies tested. At the highest frequency, it appears that the microsensor response is faster than the photo diode. The gage response time is clearly better than 1 ms (Figure 19 on page 48). It can also be seen that at the higher frequencies the input signal becomes more distorted(Figure 19 on page 48). The general characteristics of these results seem promising, alluding to the fact that when a prototype microsensor is fabricated on a heat sink and tested using a pulse laser, the results may in fact show that the time response is on the order of hundreds of kHz.

The frequency span to be tested in order to produce the frequency response function was intended to be 0-50 Hz, but it was determined that due to the voltage supply driving the chopper wheel and chopper wheel motor itself, the reliable frequency range was limited to between 20 and 50 Hz. This reliability can be seen in the power spectrum of each signal (Figure 20 on page 49). The signals don't show similar behavior until the 20 Hz frequency level is reached, following which the behavior is very similar as expected. Looking at this confidence region on the coherence plot shows that with a magnitude of 1, the output signal is indeed related to the input and therefore, the frequency response function is representative of the system. (Figure 21 on page 50). The aim of the analysis is the frequency response function or Bode plot (Figure 22 on page 51). This shows the comparison between the magnitude and phase of the output microsensor signal to the input photodiode signal. The magnitude of the frequency response function (top curve) should be constant for perfect gage response. There is a little slope up to about 30 Hz which is due to running through the frequencies too quickly as mentioned earlier. This is found to be more critical at the lower frequencies when there are less points to average in a given time period. The phase plot of the frequency response function (lower curve) shows the microsensor initially lagging the photodiode at 20 Hz by about 20 degrees. As the frequency is increased, though, the plot shows that by 50 Hz the microsensor is in phase with the photo diode. This trend can infer that at frequencies higher than 50 Hz, the microsensor could in fact be leading the photo diode, as indicated by the higher frequency time plots.

These results are very encouraging. They do not show any limitation of the heat flux microsensor response over the range tested. The data represents approximations of the microsensor performance because of the previously discussed uncertainties in the time records, and the low frequency restriction of the frequency response function. The general method for testing the frequency response has been found to be satisfactory but will be much better for future prototypes when a reliable differential amplifier is used with a pulse laser and a microsensor fabricated on metal. Future tests will be concentrated on frequencies in the kHz range on up to 1 MHz, to fully test the microsensor capabilities.

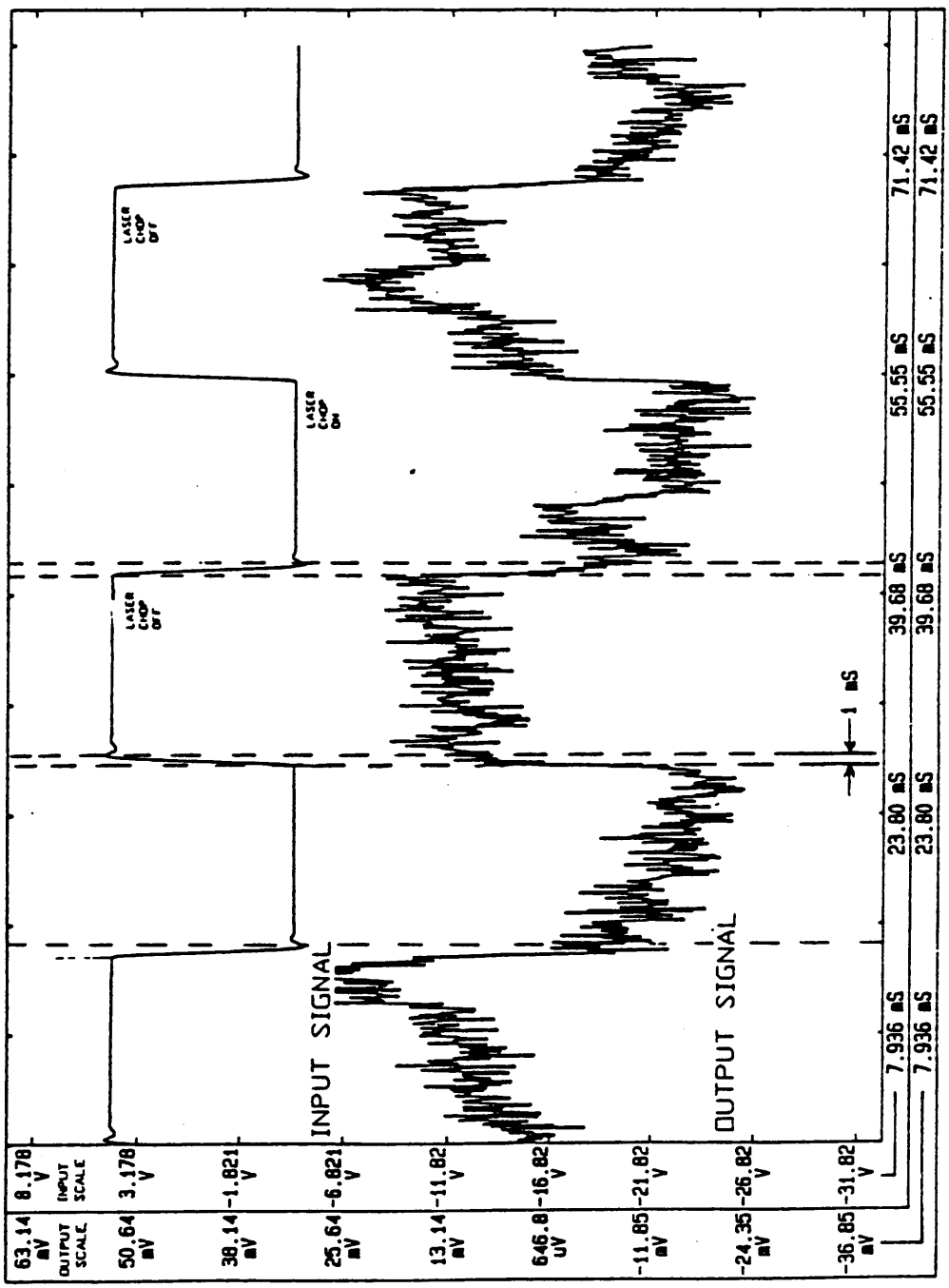

Figure 16. Time Record input 26 Hz

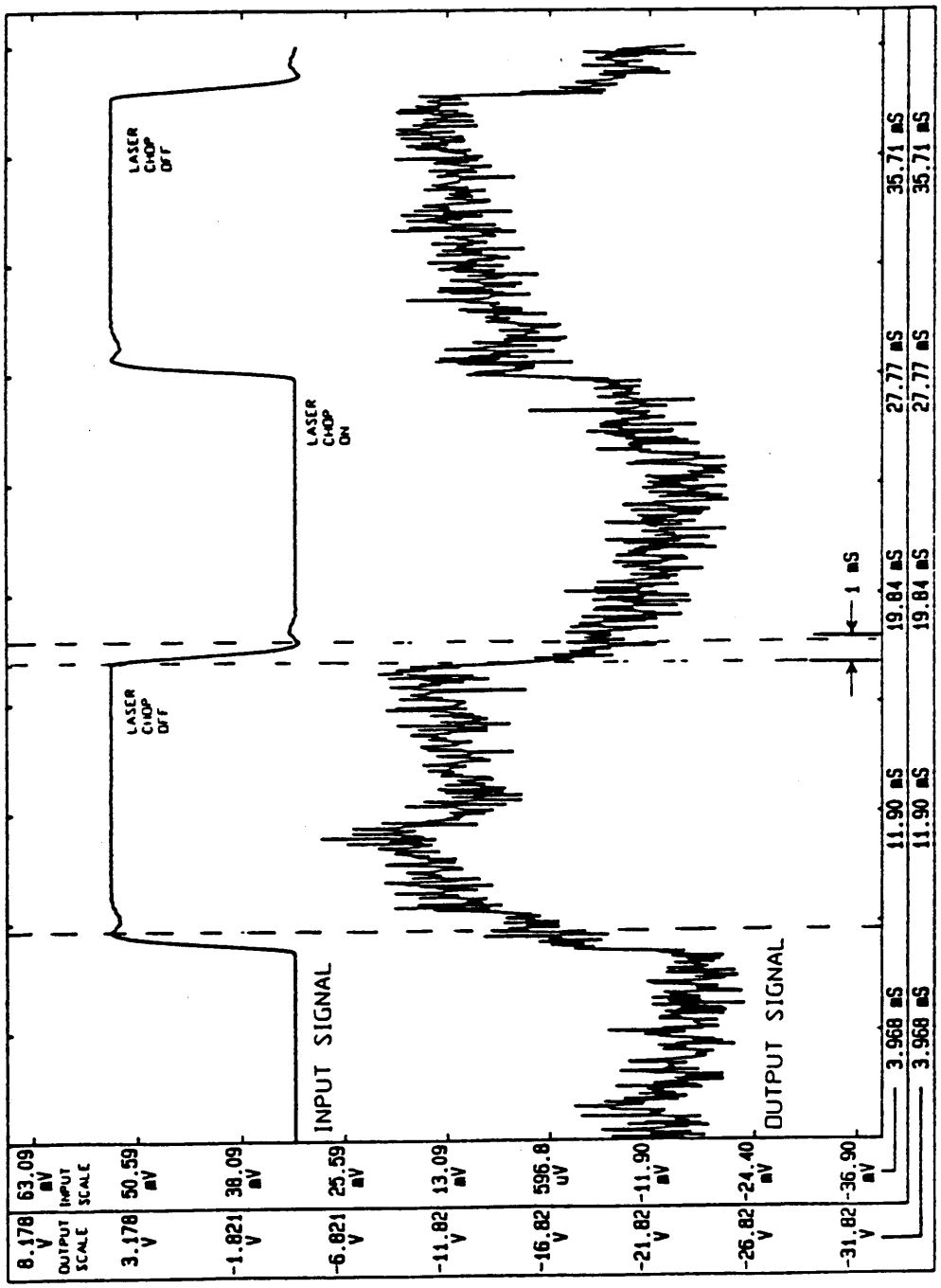

Figure 17. Time Record input 47 Hz

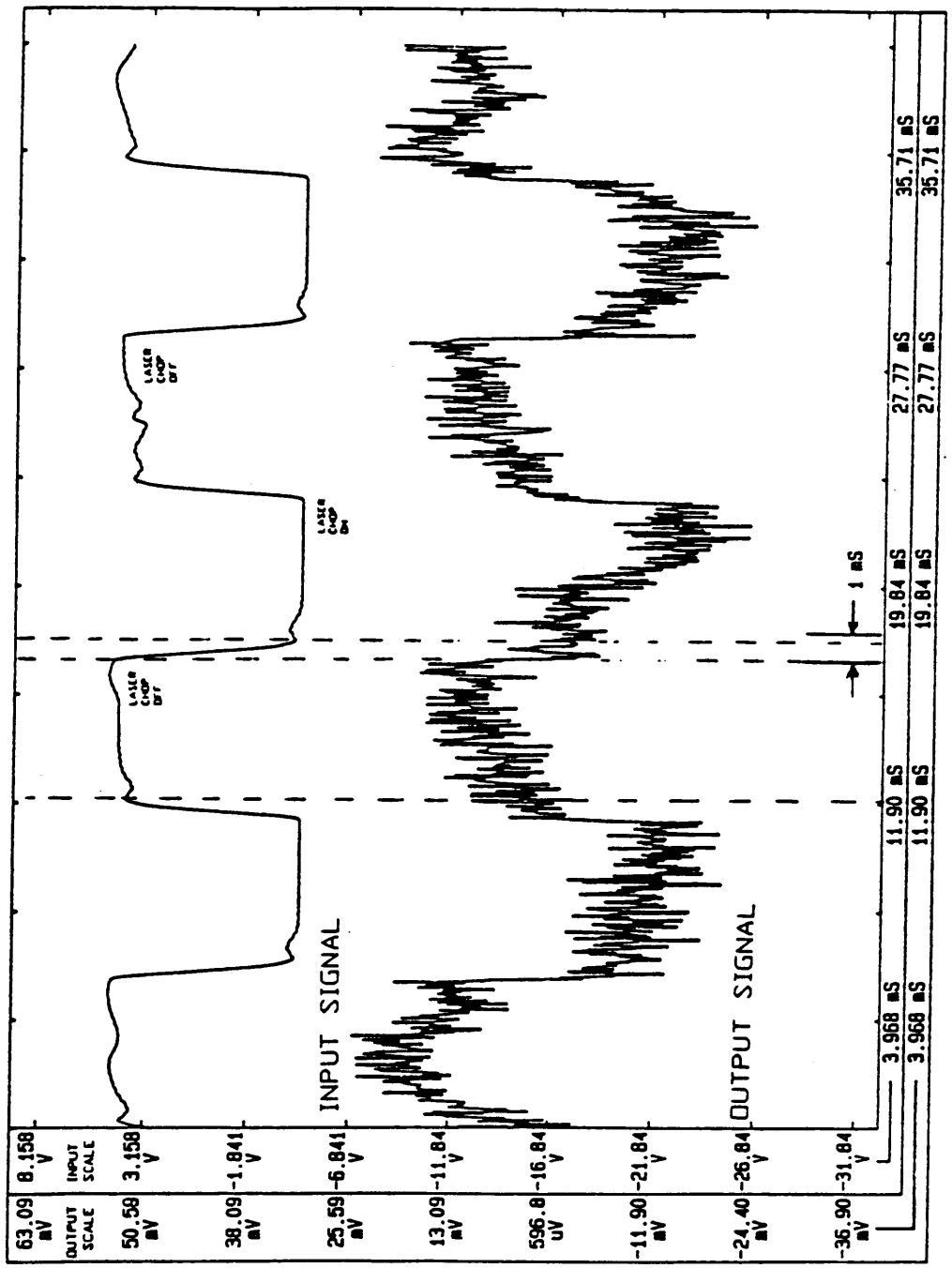

Figure 18. Time Record input 84 Hz

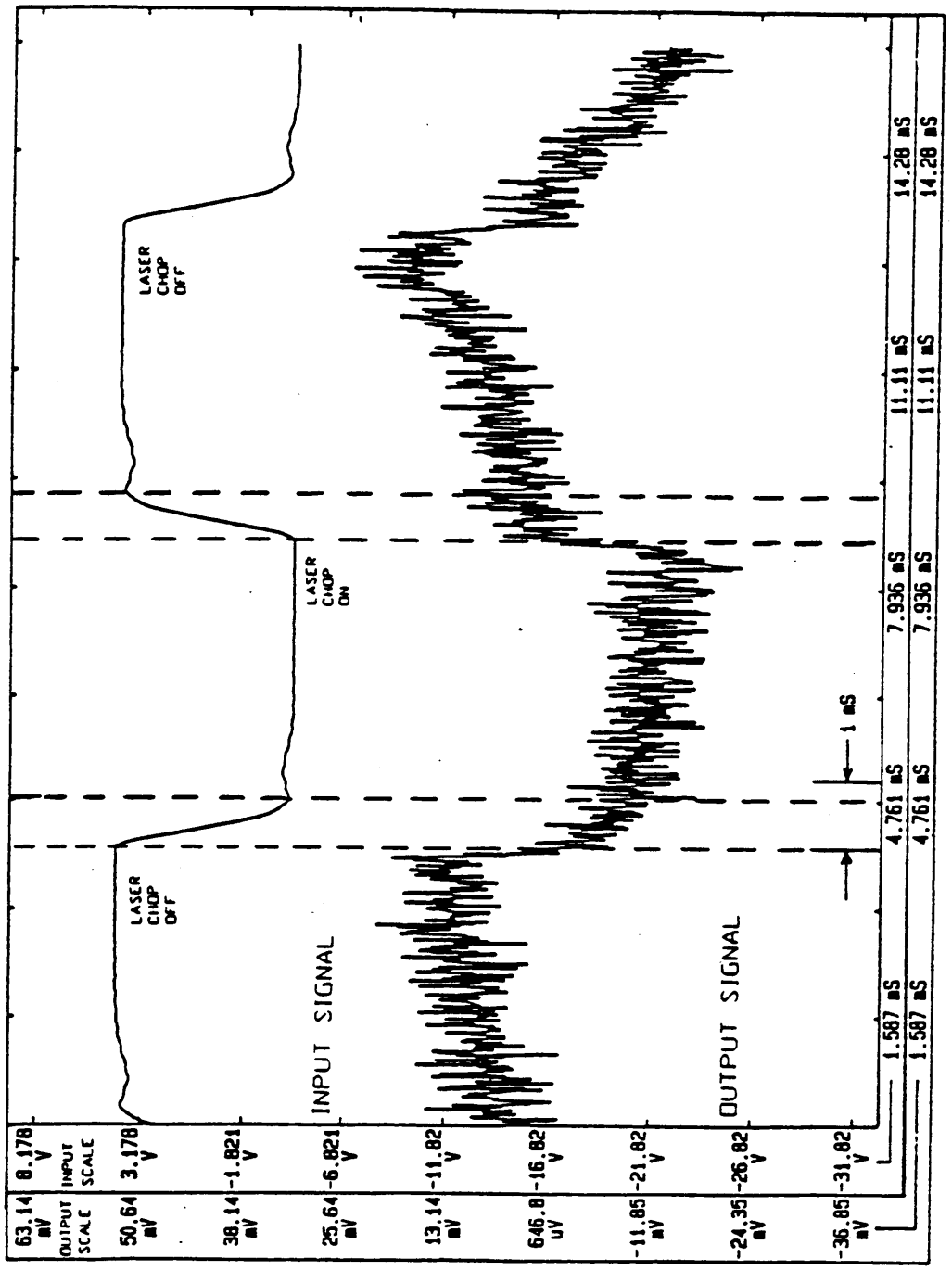

Figure 19. Time Record input 110 Hz

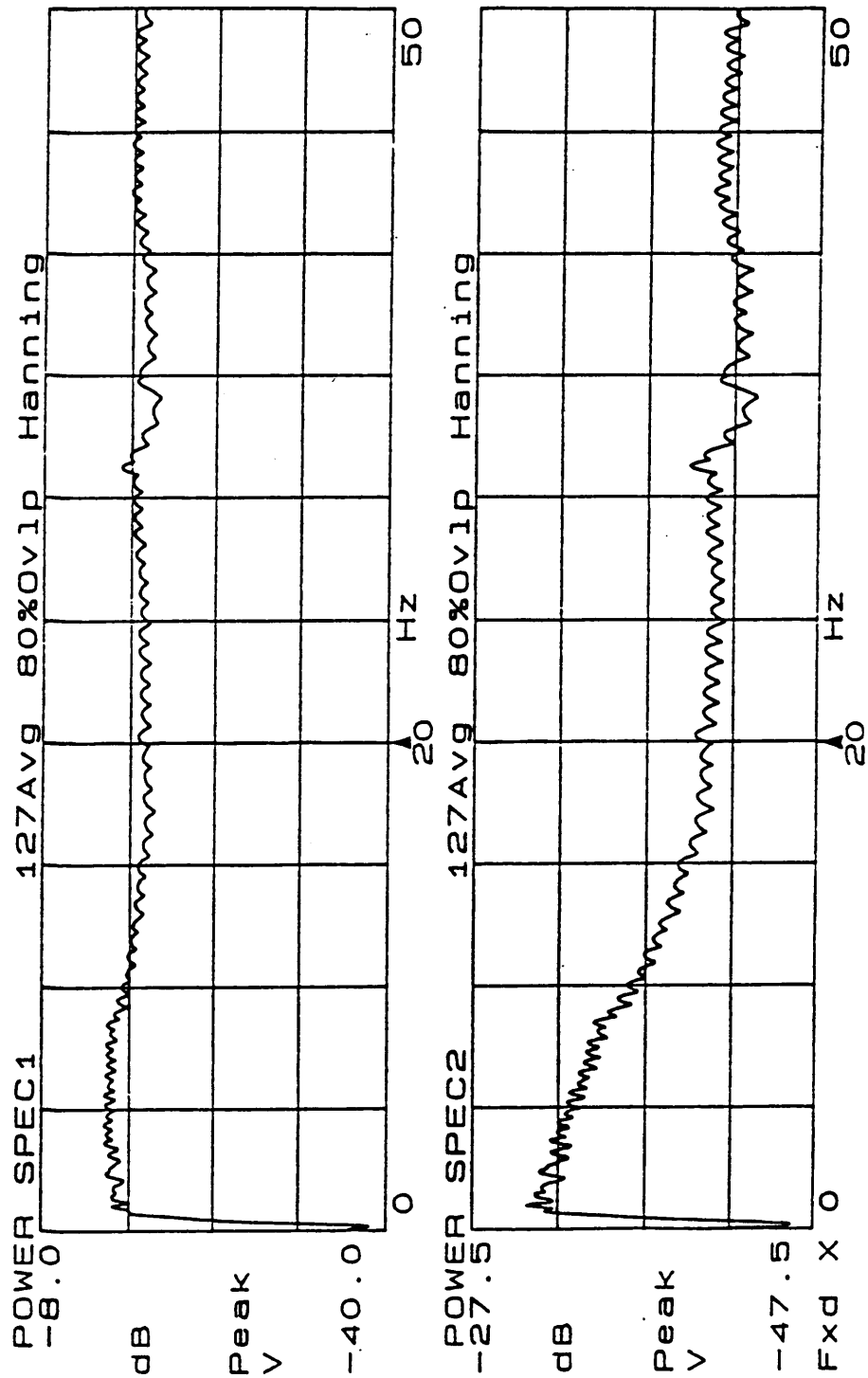

Figure 20. Frequency Power Spectrum of I/O 0-50 Hz

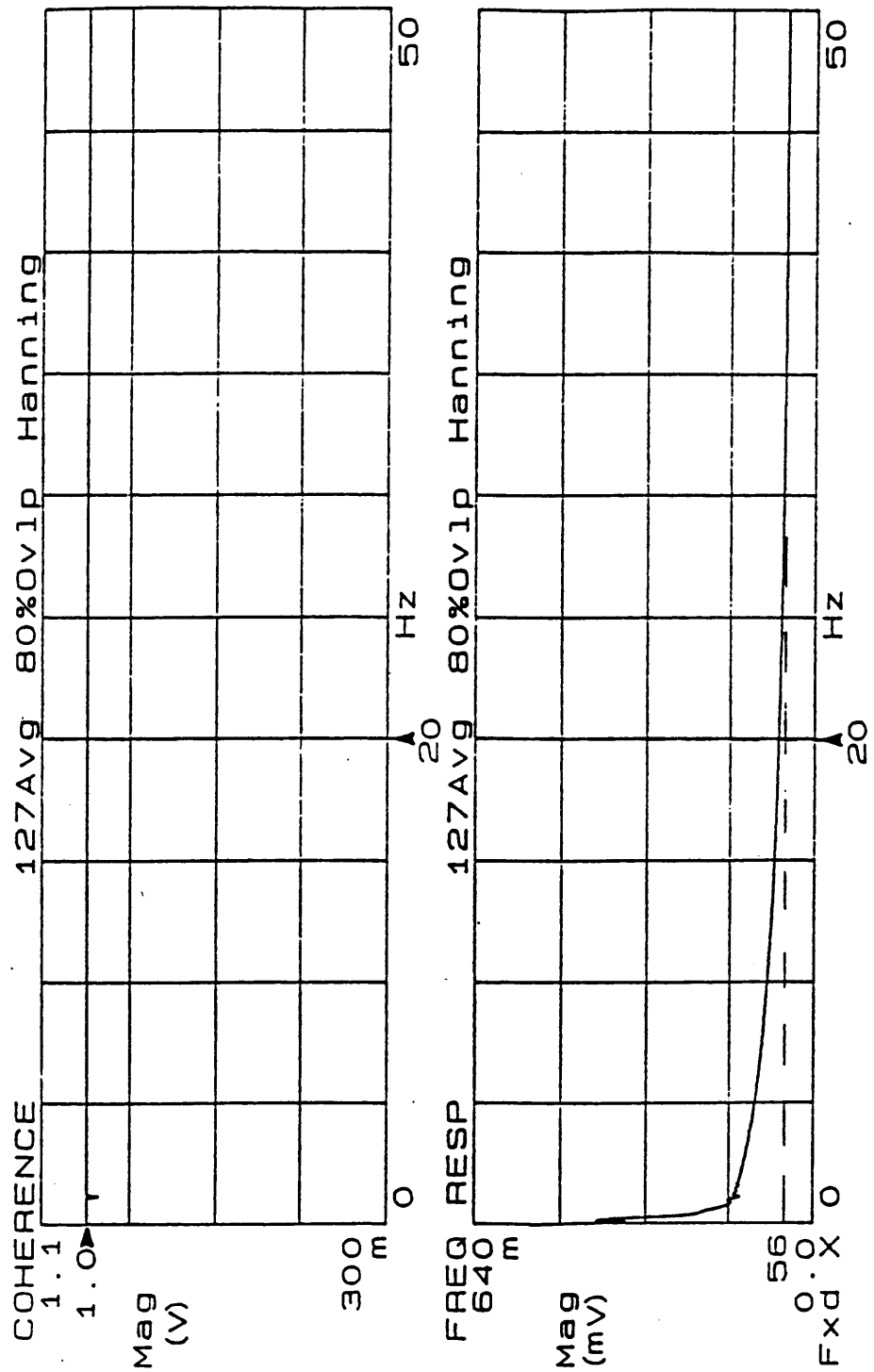

Figure 21. Frequency Coherence and Frequency Magnitude

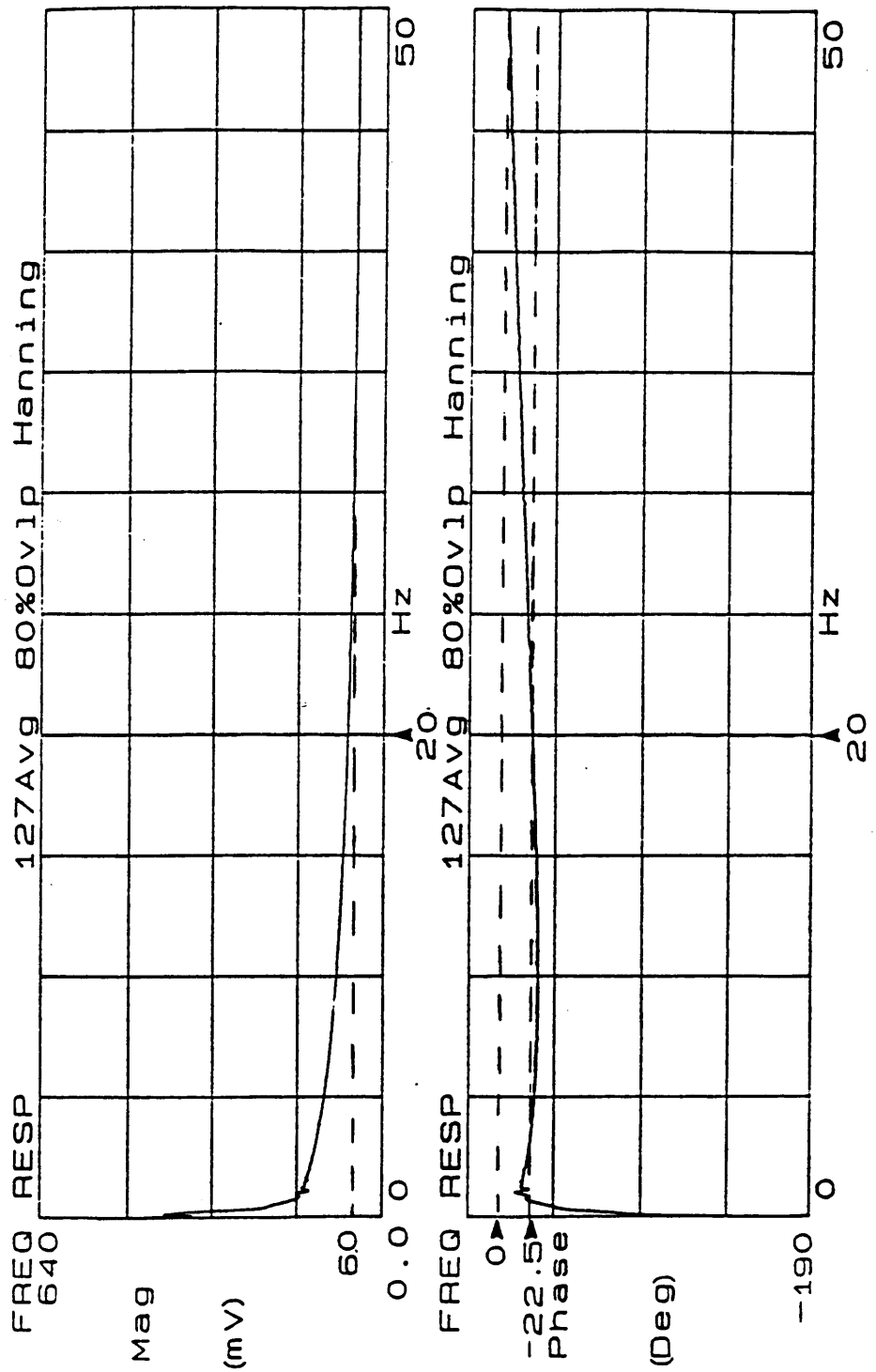

Figure 22. Frequency Response Function for Microsensor

Conclusions and Recommendations

The concept of the thin-film heat flux microsensor has been shown to be viable. By using thin-film techniques, a very small, very thin, high sensitivity, and high frequency response heat flux transducer has been developed. The following conclusions can be drawn from the present work:

1) Thin film techniques can be used to fabricate hundreds of thermocouple pairs in a very small area, 0.1 cm^2

2) Using a large thermopile generates a sizeable signal, 100μV, with a very small ΔT across the gage, 0.043°C, which corresponds to a heat flux of 6100 W/m^2. This combined with the very small thickness, <2.0μm, leads to the fact that there will be both negligible disruption of the thermal boundary condition and the physical contour of a model surface while fluid flows over it.

3) Even with the microsensor's small size, it was found to have a sensitivity of 0.164 mV per watt/cm^2, only 21% less than a

Gardon gage. Therefore the microsensor can even be used in low speed wind tunnels. These are conservative results due to a constant heat transfer coefficient assumption used in the steady-state calibration.

4) The gage thickness can be made very small allowing a very high frequency response, >1kHz. Therefore, the gage can be used to measure unsteady heat transfer fluctuations.

5) Photolithography methods have been shown to produce a gage of very intricate design for intermediate temperature application. High service temperatures should be reached using stainless steel masks.

6) These results have been shown to be better than any other available heat flux transducer. The results show that the heat flux microsensor may indeed fill the void requested by Kidd(1981).

The measurements done were conservative estimations of the heat flux microsensor performance. The following recommendations are made for future work to improve the heat flux microsensor performance:

1) The microsensor should be fabricated on a heat sink with feed-thru lead connections to improve the time response and eliminate surface flow disruption.

2) More accurate steady-state calibrations should be done using the

convection calibration apparatus. A metal substrate should be mounted in a redesigned center plate capable of reaching higher heat flux levels.

3) More accurate frequency response studies should be done using a microsensor fabricated on a heat sink and subjected to radiant flux from a pulse laser whose input is a better representation of instantaneous heat transfer changes. Concentration of performance characteristics should be in the range between 1 kHz on up to 1 MHz.

4) Stainless steel masks should be used to more reliably produce gages and to promote better adhesion allowing for high temperature testing.

5) Time-resolved heat transfer studies should be done to show the nature of heat flux fluctuations due to unsteady flow phenomena.

References

Bales, E., Bomberg, M., and Courville, G. E., Eds., 1985, *Building Applications of Heat Flux Transducers*, ASTM, Vol. 885.

Borell, G.J., and Diller, T. E., 1987, "A Convection Calibration Method for Local Heat Flux Gages," *ASME J. Heat Transfer*, Vol. 109, pp. 83-89.

Campbell, D. S., Gundappa, M., and Diller, T. E., 1989, "Design and Calibration of a Local Heat-Flux Measurement System for Unsteady Flows, accepted for *ASME J. Heat Transfer*, also in *Fundamentals of Forced and Mixed Convection*, Eds. F. A. Kulacki and R. D. Boyd, ASME, 1985 pp. 73- 80.

CRC Handbook of Tables for Applied Engineering, Eds. Bolz,R. E. and Tuve, G. L., second ed., 1973, pp. 249-261.

Diller, T. E. and Onishi, S., "Heat Flux Gage," U.S. Patent # 4779994, October 25, 1988.

Diller, T. E. and Telionis, D. P., 1988,"Time-Resolved Heat Transfer and Skin Friction Measurements in Unsteady Flow," to appear in *Advances in Fluid Mechanics Measurements Lecture Notes in Engineering*, Eds. Gad-el-Hak, M., Springer-Verlag, 1989.

Epstein, A. H., Guenette, G. R., and Yuzhang, C., 1985, "High Frequency Response Heat Flux Gage for Metal Blading," AGARD CP 390.

Epstein, A. H., Guenette, G. R., Norton, R. J. G., and Cao, Y., 1986, "High-Frequency Response Heat-Flux Gage," *Review of Scientific Instruments*, Vol. 57, pp. 639-649.

George, W. K., Rae, W. J., Seymour, P. J., and Sonnenmeier, J. R., 1987, "An Evaluation of Analog and Numerical Techniques for Unsteady Heat Transfer Measurement with Thin Film Gages in Transient Facilities," in *Proc. of the 1987 ASME/JSME Thermal Engineering Joint Conf.*,Eds. P. J. Marto and I. Tanasawa, ASME, NY.

Godefroy, J. C., Francois, D., Gageant, C., Miniere, F., and Portat, M., 1986, "Thin Film and High Temperature Thermal Sensors Deposited by RF Cathodic Sputtering," ONERA TP No. 1986-28.

Hager, N. E., Jr., 1965, "Thin Foil Heat Meter," *Rev. Sci. Instr.*, Vol. 36, pp. 1564-1570.

Hayashi, M., Sakurai, A., and Aso, S., 1986a, "Measurement of Heat Transfer Coefficients in Shock Wave-Turbulent Boundary Layer Interaction Regions with a Multi-Layered Thin FIlm Heat Transfer Gauge," NASA-TM- 77958.

Hayashi, M., Sakurai, A. and Aso, S., 1986b, "A Study of a Multi- Layered Thin Film Heat Transfer GAuge and a New Method of Measuring Heat Transfer Rate with It," Trans. Japan Soc. Aero. Space Sci., Vol. 30, No. 88.

Incropera, F. P., and Dewitt, D. P., 1985, *Fundamentals of Heat and Mass Transfer*, second ed., John Wiley and Sons, New York, pp. 758-759.

Kidd, C. T., "A Durable Intermediate Temperature, Direct Reading Heat Flux TRansducer for Measurements in Continuous Wind Tunnels," 1981, AEDC-TR-81-19, November.

Onishi, S., Eschwei, M., Wang, W. C., 1981, "Colorless, Transparent, c-Oriented Aluminum Nitride Films Grown at Low Temperature by a Modified Sputter Gun," *Applied Physics Lett.*, Vol. 39, No. 8, October, pp. 643-645.

Ortolano, D. J., Hines, F. F., 1983, "A Simplified Approach to Heat Flow Measurement," Proc. of the ISA International Conference and Exhibit Houston, Texas, October.

Ott, L., 1977, *An Introduction to Statistical Methods and Data Analysis*, Duxbury Press, Mass., pp. 105, pp. 659.

Schenck, H., 1979, *Theories of Engineering Experimentation*, Hemisphere Publishing Corp., Washington, pp.229-230.

Appendix A. Heat Flux Microsensor Layer Designs

Thin film fabrication techniques allow very intricate conductor patterns to be made in a small area on a substrate. The restriction on size and intricacy depends on the facilities and fabrication methods available. For the research involving the heat flux microsensor, lithographic techniques were used. These techniques, such as the lift-off method, require image transfers using emulsions and wet processing. Stainless steel masks are a better method because they eliminate possible chemical reaction, dust particles, or other contaminants that could damage the fine patterns. Since stainless steel masks could not be used, the microsensor design was kept simple and made relatively large to try to reduce chances of contaminant particle damage. Using a differential thermopile, to be discussed later, a series connection across multiple layers was achieved. This required the deposition of two metal layers, a thermal insulating layer, and both an electrical insulating layer and a protective barrier layer. The simplified top and side views of the design are on the following page(Figure 7 on page 22). The complete overlay of the microsensor layers is shown on the page after(Figure 8 on page 23). The individual layer designs can be found in appendix A, figures 24 through 30.

The electrical insulating layer is used for conductive substrates to prevent electrical grounding of the microsensor to the substrate. Additionally this layer has to have high thermal conductivity so as not to reduce the frequency response or the accuracy of the gage. The pattern for lead wire surface

connections, is simply a mat on which the microsensor pattern would fit. For feed-thru wire connections the terminal locations are masked out to allow for electrical contact. These are circles a few sizes smaller than the terminal diameter. The film to be used in this case would be a dielectric film, aluminum oxide-Al_2O_3. Aluminum nitride would be preferred, but the developer used in the lithographic process etches away the film. The Al_2O_3 film was chosen because of its good adhesion, and high thermal conductance, 4.184 W/m °K (Bolz, 1973). The thickness of the film was largely dependent on the surface quality of the substrate. A very thin film may not fully electrically insulate the circuit yet a thicker film may increase the thermal insulating characteristics of the layer affecting the measurement accuracy. For a metal substrate that has been hand polished on buffer wheels, the necessary thickness is approximately 1.0 μm. To ensure uniform electrical insulation, the film would be deposited twice, each layer about 0.5 μm thick, with the sample being rotated between depositions.

The second and third layers are the two metalization layers that must form the base layer of thermocouples. The requirement for this design was to create as many thermocouple junctions as possible in a very small area. This minimizes measurement error due to a substantial temperature variation across the surface of the gage, while still producing a relatively large signal. As mentioned earlier, restrictions would depend on laboratory conditions and techniques. Being the first prototype, the pattern was limited to 100 thermocouple junctions across a small strip 1.0 cm in length. The pattern of the layers can take many other forms such as a circle, a horseshoe, or a square. The decision for the strip design was due to the ease with which it could be produced by the MicroCAD software package, and also to make layer alignment simpler. To fit the large amount of junctions and to keep the pattern simple, straight lines were used for the thin-film junction leads, or *fingers*. Achieving a series connection with the upper layers, required that these metalized fingers be offset at an angle. Though only one set of leads need be offset, it was later found that by angling both leads alignment is easier, as is identification of lower layers after fabrication was complete. The first of the finger leads, copper, had to originate from a terminal pad for later lead wire connection. The rest of the copper fingers followed along the length spaced 50 μm apart. The second metalization,

nickel, is connected to each of the copper fingers in a row below. Copper and nickel were chosen to form the thermocouples, over higher service temperature metal combinations, because of their lower cost for sputtering targets and their more consistent sputtering characteristics. Later, during the development of a metal substrate gage, copper was replaced by silver because of base Al_2O_3 interaction. Additionally, the copper-nickel thermocouple produces a reasonable signal and can attain service temperatures around 700 °C.

The thermal insulating layer is the most critical layer of the microsensor. It must be a thin film of high thermal resistance and excellent electrical insulating properties. The thickness of the film is very important in determining the gage sensitivity. A thicker film would give a greater output because it would set up a larger ΔT across the gage. Too thick of a layer risks thermal disruption of the model surface, if the gage surface temperature becomes much greater than the model surface temperature. The thickness of the thermal resistance layer is limited by the step coverage of the metalization layers deposited on top. Because high steps break the electrical continuity of the metal films, the thickness of the thermal insulating layer was kept below 1.0 μm. An effect called shadowing, only achieveable with stainless steel masks, results in smooth transition from the base to the top of the layer allowing for greater film thickness. The film must cover the thermocouple junctions along the centerline. Due to the gage design incorporating the surface thermocouple, though, and to limit the heat flow to 1-D conduction, the film must extend considerably beyond the centerline. To achieve thermopile connection, though, the ends of the lower fingers must be left exposed. To achieve the material properties necessary, a dielectric film of silicon dioxide, or fused silica with a thermal conductivity of 1.38 W/m K (Incropera and DeWitt, 1985), was tried initially. Due to problems encountered resulting from the expansion qualities of the SiO_2 layer, it was replaced by silicon monoxide. Silicon monoxide has an expansion coefficient on the order of the metal films, about 100 times that of silicon dioxide whose thermal expansion coefficient is $0.55x10^{-6}$ /°K (Bolz, 1973). Using silicon monoxide reduced the previously encountered adhesion problems. Although the insulating properties are less than silicon dioxide, the results were more than satisfactory.

The metalization layers, fifth and sixth, are deposited on top of the thermal insulating layer. These layers consist of copper and nickel fingers forming a strip of thermocouple junctions above the lower junctions. This upper layer of fingers was aligned perpendicular to the centerline of the gage so that it could be distinguished from the lower layer and also continue the series connections between layers. These connections are at the portions of the fingers that protrude beyond the thermal insulating layer. Following the last junction, the copper finger attaches to a terminal pad for lead wire connection. This terminal falls on the opposite end of the gage from the lower layer terminal. As mentioned previously, a surface thermocouple was incorporated in the gage design to monitor the gage surface temperature and is deposited along with the upper metalization layers. The thermocouple, which has its junction at the center of the upper surface, originates from two individual terminal pads which fall in line with the gage terminal pads.

The top layer of the gage is a very thin film of aluminum nitride. Not only is this top, or barrier layer, used for electrical insulation, but is also used for overall protection of the delicate microsensor. Aluminum nitride was chosen because it forms a very tough, scratch resistant film of high thermal conductivity. Consequently, it is able to protect against a majority of the test flow particles that may strike it, without hampering thermal performance. For most cases, except for very extreme environments, a very thin film on the order of 0.06 μm is sufficient. The pattern of the the barrier layer is largely dependent on the lead wire connections to be used. For surface connection the design requires four circles a little smaller than the terminals, the same pattern as that used for the base insulating layer when feed-thru leads are used. This allows for silver paint connections of the lead wires to the gage surface. Not only does this layer protect the gage from the test environment, but it also protects against the silver paint running onto the metal circuit shorting out the sensor. For the case of feed-thru lead connections, the entire gage surface is coated including a small region around the perimeter to ensure protection. This is of course the best method because it entirely eliminates any possible flow disruption on the gage surface.

The pages that follow display the individual layer patterns used in the photolithography construction of the heat flux microsensor. Seven layers are shown in order, from the base dielectric layer to the top protective layer. All are displayed at 15X scale.

Steady-State Results-Data Sets 1 and 2

The first data set, set 1, was done without monitoring the microsensor surface temperature. A 1.6 cm free jet was used to try to attain higher heat transfer coefficients than the 4 inch square jet usually used with the calibration apparatus. The tube was aligned so that the stagnation point on the plate occurred in between the two gages. It was assumed that for this data set the two gages would measure the same heat flux. The output of each gage was measured using the HP data acquisition system and was averaged over 50 readings per data point. The heat flux, as measured by the Gardon gage, taken as the boundary condition for the microsensor, ranged from 0-1500 W/m^2. From this information, calculations using the output of the sensor and the heat flux measured by the Gardon gage

$$S = \frac{q_c}{E_m} \tag{11}$$

resulted in an average sensitivity of 0.086 mV per watt/cm^2 with very little standard deviation, $2.116x10^{-3}$, about 2.4%(Table 3 on page 73). This sensitivity was more than twice that predicted. At ambient conditions, a signal of 2.97 μV had been measured which was taken as an offset from the multimeter. The microsensor resistance was measured before and after the calibration and was found to be consistently 6.2 kΩ. This indicates that there was no physical alteration to the gage during the calibration. Upon later analysis of the experimental setup, it was realized that the heat flux to the two gages was indeed not the same. Because the microsensor was fabricated on a 2 mm thick glass substrate mounted on the surface of the plate, the surface temperature was up to 30°C

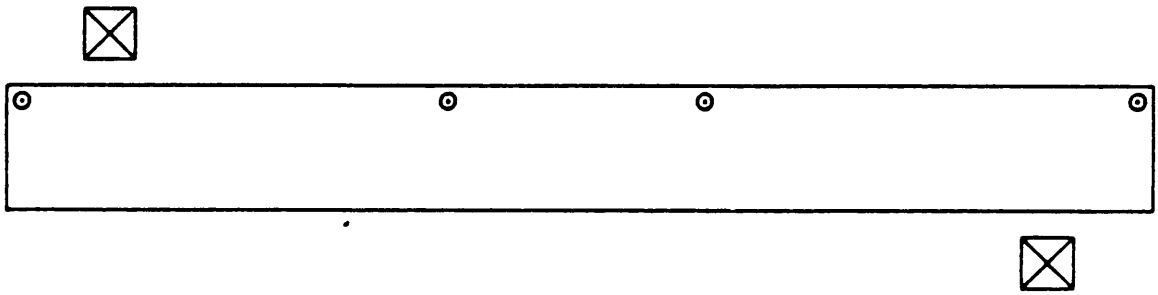

Figure 23. Base Dielectric-Al_2O_3

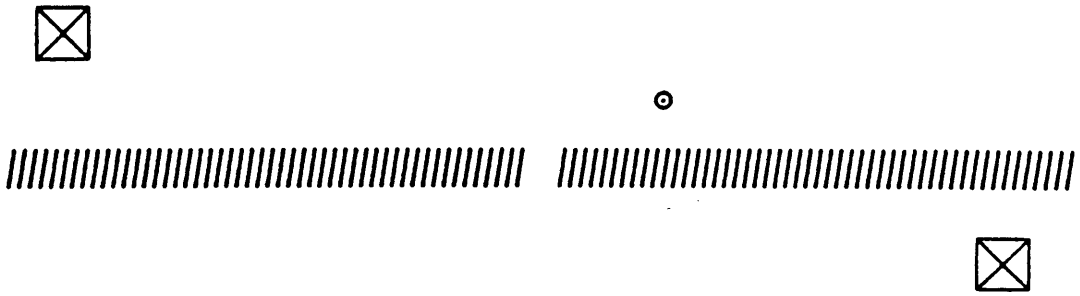

Figure 24. Lower Metalization-Ni

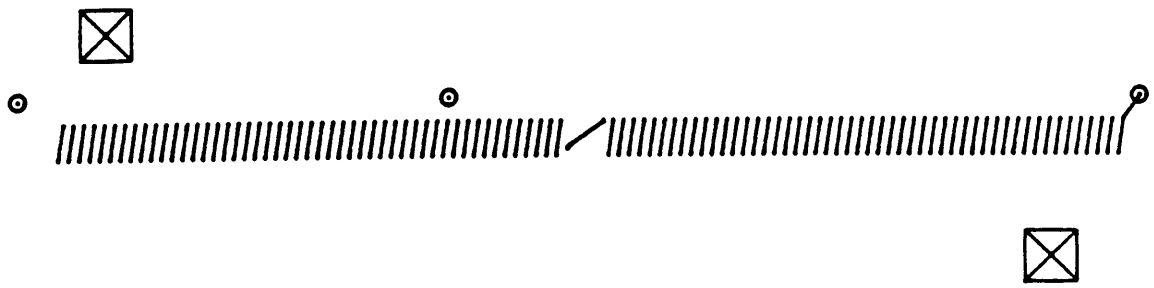

Figure 25. Lower Metalization-Cu

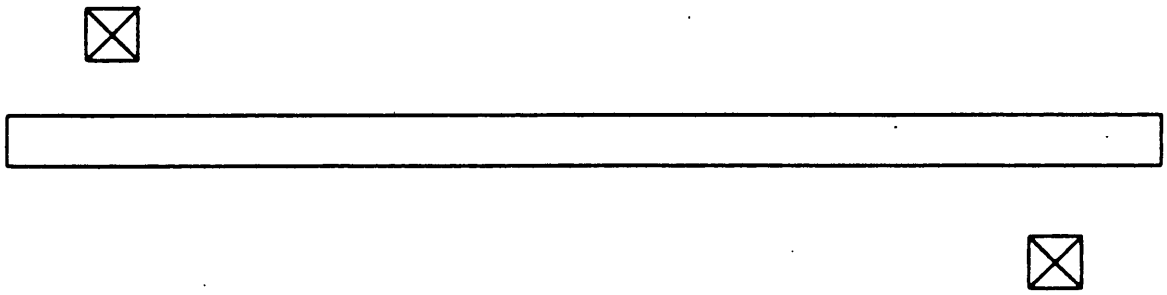

Figure 26. Thermal Resistance-SiO

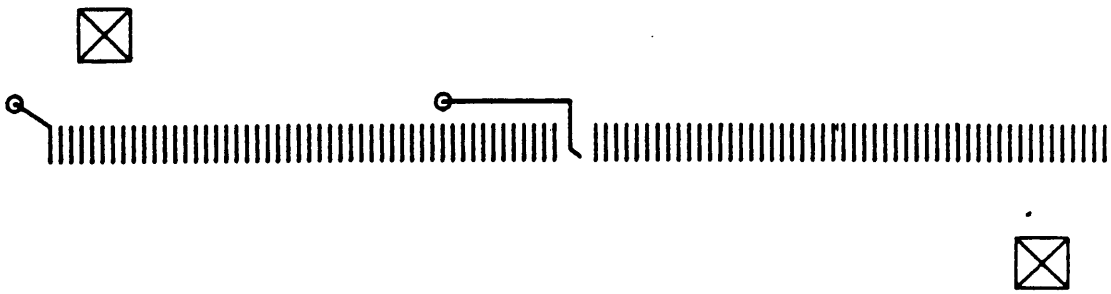

Figure 27. Upper Metalization-Cu

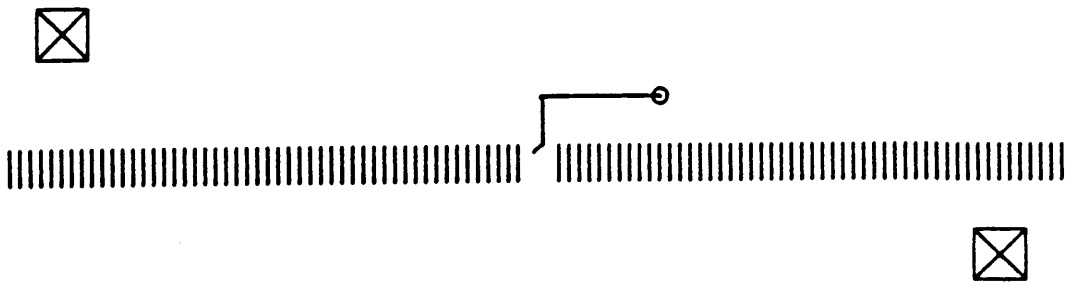

Figure 28. Upper Metalization-Ni

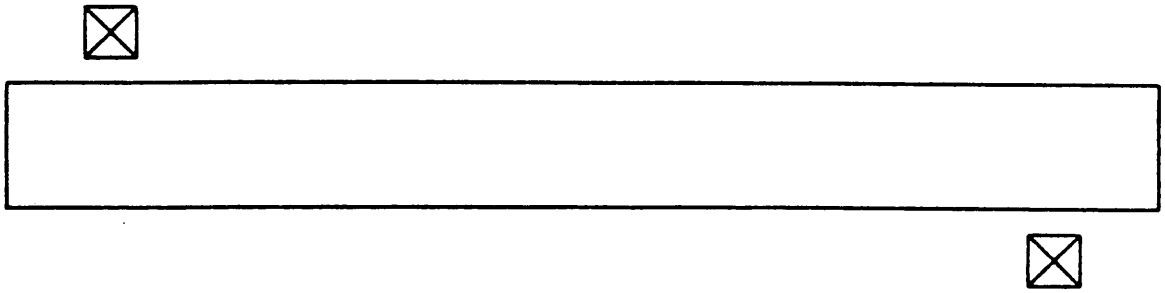

Figure 29. Protective Barrier-AlN

lower than that of the plate. Therefore, the microsensor did not experience the same heat flux as the plate.

The required temperature correction determined by the preceding calibration was taken into account with data set 2. This data set used the same microsensor. The gage resistance was again checked and found to be 6.148 kΩ assuring that no physical damage occurred during any subsequent tests performed. During preliminary frequency tests in this time period, it was found that the microsensor signal contained substantial AC line noise. To reduce the noise, the output signal was connected to a Dynamics differential amplifier reducing the noise level from 473 μV to between 10 and 20 μV. The noise was determined to be due to the ungrounded sensor whose uninsulated high-impedance silver paint connections caused the sensor to behave like an antenna attracting electrical disturbances. The differential amplifier amplifies the two input leads separately and then subtracts out the common noise signals through a differential op-amp. Although it was not necessary for the steady-state tests, the differential amp was incorporated in the second calibration. Now both the Gardon gage and the microsensor were amplified. The Gardon gage was amplified through 2 amplifiers for a gain of 10,054, while the microsensor was multiplied 1000 times for easy conversion of the output signal. Both were measured using the HP data acquisition system. The thin-film thermocouple was included in the calibration to monitor the surface temperature of the microsensor, as described previously. The air jet was aimed on the Gardon gage and it was assumed that the heat transfer coefficient of the Gardon gage would be the same for the microsensor and the thermocouple. Both were attached to the calibration plate surface in the same manner. The calibrated Ni-Cu thermocouple was referenced to 0 °C with an ice bath and its output was measured with a voltmeter. The calibrated sensitivity was found to be 23 μV/ °C. The ambient temperature value was checked and found to be equivalent to that measured by the T-type thermocouples of the calibration plate.

Using the calibrated Gardon gage, with a sensitivity of 0.241 mV per watt/cm^2, a heat flux range of 0-20,000 W/m ^{2} was covered. From the experimental data, the corrected heat transfer coefficient was determined using equations (3) and (4). These values were now used as the boundary condition

for the microsensor measurement. Since the heat transfer coefficient is largely a function of the flow, it was assumed to be constant across the region close to the impingement point of the jet. This is not entirely true since the Gardon gage is at the stagnation point of the flow and thus would have a higher heat transfer coefficient than the microsensor. This can be shown on a plot of the Nusselt number versus gage location in the impingement region(Figure 13 on page 36). This information displays the fact that the results calculated using the constant heat transfer coefficient are conservative estimates. The heat flux incident on the microsensor was calculated using the corrected heat transfer coefficients, which were consistently around 351 W/m^2K and the temperature difference between the surface temperature detected by the thin-film thermocouple and the air jet temperature. This resulted in a considerable correction in heat flux. The maximum ΔT for the microsensor was found to be about 25 °C. The resulting heat flux incident on the sensor was up to 2.5 times less than that detected by the Gardon gage. The measured heat flux range was therefore only 0 - 8588 W/m^2. Comparing the results from using the Gardon heat flux as the boundary condition, uncorrected, to that when the heat transfer coefficient is used as the boundary condition, corrected, can be seen on the plot of data set 2 (Figure 30 on page 74). One can see that the slopes of the curves, sensitivities, are considerably different. The corrected results show a much higher sensitivity, as much as 4 times. This would be expected since the output is the same but the input flux used to generate the output is much less. Since the correction made such a difference, the results of data set 1 were not valid. The results of data set 2 generated an average sensitivity of 0.19 mV per watt/cm^2 with a standard deviation of $9.5x10^{-2}$ (Table 2 on page 72). This standard deviation was very high, so the data was reanalyzed. Noting the first data point sensitivity of 0.416 was 2.5 standard deviations from the mean, it was determined to be offseting the true results. A popular statistical test, Chauvenet's criterion, was used to analyze this data point (Schenck, 1979). The criterion states that

> ".. any reading out of a series of readings shall be rejected if the magnitude of its deviation from the true or mean value is such that the probability of the occurrence of such deviation does not exceed 1/2n."

For this data set of 9 readings, the value can be rejected if it is more than 1.9 standard deviations from the mean. The value in question satisfies this criterion and was thus rejected. The remaining

data in this set (Table 3 on page 73), resulted in a mean value of sensitivity of 0.162 mV per watt/cm^2, almost twice that found with data set 1. Even after rejecting an irregular data point, the standard deviation of the remaining data is still poor, $4.6x10^{-2}$, a variation of about 28% from the mean. This corresponds to a 95 percent confidence interval of $\pm$ 24%. Looking at the plot of set 2, corrected versus uncorrected, shows this scattering of data points(Figure 30 on page 74). After more analysis of the data and the experimental technique, it was determined that the errors could be due to two possible factors. The differential amplifier used was very old and at times had radically altered the signal either due to saturation or overheat. Secondly, after the data was collected it was noticed that the glass substrate with the thin-film thermocouple on it may have separated from the plate surface a little. If this were the case, the temperature correction would not be reliable. Taking into account both of these factors, a third data set, set 3, was taken. Looking at the comparison plot of corrected data set 2 versus corrected data set 3 (Figure 31 on page 75), one can see the improvement with data set 3. The average sensitivity of data set 2 was 0.162 mV per watt/cm^2 while the average sensitivity for data set 3 was 0.164 mV per watt/cm^2.

Overall, the improvement in the confidence and the accuracy of the calibration from data set 1 to data set 3 was very noticeable. The improvement in simply the experimental method can be displayed by the plot of the uncorrected data of all 3 sets(Figure 32 on page 76). The data of set 3 shows to be fairly consistent and falls within the upper and lower limits set by the previous data sets. All of the factors that were able to be controlled to limit the error were taken into account to produce data of reasonable confidence. This is the data set which is presented in the main body of this text.

Table 2. Convection Calibration Results (ALL SETS)

Sens 1 (mV/W/cm^2)	Sens 2 (mV/W/cm^2)	Sens 3 (mV/W/cm^2)	
0.082	0.416	0.287	
0.085	0.254	0.199	
0.085	0.203	0.183	
0.086	0.173	0.179	
0.087	0.135	0.166	
0.088	0.155	0.157	
0.088	0.130	0.151	
	0.127	0.163	
	0.119	0.145	
		0.132	
	$\overline{Sens}$	σ	95% conf.
SET 1	0.086	0.00212	$\pm$0.0020($\pm$ 2%)
SET 2	0.190	0.095	$\pm$0.0730($\pm$38%)
SET 3	0.176	0.044	$\pm$0.0315($\pm$18%)

Heat Flux Microsensor (original data table)

Table 3. Convection Calibration Results (ALL SETS)

Sens 1 (mV/W/cm^2)	Sens 2 (mV/W/cm^2)	Sens 3 (mV/W/cm^2)	
0.082	0.254	0.199	
0.085	0.203	0.183	
0.085	0.173	0.179	
0.086	0.135	0.166	
0.087	0.155	0.157	
0.088	0.130	0.151	
0.088	0.127	0.163	
	0.119	0.145	
		0.132	
	$\overline{Sens}$	σ	95% conf.
SET 1	0.086	0.00212	$\pm$0.0020($\pm$ 2%)
SET 2	0.162	0.046	$\pm$0.0385($\pm$24%)
SET 3	0.164	0.020	$\pm$0.0150($\pm$ 9%)

Heat Flux Microsensor (after discarding 2 data points)

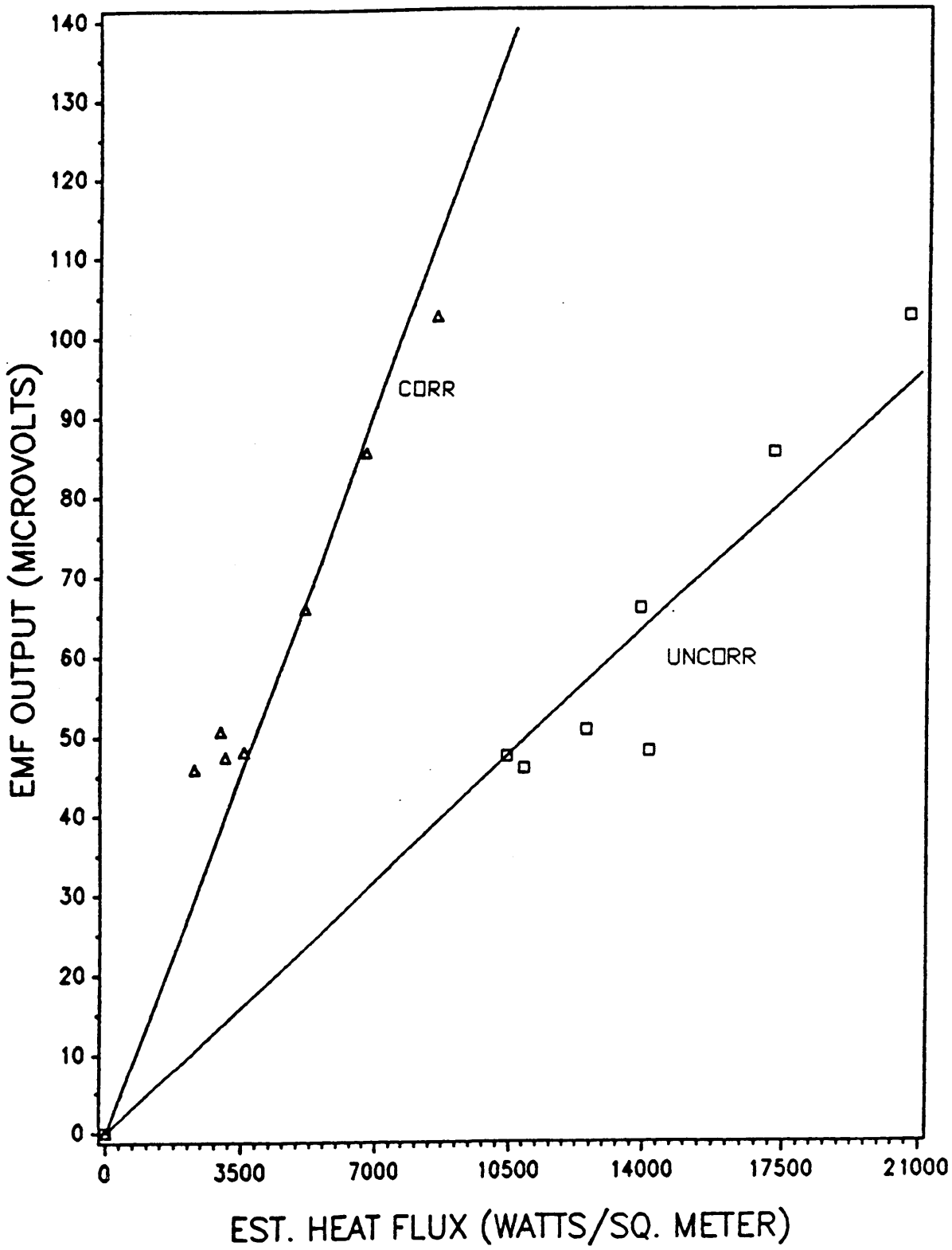

Figure 30. Steady State Plot Set 2 (corr vs. uncorr)

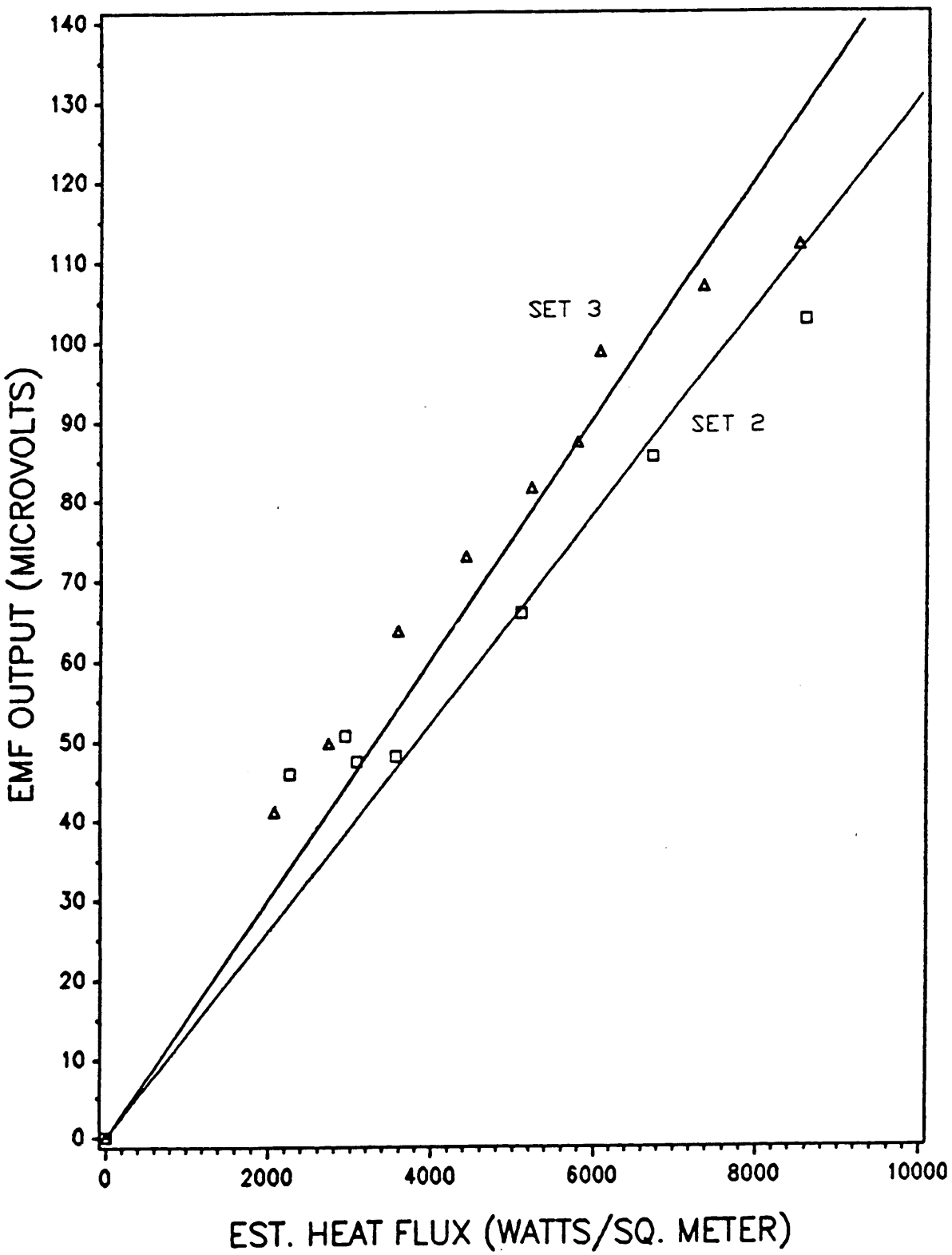

Figure 31. Steady State Plot Set 2 vs. 3 (corr)

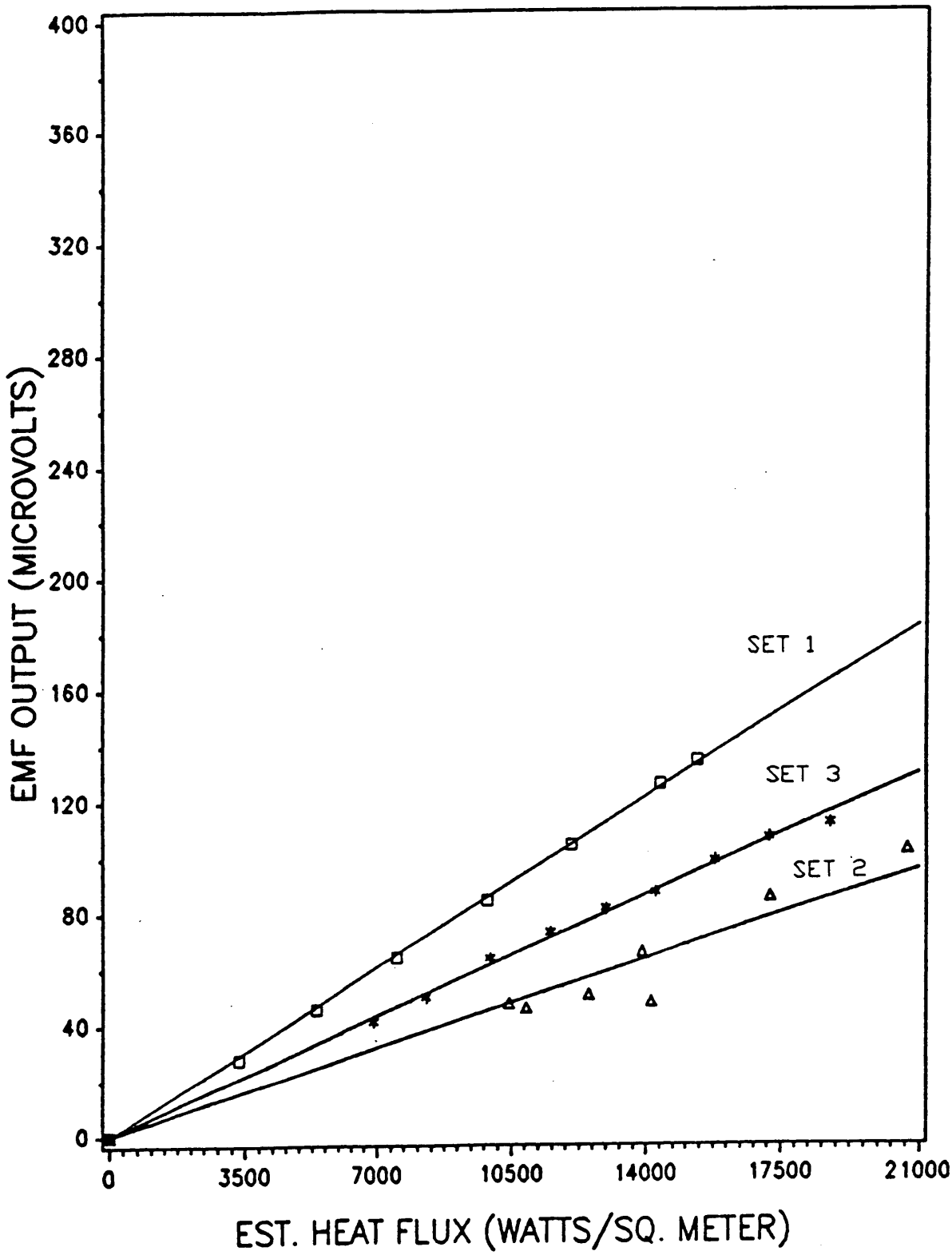

Figure 32. Steady State Plot Sets 1,2,3 (uncorr)

Appendix B. Raw Data for Steady State Calibration

Convection Calibration Data

Gardon Gage vs. Heat Flux Microsensor(10/2/88)

Initial conditions -

Ambient temperature : 22.8 °C

Jet air temperature : 27.5 °C

Ambient conditions Microsensor output : 2.97 μV

NOTES:

AC signal noise - 473 μV without input flux

no change with all instruments on

plate temperature of 94.3 was the maximum attainable

single 1.0″ tube jet was used

gain for Gardon gage 502.72 x 20

Table 4. Convection Calibration Data (SET 1)

T_p (°C)	E_m (μV)	E (μV)	q_c (W/m^2)
22.8	00.00	00.0	0000.0
40.0	27.57	81.0	3342.8
50.0	45.54	129.0	5365.0
60.0	64.03	181.0	7511.0
70.4	84.57	237.7	9863.4
80.0	104.59	290.0	12050.6
90.3	126.16	346.0	14361.7
94.3	134.54	369.0	15352.2

Gardon Gage vs. Heat Flux Microsensor (10/2/89)

Convection Calibration Data

Gardon Gage vs. Heat Flux Microsensor (1/16/89)

Initial conditions -

Ambient temperature : 24.5 °C

Thin film temperature : 32.9 °C

Plate temperature : 37.0 °C

Ambient conditions Microsensor output : 17.0 μV

NOTES:

gage resistance at ambient conditions : 6.148 kΩ

thin-film thermocouple copper-nickel (23 μV/ °C)

gage fabricated on Corning 7059 glass substrate

Microsensor made of copper-nickel junctions

mounted using Thermalcote to the front surface of the plate

gain for Gardon gage 502.72 x 20

Table 5. Convection Calibration Data (SET 2)

T_p (°C)	T_m (°C)	T_∞ (°C)	T_a (°C)	E_m (μV)	E (μV)
24.5	24.5	24.5	24.5	00.00	000.00
49.0	29.7	22.9	27.3	34.49	157.34
53.6	31.9	23.0	27.4	40.00	191.86
58.4	33.9	23.0	27.5	45.82	227.66
63.4	35.9	23.3	27.5	50.66	261.97
67.8	37.7	23.4	27.6	47.99	295.89
58.3	37.1	24.6	28.3	47.33	218.81
67.8	42.9	25.1	28.5	65.87	290.42
76.9	47.4	25.2	28.5	85.42	360.04
86.9	52.8	25.3	28.6	102.60	432.65

Gardon Gage vs. Heat Flux Microsensor (1/16/89)

Table 6. Convection Calibration Calculations(SET 2)

h_i. (W/m^{2}K)	h_c (W/m^{2}K)	ΔT_p (°C)	ΔT_m (°C)	q_c (W/m^2)	q_m (W/m^2)
000.00	000.00	00.0	0.0	0000.0	000.0
300.85	345.59	21.7	2.4	7499.3	829.4
303.84	349.54	26.2	4.5	9157.9	1572.9
305.69	351.99	30.9	6.4	10876.5	2252.7
302.77	348.12	35.9	8.4	12497.5	2924.2
305.39	351.59	40.2	10.1	14133.9	3551.1
302.62	347.93	30.0	8.8	10437.9	3061.8
306.61	353.21	39.3	14.4	13881.2	5086.2
308.63	355.89	48.4	18.9	17225.1	6726.3
307.88	354.89	58.3	24.2	20690.1	8588.3

Gardon Gage vs. Heat Flux Microsensor (1/16/89)

Convection Calibration Data

Gardon Gage vs. Heat Flux Microsensor(1/17/89)

Initial conditions -

Ambient temperature : 22.1 °C

Thin film temperature : 22.1 °C

Plate temperature : 23.7 °C

Ambient conditions Microsensor output : 2.0 μV

NOTES:

gage resistance at ambient conditions : 6.148 kΩ

thin-film thermocouple copper-nickel (23 μV/ °C)

gage fabricated on Corning 7059 glass substrate

Microsensor made of copper-nickel junctions

mounted using Thermalcote to the front surface of the plate

gain for Gardon gage 502.72 x 20

Table 7. Convection Calibration Data (SET 3)

T_p (°C)	T_m (°C)	T_∞ (°C)	T_a (°C)	E_m (μV)	E (μV)
22.1	22.1	22.1	22.1	00.00	000.00
43.9	31.3	24.0	28.2	29.52	109.86
48.4	33.4	22.4	27.0	41.04	146.20
53.2	35.8	22.8	27.2	49.64	175.42
58.0	38.3	23.0	27.3	63.62	210.37
63.0	40.9	22.8	27.2	72.92	243.53
67.7	43.5	22.8	27.2	81.56	274.29
72.1	45.8	23.7	27.8	87.22	301.43
76.7	46.6	23.4	27.9	98.72	334.28
81.4	50.8	24.2	28.0	106.80	364.22
86.4	54.5	24.0	28.1	112.00	397.15

Gardon Gage vs. Heat Flux Microsensor (1/17/89)

Table 8. Convection Calibration Calculations(SET 3)

h_i. (W/m^{2}K)	h_c (W/m^{2}K)	ΔT_p (°C)	ΔT_m (°C)	q_c (W/m^2)	q_m (W/m^2)
000.00	000.00	00.0	0.0	0000.0	0000.0
290.34	331.79	15.7	3.1	5209.1	1028.5
283.46	322.84	21.4	6.4	6908.8	2066.2
277.80	315.52	26.2	8.6	8266.6	2713.5
284.32	323.95	30.7	11.0	9945.3	3563.5
282.24	321.26	35.8	13.7	11501.1	4401.3
280.99	319.64	40.5	16.3	12945.4	5210.1
282.31	321.35	44.3	18.0	14235.8	5784.3
284.19	323.78	48.8	18.7	15800.5	6054.7
282.97	322.20	53.4	22.8	17205.5	7346.2
282.62	321.75	58.3	26.4	18758.0	8494.2

Gardon Gage vs. Heat Flux Microsensor (1/17/89)

Appendix C. Frequency Response Input Signal

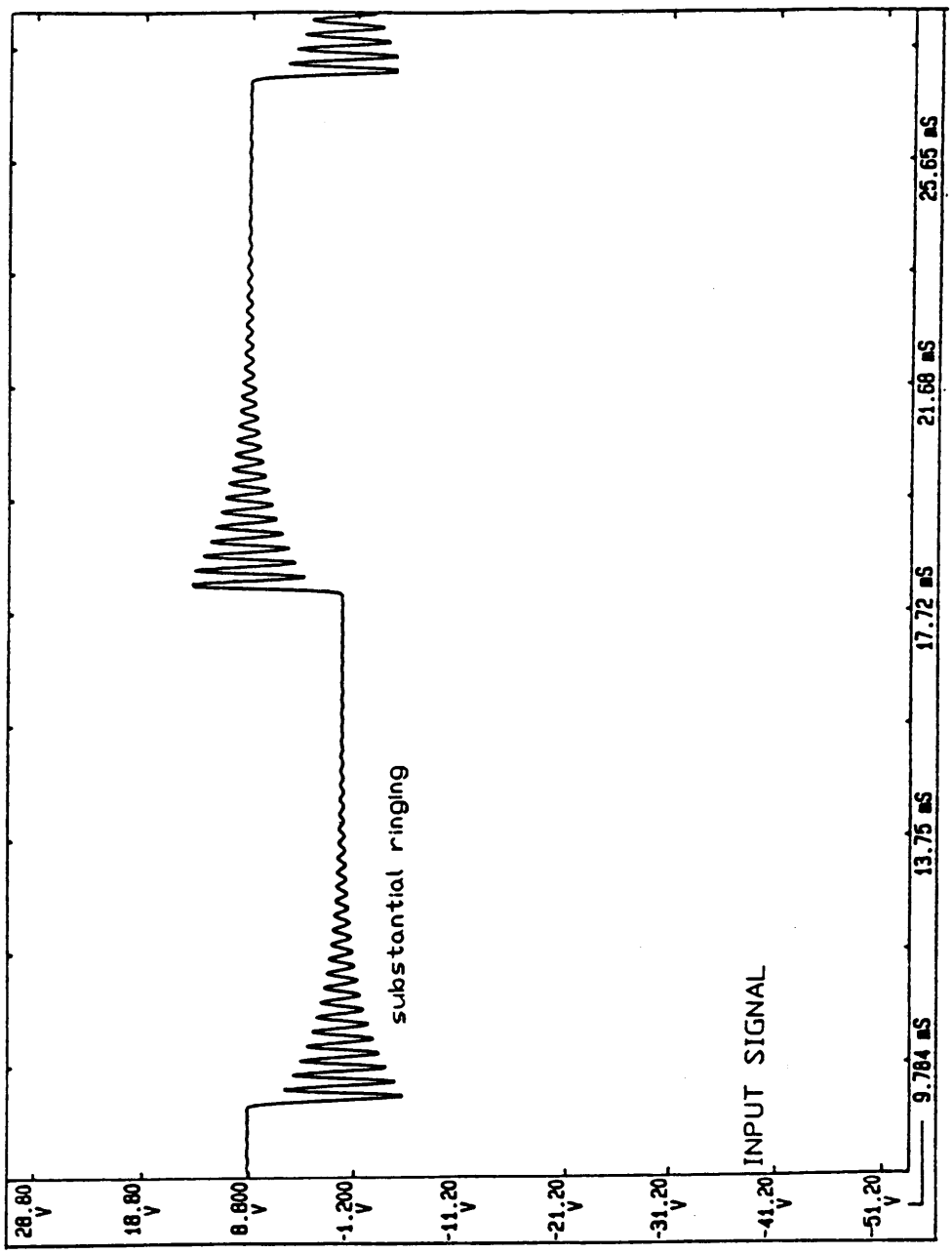

Figure 33. Photo Diode Signal direct

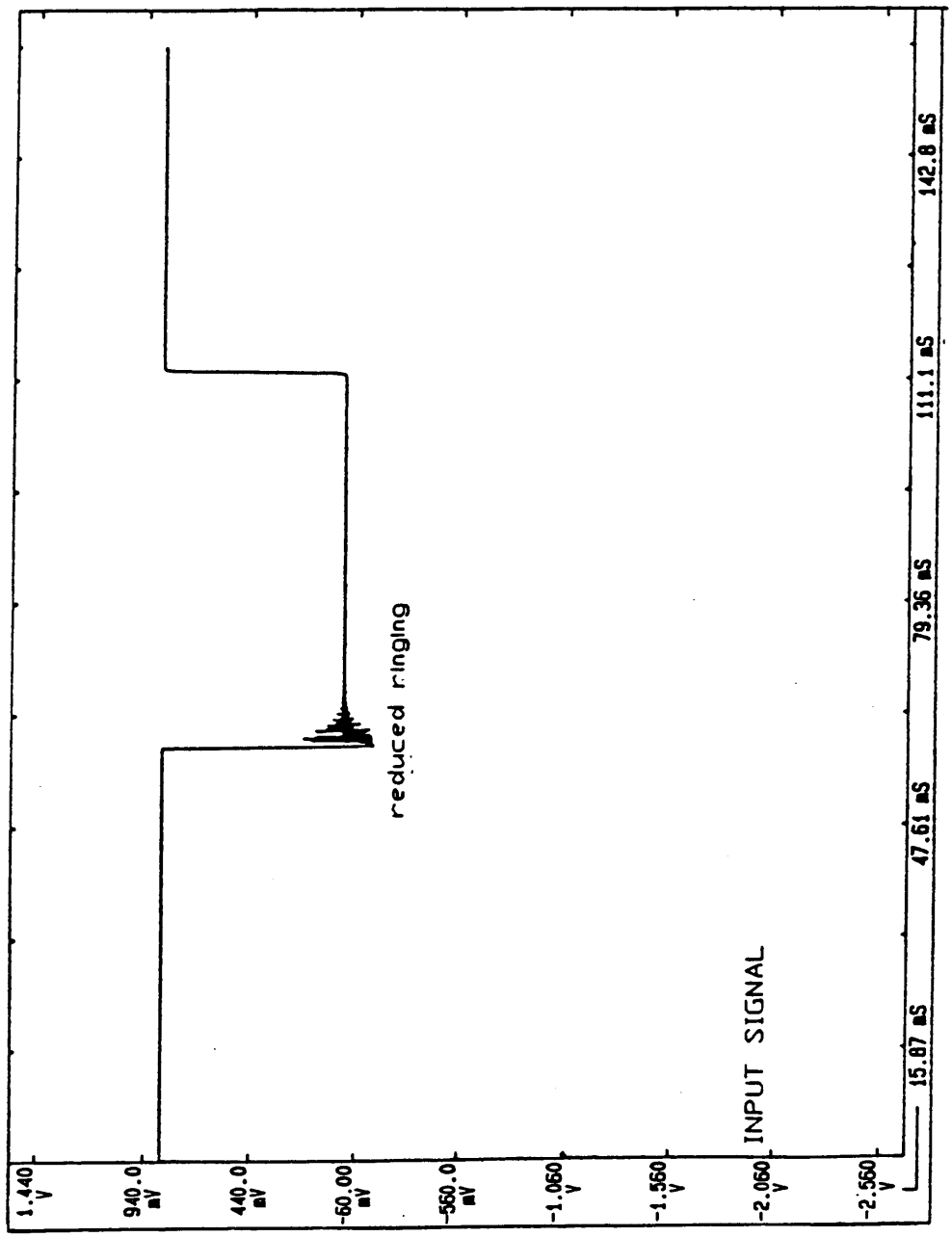

Figure 34. Photo Diode Signal filtered above 2 kHz

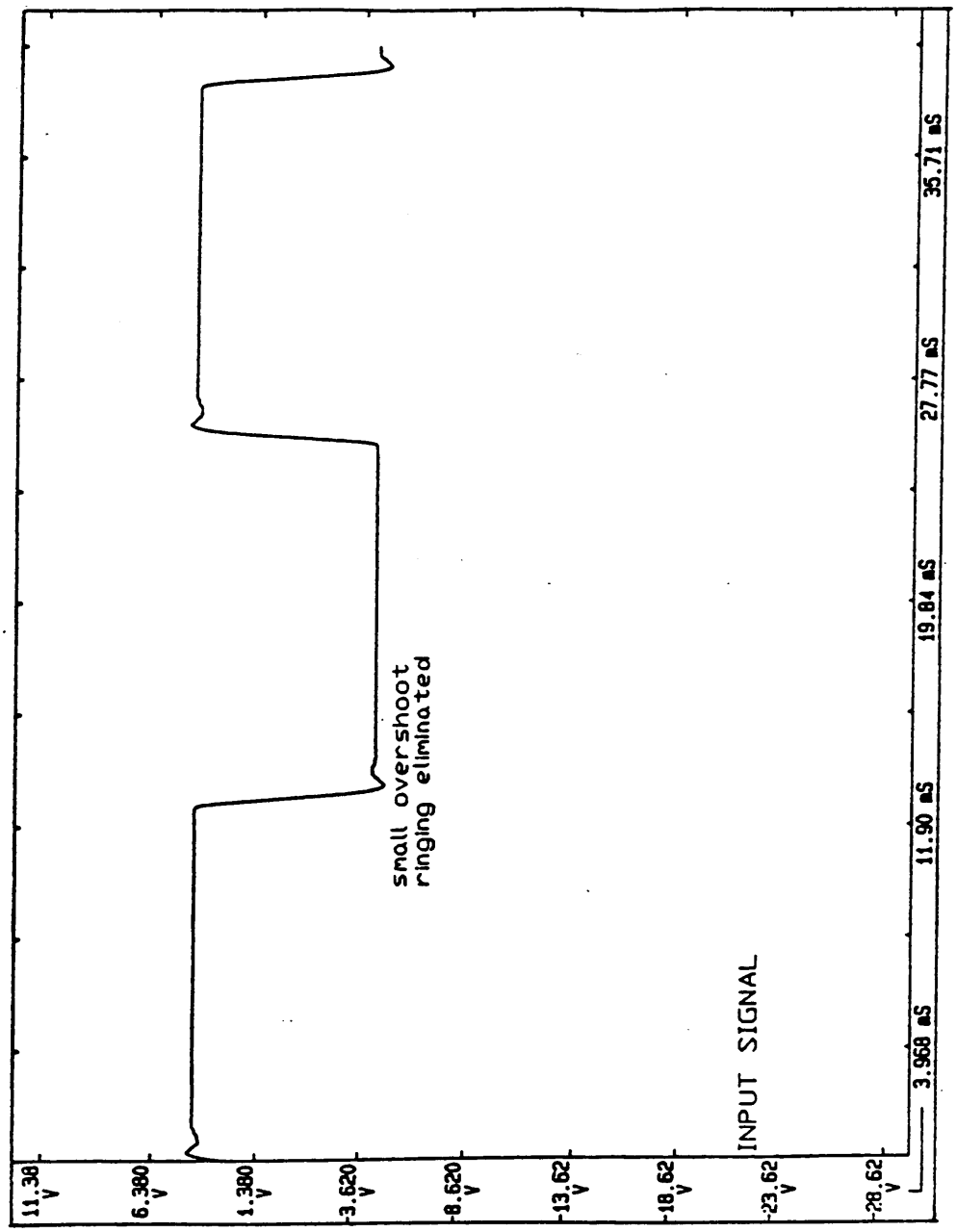

Figure 35. Photo Diode Signal filtered above 1 kHz

Appendix D. Thin Film Construction Technique

D-1 Reduction Process

The process of producing a "working image" from which a microcircuit can be fabricated is a matter of creating a series of positive - negative images of each layer of the microcircuit. These working images are masks or hard copies of each circuit layer which can be successively transferred to a particular substrate by photolithography in conjunction with the sputtering process.

The first "positive" image, which represents the image desired after the sputtering process is complete, is created by a Micro-CAD software package developed for micro computer systems. Each layer is drawn separately with the aid of cursor arrows and various block indexes and the program stores each of the layers separately. The circuit layers can then be viewed as any combination of overlays. After the drawings are completed, they can be compiled by a Hpplot software package and plotted at any magnification on a HP clone plotter. The plots produced are scribed images on rubylith, a red-clear lamination of mylar. The scored portions are then peeled off exposing clear regions representing the circuit pattern. The rubylith is a large scale positive red-clear image which must be reduced to actual circuit size onto the mask.

The large scale image for thin-film circuits is usually on the order of 60X scale. The size is limited by the size of the exposure light board, which backlights the clear images for film exposure, and the lens reduction system. The positive image is attached to the light board with masking tape and a fixed mount box camera is used to produce a 60X reduction negative image of the pattern in a safety lit darkroom facility. Care must be taken to carefully wipe the dust from the light board and mylar images in order to expose a defect-free image. To obtain a one step reduction, a Nikon 28:2.8 lens was adapted to the Microcrasm reduction system(Figure 36 on page 93). The camera must be focused using a frosted piece of glass mounted on a camera backplate which is positioned so that the focused image appears in the same location as the surface of the negative will be. Focusing is best done using the largest lens aperture so the larger image is better observed, but the aperture must then be closed to the lowest setting to obtain the reduction and a crisp negative image. A grooved

camera backplate, attached to a vacuum source, is used to secure a piece of Kodalith portrait quality film for exposure. The negative of each layer is created under timed exposure by the light board. For each different set of circuit images the optimum exposure time varies and must be obtained by a series of trial pictures. This is usually done by starting with one minute exposure time and then continue to reduce this time by half this exposure time for successive photographs. The negative is developed by standard black and white film processing. Note that overexposure will tend to widen lines or enlarge bright images, underexposure will lead to spotty dark regions on the negatives, and a poorly focused image will appear blurred and irregular which must not be confused with overdeveloping. An overdeveloped image, on the other hand, appears runny or bled and usually only occurs if an image is developed one-and-a-half times too long. Once an image appears crisp and uniform in the solution, the developing is complete. This is largely a matter of practice.

The negative film images are now of the actual gage size and must be transferred to an iron-oxide glass mask or working image. An intermediate step must be carried out if a positive working image is needed for positive lithography techniques. This step is a negative-negative contact print which is done using the lens system again. The emulsion side of the negative is mated face to face with the emulsion side of a piece of film and secured against the backplate of the camera using a clear glass cover plate and clamps. This is then exposed to a blank light board for the same time determined in the reduction process. Care must be taken to center the negative on the backplate to prevent transferring an incomplete image.

The production of the working image is the same regardless of film image, a positive mask for the positive lithography process and a negative mask for both the negative lithography process and the etching process. Before processing it is very important to check that all lights are out except for the golden safety lights of the flow hoods. The emulsion side of the developed film is mated to the emulsion side of a 3 inch square Feroxoplate iron-oxide glass mask. Two images can be placed on one mask, depending on their size, yet the corners and sides of the glass mask should be avoided for better results. A clear piece of glass and clamps are used to secure the film which is then exposed to using a UV vertical exposure system, (Figure 37 on page 95). This produces a replicate of the

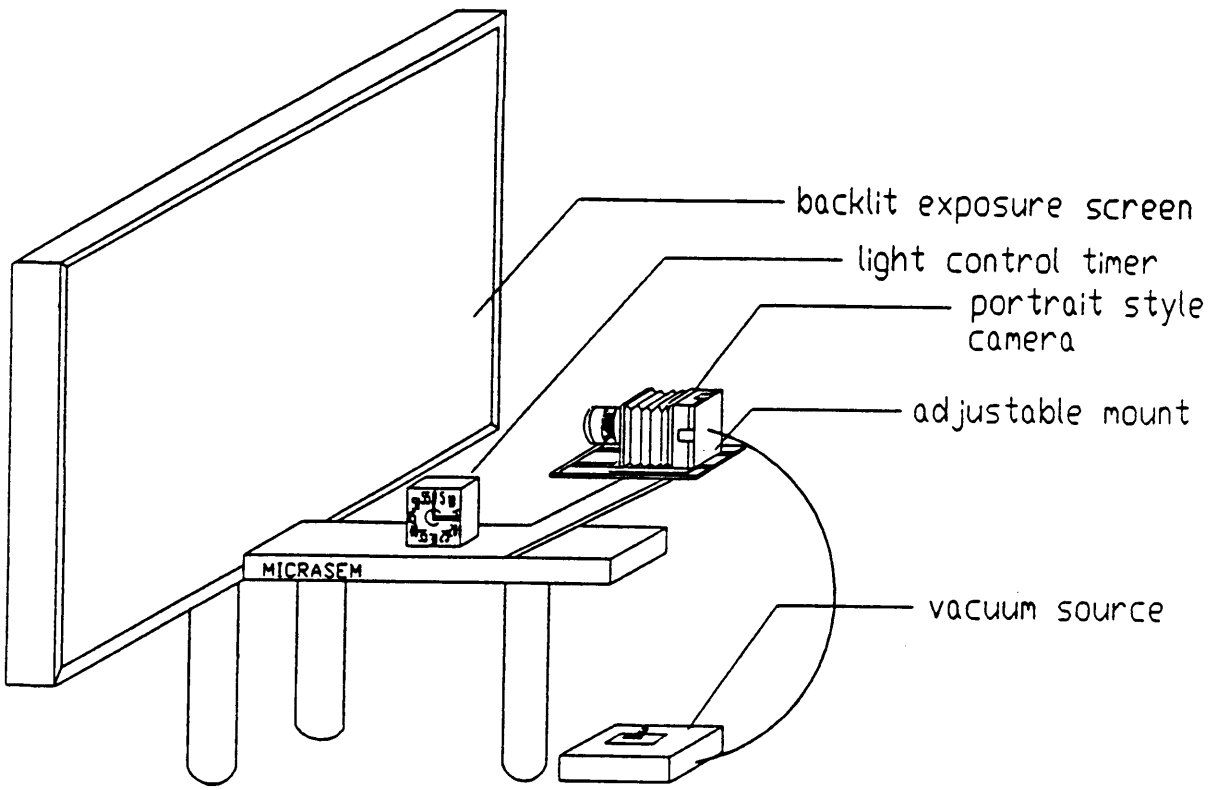

Figure 36. Photoreduction Apparatus

film image on a durable rigid surface for future multiple image transfers. Note that one should never expose their eyes or skin to direct UV light because it is very harmful. The UV exposure system must be allowed to reach full power before exposure is to be done, and the timer should be set to the correct exposure time. Typically the best results were found using 9 seconds exposure, but just as with the film processing this can be varied to find the optimum times for the particular circuit set. The variation in times are very dependent on the lab environment. The exposed iron-oxide mask is developed in a shallow dish of Shipley 353 developer by slowly agitating the glass until the image appears and no more emulsion seems to be dissolving off, around 1 ½ minutes. Immediately the mask must be rinsed thoroughly with deionized water to remove all the developer, and then blown dry with nitrogen or a dry air gun. The best results are achieved by initially rinsing with a stream of tap water followed by a final rinse with deionized water. Now the exposed regions of the mask can be etched off to form the working image by placing the mask in a beaker of $FeCl_2 \bullet 6H_2O$ etchant. The etching process takes about one to two minutes but may vary due to strength of the solution and temperature. To determine if the process is complete the mask should be removed and rinsed to see if the exposed portions appear perfectly clear without any emulsion spots. When the results are determined sufficient, the glass must be rinsed thoroughly with deionized water, followed by substantial cleaning and rinsing with acetone and a cardboard shaft cotton swab. The glass mask can now be inspected for quality and stored until the lift-off process is to be performed. This is repeated for each pair of layers to form the working images that can be used to construct the desired circuit, in this case the 7 layer heat flux microsensor.

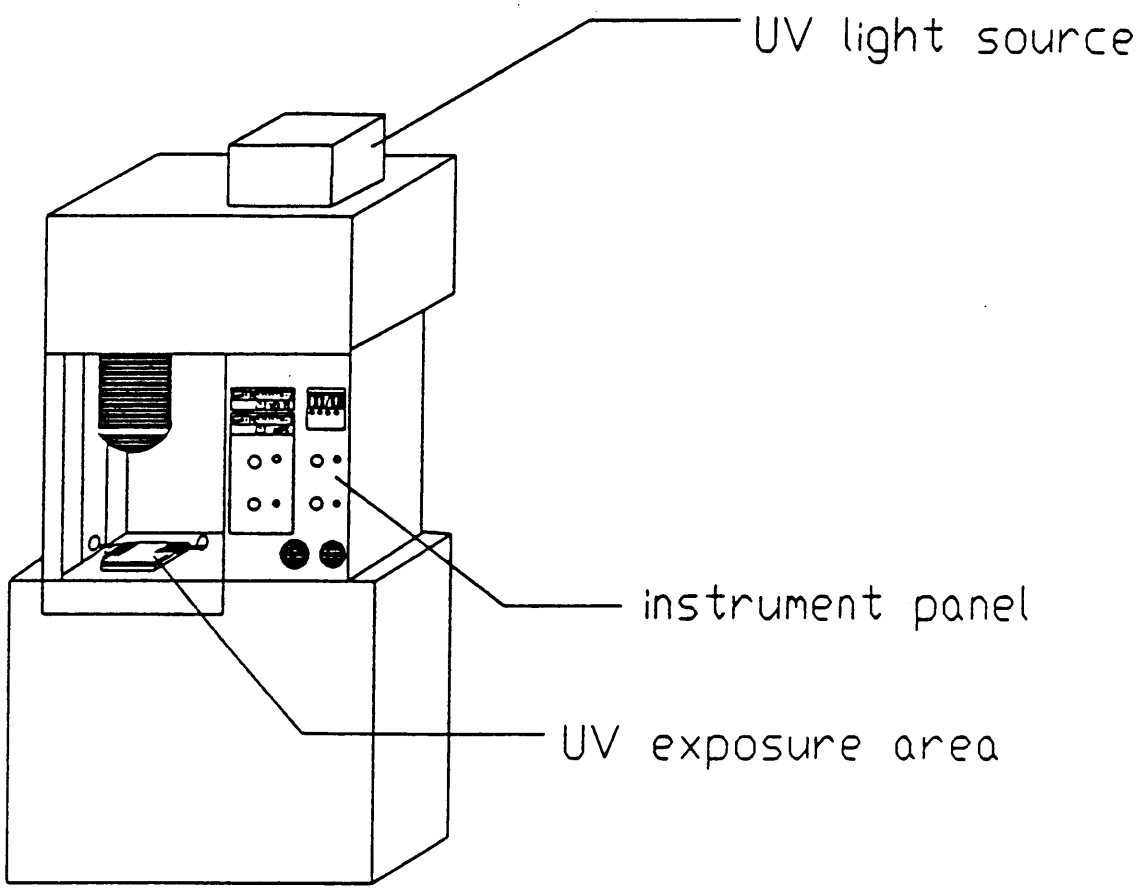

Figure 37. UV Exposure System

D-2 Lift-off Process

The lift-off process is one of the lithographic techniques for fabricating a multilayer circuit. The process is used in conjunction with the sputtering process and can be looked on as a pre-sputtering method, where the image is developed on the substrate before deposition. The substrate is the sample whose surface the circuit is to be fabricated, before deposition. Basically, the desired material is sputtered over the whole substrate and the undesireable material regions are lifted off using a lift-off agent afterwards(Figure 38 on page 97).

Of foremost importance throughout the lift-off process, is to make sure the substrate is as clean and dust-free as possible. With thin-film integrated circuits techniques dimensions are on the order of 2 to 5 μm and therefore any dust particles can easily damage a circuit layer. Due to poor laboratory conditions it was found best to cover the samples at all times with a clean beaker, and only handle samples with tongs or clips. Initially the substrates, either metal or glass, are prepared to be clean and smooth as possible. If the substrate is metal, it should be polished extremely smooth using down to 0.5 micron polishing suspension. To retain a flat surface it is best to use diamond paste and polish on a hard flat polishing surface. Regardless of the sample, it must be cleaned carefully using a very mild abrasive powder, followed by a strong soap solution in an ultrasonic bath. One must be careful not to let the sample touch the sides or it will be scratched and damaged. The sample should then be thoroughly rinsed in deionized water and dried using nitrogen or a dry air gun. The dried substrate is placed on a hot plate set to 85 to 90 °C to warm. Warming the substrate promotes better molecular adhesion between the photoresist, an organic emulsion used to transfer the working image, and the substrate. While the substrate is preheating, the UV exposure system should be turned on and allowed to reach a steady state power level. At this point the desired exposure time should be set. This again varies in order to obtain a sharp image for a particular circuit layer set, but best results were found to be 9-10 seconds. Care must be taken to never let ones' eyes or skin be exposed to UV light for it will be very hazardous. After warming for a few minutes, the substrate is placed onto a spinner which holds the sample in place by creating a vac-

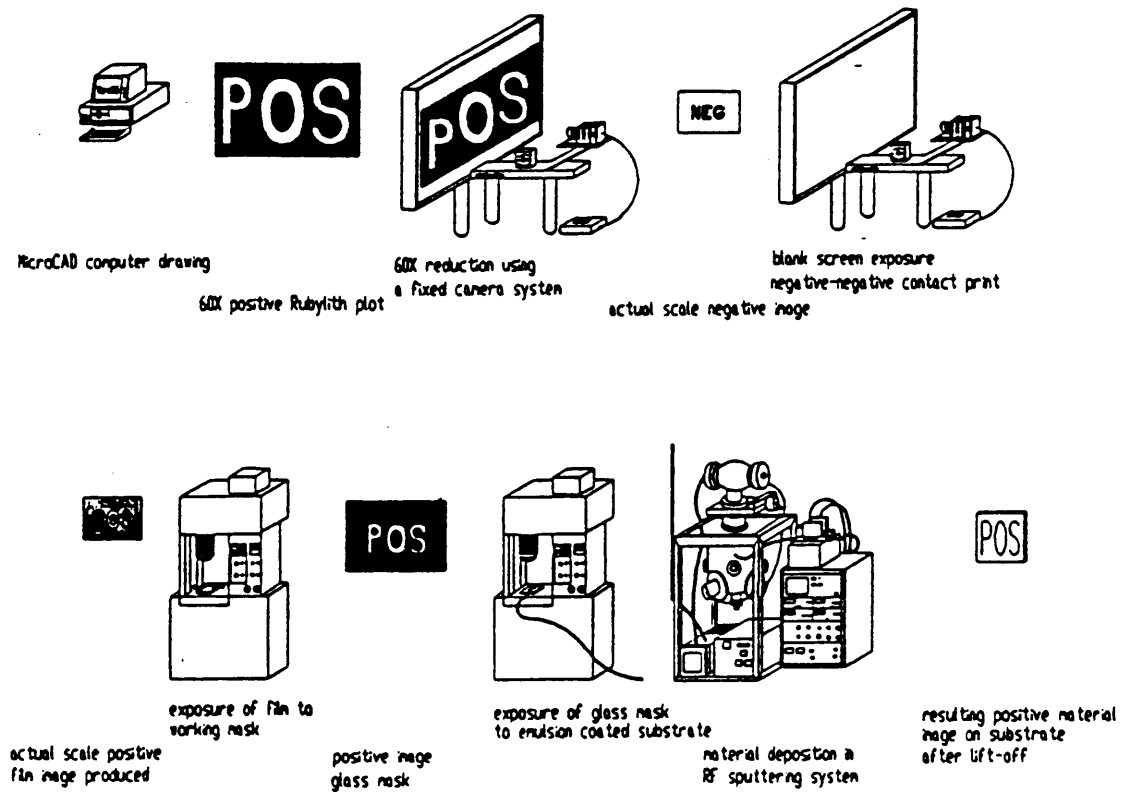

Figure 38. Thin Film Image Transfer Process

uum through a hole in the spinner head. The spinner will not spin unless a perfect seal, or vacuum interlock, is obtained, so the glass beaker can safely be used to cover the substrate while spinning. At this time the settings for the speed and time of spinning should be checked. The time need not be more than 35 seconds, but the speed can be varied to adjust the thickness of the photoresist layer. Too thick or too thin a layer can lead to problems, a good setting for 1 inch square glass samples was found to be about 3000 rpms. The thickness of the photoresist layer largely depends on how thick a deposited layer is needed, thicker layers need thicker layers of photoresist. Turning on the spinner requires pressing the first foot activated button on the floor which will buzz when depressed (the other button is an emergency stop). A small disposable pipet is filled with photoresist. While the spinner is spinning, the pipet is held over the center of the glass, close to the surface, and several quick drops are discharged. Keep the substrate covered with a beaker as much as possible, even while it is spinning. When the spinner stops, the substrate should be transferred to the hot plate, covered and allowed to soft bake at 85 to 90 °C for about 10 minutes.

The next part of the process is to transfer the working image to the substrate. Depending on which type of photoresist is used, will depend on which mask to use. A positive image mask is used with a positive photoresist and a negative image mask is used with negative photoresist. For the processing described above, positive photoresist was used because it is much easier to work with. Before transferring the image the glass mask should be cleaned thoroughly with deionized water and inspected under a microscope to be sure there are no imperfections. The substrate is removed from the hot plate when the soft baking is complete and is briefly inspected for dirt or nonuniformities in the photoresist layer. If a defect is found, the sample should be cleaned with acetone and the above process should be repeated. The reason why this inspection is not done before baking, is that the photoresist is very sticky and seems to attract any dust in the air. If all is well the substrate should either be placed in a vacuum chuck or in a mask aligning unit. The vacuum chuck is a simple tool which holds the substrate, and with the aid of a pump draws suction, mating the mask directly to the face of the substrate. The mask aligner, on the other hand, mechanically holds the substrate and mask in just near intimate contact until alignment is complete and then the mask and

substrate are mechanically mated. Though the mask aligner is better, it is not always available. The vacuum chuck is a little more difficult to use, especially when aligning successive layers, and can be damaging to both substrate and mask because of possible movement during direct contact. Since it is a simple design, though, the vacuum chuck is easily made. If it is the first layer to be deposited, the alignment is simply a matter of placing the image near the center of the substrate. This should be done under a yellow safety lit microscope in order to avoid any exposure effects. If the layer is to be deposited on an existing layer, it must be aligned more carefully under a safety lit microscope with the aid of alignment marks beside the images, and checking junction points between the circuit layers. This can be very painstaking using the vacuum chuck. When the mask is in position, the mated pair can be exposed under the UV light source. The substrate is removed and developed using Shipley 353 developer in a shallow dish agitated until the emulsion stops dissolving off, or about 1 ½ minutes. This time is of course variable depending on the image, the photoresist thickness, and the laboratory environment. The substrate must be thoroughly rinsed with deionized water and dried with either nitrogen or a dry air gun. Now the sample is inspected for quality before continuing with the sputtering process, which is described in the next section.

After the sputtering process is complete, the sample is allowed to come to room temperature. The sample is then carefully placed in a small dish of acetone, the lift-off agent used, and allowed to soak for a few minutes. After this time the excess metal, that was deposited on the photoresist, should seem partially lifted from the substrate. The sample is sprayed with a stream of acetone across the image to lift-off the unnecessary metal. If necessary, the image can be lightly brushed with a cardboard shaft cotton swab wetted with acetone, but if the photoresist-metalization is correct, the acetone spray should do the job. Note that one should always brush in the direction of the lines of the circuit. The circuit layer should be the only metal remaining in the image region and can now be inspected for quality. Some spots may remain which represent dust particles that blocked the photoresist. If the image is good quality and complete, the process can be repeated for the remaining layers. From this point on there should be no need to clean the sample with soap, acetone should be sufficient as long as the sample is handled with tongs or clips.

D-3 Etching Process

The etching process is a different type of lithographic technique used in fabricating a multilayer circuit. This method is used in conjunction with the sputtering process but is looked on as a post-sputtering method, in which the image is laid down on the substrate after the material film is deposited. In this manner the entire substrate is sputtered with a film and the undesired areas are etched off with an etching solution. The advantage of this process is that the material film can be deposited at a much higher temperature since there is no photoresist used during sputtering. Deposition temperatures near 400 °C will markedly increase the adhesion between film and substrate.

The most important precaution to keep in mind throughout any microcircuit processing, is to make sure the substrate is as clean and dust-free as possible. With the etching process the sample must also be as smooth as possible. If the substrate is metal, it must be polished down to at least 0.5 micron polishing solution. This is again best done on a hard, flat polishing surface using diamond paste. Regardless of the material, the cleaning process is the same. The sample is thoroughly cleaned with a mild abrasive and then immersed in an ultrasonic bath of a strong detergent solution. Care must be taken that the sample does not fall out of the holder or touch the sides of the container because the sample will be scratched. After about 10 minutes the sample can be removed and placed in an ultrasonic rinse of deionized water, followed by a thorough rinsing using a deionized water spray gun. Carefully blow dry the substrate using nitrogen or a dry air gun, and inspect for cleanliness. The substrate should be heated for a few minutes to bake off any moisture. The sample is then ready for the sputtering process which is described in the next appendix.

Following the sputtering process, the substrate will be completely covered by a continuous film of the deposited material. There should be no noticeable surface defects such as pinholes due to electron bombardment of the substrate. If the surface is satisfactory, it can be set on the spinner with a few drops of acetone on the surface and spun dry to rinse off any excess particles acquired during removal from the chamber. At this time be careful to keep the substrate covered as much

as possible to eliminate dust accumulations. The substrate is then placed on a hot plate set at 85 to 90 °C for preheating. The preheat tends to increase molecular adhesion between the material film and the photoresist to be used next, and it removes any excess moisture. The substrate is carefully moved to the spinner which is set to a speed of 3000 rpm and a time less than 35 seconds. The speed and time can both be adjusted to meet the needs for the particular circuit. The speed is used to adjust the thickness of the photoresist layer needed, which is a matter of trial and error. The time, on the other hand, is more of a matter of preference, 20 seconds being the minimum. A disposable pipet is filled with photoresist solution and held over the center of the substrate, very close to the surface. The foot activated button is depressed and as the sample spins, a few drops are rapidly discharged onto the surface. When the spinner stops, the sample is transferred to the hot plate and covered to soft bake for about 10 minutes.

The next step in the process is to transfer the working image to the substrate. This step depends on which type of photoresist emulsion has been used. If the resist is a positive, then a negative circuit layer image must be transferred; if negative resist is used, then a positive image is transferred. Same as with the lift-off process, the iron oxide mask should be cleaned with deionized water before exposure. At this time the UV exposure system can be turned on to allow to reach a steady state power level and the exposure time can be set. This should be that time determined from trial and error since different exposure times are necessary for different images, unlike the lift-off process. Eight seconds exposure has seemed to be sufficient for this application. The substrate is placed in either a vacuum chuck or a mask aligner, preferably a mask aligner because it is much easier to use and is more accurate. If the image is of the first layer, it should be placed as close to the center as possible, avoiding any noticeable imperfections. For the layers to follow, care must be taken to mask out the previous layer also, especially if the latter etchant for the material is the same as the former, which happens to be the case with the copper-nickel combination. After exposure, the image is developed in a shallow dish of Shipley 353 developer for approximatly 1 minute while agitating the dish. This time, as in all developing processes, is adjusted by a few trials to obtain

optimum results. The substrate is rinsed thoroughly with tap water followed by deionized water and blown dry using nitrogen or a dry air gun.

The etchants for the materials used must be determined and prepared. Etchants for most materials can be found in materials or chemistry handbooks, and are different combinations of acid solutions. After the etchant is determined it should be prepared to a concentration which takes about 5 to 10 minutes to etch the material completely. In this way, the etching process can be easily monitored so as to prevent over or under etching. This dilution should be done with deionized water. In some cases, as with copper and nickel, the same etchant $FeCl_2 \bullet yH_2O$ is used for both materials, but the concentrations may be different. When the sample is placed in the etching solution, the etchant will chemically remove the excess metal which was exposed by the UV source and thus not protected by photoresist. The sample must be carefully monitored, though, because the etchant will slowly etch even the protected metal, known as side etching. Noting this, it may be a good idea to overexpose the transferred images to increase the circuit line width protecting them from etching damage. The best method is to observe a large unprotected region, looking for the moment when there is essentially no material residue left. When determined complete, the sample is removed and thoroughly rinsed with deionized water.

The process is repeated for the successive layers. This is where the problems occur when using two materials which use the same etchant. If the etchants are different, the substrate would again be placed in the sputtering chamber and the next material would be deposited over the entire surface. After the respective image is laid down and the sample is etched, the lower layer will be exposed again, at least in the regions where the two layer images don't overlap. For the case of similar etchants there would be nothing to protect the lower layer. In order to do this, the lower layer must be protected before the sputtering process. Of course this could be done using photoresist but this would omit the one major advantage of the etching process, deposition at high temperature. The better way is to protect the lower image with a piece of stainless steel covering those regions which would be affected. This is easy if the patterns are simple as with the gage and the single

thermocouple, but if the patterns are heavily intertwined the sheet metal essentially become a stainless steel mask.

Stainless steel masks are similar to the positive image iron oxide glass mask, except that the clear regions are etched holes in the thin stainless steel. Therefore, the best of all methods is achieved by using these masks for all layers. The pattern itself can be deposited at high temperature, eliminating both pre and post sputtering processes. The difficulties in this process are largely dependent on equipment availability. Making a stainless steel mask is possible in existing facilities if the patterns are simple and line clarity is not a problem, but for fine images it is best to send out to a company better equipped for the process. Stainless steel also help to reduce aligning problems. If the masks are manufactured by a computer they can be prealigned with peg holes. Using this method enables the stainless steel masks to be simply placed on pegs surrounding the substrate, aligned slightly, secured and then placed in the sputtering chamber for deposition. There would be great difficulty in major aligning the masks by hand because there are not enough translucent regions to judge location. This is not a problem if they are made accurately enough. One of the additional problems is involved with making sure the mask and the substrate mate cleanly, preventing excess shadowing. The method for holding down the mask is largely dependent on the patterns used. Having the edges of the pattern slightly lifted will tend to increase shadowing. Shadowing, having the material film slowly reduce in thickness underneath the mask, is essential, especially if the film layers are to be thick. Too much shadowing, though, could tend to run nearby images together. Shadowing causes the image outlines to act as ramps for the overlapping layers instead of the sharp shelf-like corners produced in the lift-off method. The overlapping layers then tend to have less surface stress and achieve better adhesion. Too thick of a layer using the lift-off process leads to a circuit line discontinuity. Of course this sounds like the best solution, but the big disadvantage of manufactured stainless steel masks is the cost. The initial cost, hundreds of dollars, is just for the machinery set-up fee for each individual layer. For circuit production purposes, this investment is a must.

D-4 Sputtering Process

The sputtering process is the method by which the circuit photo image becomes a working material layer. This process is done by using a high vacuum sputtering apparatus in which material is deposited onto the desired substrate by a magnetron sputtering S-Gun under high vacuum conditions. To briefly describe this process, the vacuum environment is usually some sort of semi-spherical stainless steel chamber which uses a rotary vane type roughing pump to draw the low vacuum and a turbo molecular pump mounted on top to reach the high vacuum status (Figure 39 on page 105). This chamber in which the substrate is mounted is purged with a constant flow of purified argon which acts as the ionizing gas to forming a plasma which is essential to the sputtering process. The plasma is a mixture of argon ions and electrons. This plasma is created by rf discharge on a target of the desired deposition material mounted in a sputtering gun unit mounted in one of the chamber ports whose cathode center is powered to about 200 watts (with negative potential). The target, consisting of two concentric rings; main and secondary targets, has the smaller ring charged at this power level and the larger grounded, as is the rest of the chamber. This results in a cathode-anode discharge creating the high density plasma of electrons on the surface of the target held there by a permanent magnet encased in the gun unit(Figure 40 on page 106). When these electrons bombard the argon molecules, they become ionized. Due to the positive ionization, the ion accelerates toward the highly negatively charged target and bombards the surface with a sufficient velocity to release, or sputter, target material molecules in the direction of the substrate where they will deposit as a film. Though the process is more involved than this, the physics would be beyond the scope of this document.

The procedure for the sputtering process must be followed carefully because mistakes may cause severe equipment damage. After the substrate has been prepared either for the lift-off, etching or stainless steel mask process, it has to be mounted on the substrate holder. The substrate holder design varies with each particular chamber but the general structure is the same. The dimensions of the holder are restricted by the diameter of the port in which the holder will be secured and the

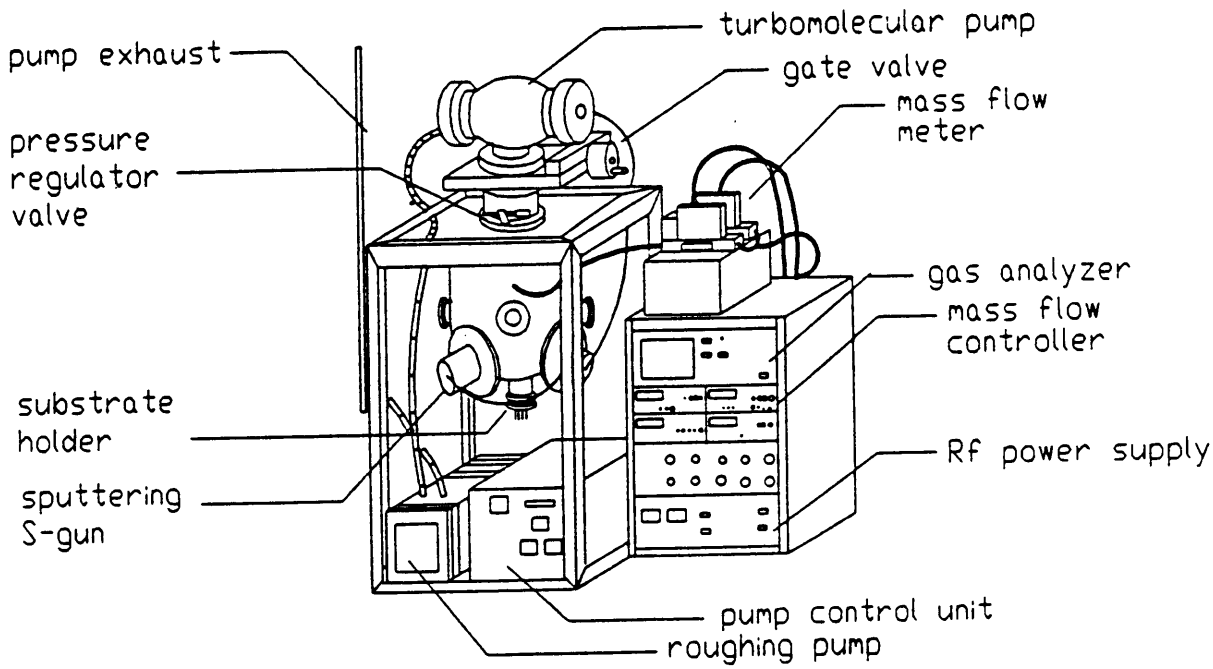

Figure 39. High Vacuum Sputtering Apparatus (Onishi)

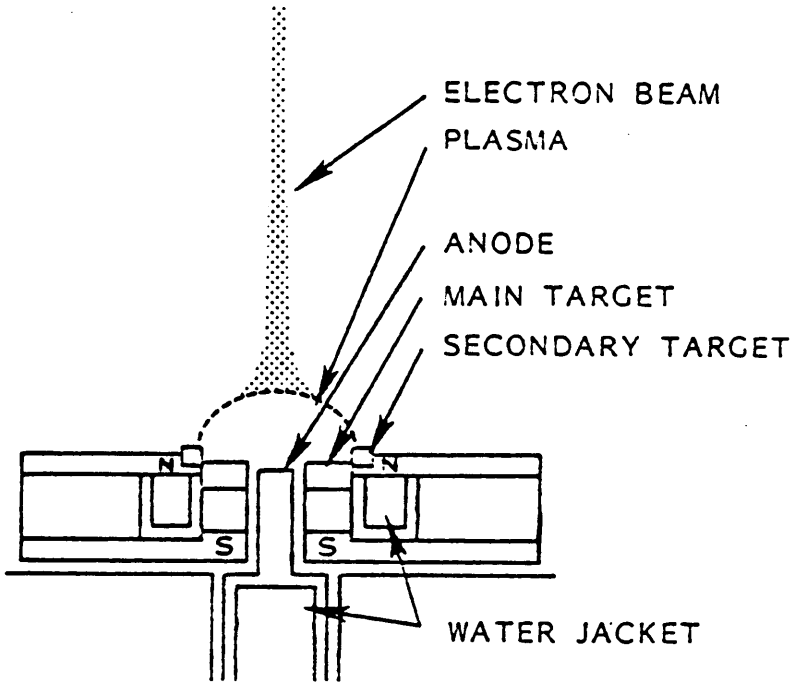

Figure 40. Sputtering S-gun Principle (Onishi, 1987)

depth of the chamber. For the sputtering system shown in the figure, a 2 inch diameter port limited the substrate holder width to less than 2 inches. The substrate is secured to a thin piece of stainless steel by spot welded spring clips or corner screws. This plate closes off a semicircular shroud enclosing a quartz heater used to maintain the substrate at a particular temperature. This is all attached to the end of a stainless steel speed flange, or quick flange connected to the port cover which can be angled in the necessary manner to optimize a uniform deposition rate. The substrate holder can now be carefully slid into the chamber and rotated to the particular angle corresponding to the chamber design. The port cover is clamped to the flange and the necessary instrument connections are made to the protruding electric feed-thru prongs which run out through the center of the insulated port cover. In this case these connections included the power source for the heater and a temperature readout for the K-type thermocouple used to monitor the substrate. There is a up-to-air, or air bleed, valve on the opposite side of the chamber which must be closed and then the gate valve which partially separates the chamber from the turbomolecular pump can be opened by the rotary crank. The micrometer adjusted variable orifice, which is used to regulate the chamber pressure by increasing or decreasing the pump load, should be partially opened for initial start-up. The main power to the pumps is turned on and the roughing pump is started by pushing the operation button. As soon as this is done it is extremely important that the cooling water system be checked to see that it is flowing. If this step is forgotten, the water-cooled turbo molecular pump and possibly the sputtering guns could overheat during the pump down and sputtering process. The regulatory valve is now opened fully to allow the pumps to exhaust the chamber of moisture and unwanted gases during pump down. The gas lines should be checked to see that the necessary valves are opened and that the desired flow rates have been set on the flow meters. Also, if the meters need zero adjustment that should be done too.

The time necessary to pump down the chamber to the necessary sputtering conditions varies with each station size and previous chamber conditions. Generally three hours should be sufficient to obtain a dry and clean enough chamber environment to start the deposition process. There are many ways to reduce this pump down time. The best of which incorporates a sub chamber con-

nected to a main chamber port separated by a vacuum seal valve. This allows the main chamber to always be at deposition conditions and requires only the small sub chamber be pumped, which takes a short time. The substrate holder, which initially enters the sub chamber is transferred to the main chamber by a lead screw manipulator device after the two chambers are at similar conditions. This accessory is not always available due to cost, so the main chamber must be bled and purged with air to ambient conditions, after each deposition. The three hour pump down is based on the situation where this purging in done through the up-to-air valve directly from the laboratory air which introduces excessive moisture. If instead the valve is connected to a filtered air source which runs through an air dryer, the pump down time can be cut at least in half. Finally to aid in any of the above processes, the heater can be turned on for a few minutes to help vaporize any substrate moisture and the chamber can be purged with argon every 5 to 10 minutes to help exhaust the unnecessary gases.

The chamber conditions can be checked after the minimum time by using the gas analyzer. With the sensing filament on, the display will show a peak scan of all the residual gases in the chamber sorted by their molecular weight. Exact amounts can be checked using the tabular display, but usually looking at the spectral display for the ratio of the peaks is all that is necessary. If after the argon is turned on, usually to a set point of 3.0 cc/min, the undesired gases such as oxygen and especially water, are less than two decades lower than the argon level, the conditions should be satisfactory for sputtering. This may not be easily achieved until presputtering later. At this time the zero level on the required flow meters should be rechecked in case any drift occured during pump down. The argon is be turned on and other additional gases are turned on if reactive sputtering is needed. Reactive sputtering involves bombarding a metal target, aluminum, and purging the chamber with a particular gas, nitrogen, to form a secondary compound when the metal particle heads toward the substrate. Aluminum and nitrogen combine to form a ceramic film, aluminum nitride, to be deposited on the substrate, providing the gas ratios are sufficient, typically 3.0:0.8. This is very important because if there is too little gas, some pure metal film may be deposited which may destroy the ceramic layer.

Now that the chamber environment has been determined to be at suitable conditions, the plasma, referred to as the glow discharge, may be initiated. This is done by initially adjusting the regulatory valve to obtain a total chamber pressure of 2.0 millitorr, which will be the pressure value needed after the glow has been initiated, so the micrometer reading should be noted. The regulatory valve is then adjusted to the closed position so that the chamber pressure rises rapidly. When the total pressure has risen above 10 millitorr, the RF power supply can be turned on and the power level can be slowly increased to about 40 watts at which time the regulatory valve is set back to the previously noted position and the colored glow is observed through the chamber view window. The color depends on the particular material and gas combination used. The power level remains at this value for about 2 minutes or until the moisture level drops about 2 decades below Argon. This is known as pre-sputtering. If a shutter is used to block the substrate from deposition, the pre-sputtering time can be reduced by using full power. When the conditions are favourable, the power level can be increased to the desired value and the deposition timer can be started. The reflected power meter should be checked to see if it is too high, over 15 watts, or if it is unstable. If either is the case, the power level should be lowered slightly or the tune knob on the tuning network should be adjusted to reduce the reflected power level. In reducing this level the tuning network is balanced with the power frequency of the gun. The RF frequency used with the S-gun is 13.56 MHz. This poor condition can also be observed in the glow discharge which would be flickering or varying in brightness showing poor quality of deposition. Some instability of the pressure and flow meters and especially on the gas analyzer can be expected in the initial 4 minutes of deposition. This is largely due to the changing chamber conditions as a result of the discharge of gases and moisture from the chamber walls. Since it usually takes about 4 minutes for the conditions to reach equilibrium, it can be very advantageous to have a shutter covering the substrate from deposition until the conditions are optimum. The time for deposition depends on the desired film thickness. This can be determined by using published data on pure film deposition rates at particular power levels in coordination with the estimated efficiency of the chamber. A much better method is to deposit film layers at a set power level for various time periods and measure the film thickness by surface scan methods. One must make sure that a portion of the substrate remains uncovered so

that the layer thickness can be measured by the scan method which uses a scan stylus connected to a strip chart recorder to map surface topography.

At the end of deposition, the power level can be rapidly reduced and then the RF power supply can be turned off. The reactive gas supply is also turned off but the argon supply should remain on. The pump is switched to stand-by mode and the main gate valve is closed to take the load off the pumps and allow them to slow down in speed. The pumps should be allowed about 4 minutes before turning off the roughing pump power. Another 4 minutes is needed before the main power to the turbomolecular pump is turned off. The chamber is ready to be bled by opening the up-to-air valve mentioned earlier. When this is complete, the substrate holder may be removed from its port and the sample is taken off to complete the image fabrication process. At this time if reactive sputtering had been done, the film may be briefly inspected for quality before proceeding with the necessary lithographic process.

It should be noted that when the chamber is not going to be used immediatly it should be placed in a stand-by vacuum status. This requires following the previously described pump down procedure except that a substrate is not necessary, the gas supply need not be turned on, and the pumping unit is to be in stand-by mode. The advantage of leaving the system in this condition is that it reduces the opportunity for moisture and impurities to migrate and be absorbed by the stainless steel chamber walls and the target. In order to change the target for each different deposition material manufactureres methods should be followed carefully. In many chambers, a few required targets are mounted in various sputtering gun ports throughout the chamber, and a shroud or shield is used to protect the unused targets and chamber walls from material deposition. This eliminates the need to fully open the chamber to change targets.

Appendix E. Thin Film Thermocouples

The preliminary work involved in fabricating a working thin-film heat flux gage required that the basic unit, the thermocouple, be fabricated first. The design used was a little more complex than needed, but it was chosen in order to find the limits of the fabrication technique. To form a simple straight line thermocouple is an easy task, but a more complex version better represents some of the design characteristics of the microsensor. The thermocouple was also necessary to determine the thermoelectric sensitivity of the copper-nickel combination.

The thermocouple leads were kept narrow and included sharp bends to see the limits of resolution using lithographic techniques, specifically the lift-off process. The pattern was designed to incorporate feed-thru leads, so terminal pads were drawn at the end of the leads. The basic layers of the thermocouple sensor are the same as the gage except that there is no need for the silicon monoxide thermal insulating layer. A base insulating layer, needed for electrically conductive substrates, either incorporated unprotected holes for feed-thru terminals or just a continuous film when surface connection was used. The film thickness was varied to determine the minimum thickness needed to achieve electrical insulation. Aluminum oxide was chosen for the base film because of its low electrical conductivity and its high thermal conductivity, 4.184 watts/cm °K . If a very thin base film is used, the thermocouple will measure the substrate surface temperature with good accuracy. The thermocouple junction was formed using nickel and copper, the same materials used for the

heat flux microsensor. Metal film thicknesses were varied until a good quality, uniform film was achieved. This preferred film thickness was found to be between 0.1 and 0.2μm. The top barrier layer was again aluminum nitride, which when a stable sputtering gas ratio was achieved, resulted in a tough, transparent film of high thermal conductivity(30 watts/m°K) with good adhesion capable of withstanding well over 300 °C. The barrier layer only needed to be about 0.1 microns for good protection from particle and chemical contaminants that the sensor may be subjected to in a test atmosphere. The top layer design depends on the instrument lead connection used. A continuous film was used for feed-thru lead connection and a film covering all but the terminal pads was used for surface wire connection.

Since the nickel-copper thermocouple pair was not a well published combination, the thermocouples had to be calibrated. The calibrations were done on thermocouples fabricated on Corning 7059 glass with surface mounted leads. The lead wires were attached to the unprotected terminal pads using silver paint and epoxy. The teflon coated lead wires, 0.010″ in diameter, were stripped back about 2.0 millimeters and then placed on a drop of silver paint on the terminal pad. While carefully holding the wire in place, another drop of silver paint was put over the connection. The wires were temporarily secured to the edge of the substrate with small clamps when the sample was placed in an oven set to 105 °C. The substrate was baked for 30 minutes, the time required for the silver paint to cure and achieve a low resistance bond. After the substrate cooled to room temperature, epoxy was applied in place of the small clamp to further secure the wires. The calibrations were done in a thermostat controled oven capable of 300 °C. The oven included a digital readout of both the setpoint and the actual temperature. The thermocouple was placed on the oven shelf and the lead wires ran through the side access hole. The nickel end of the thin-film thermocouple lead was spot welded to another copper lead to form a second thermocouple junction. This junction was used as an ice point reference by submersing it into a cryogenic dewar filled with ice slush. The signal from the thermocouple loop was measured with an HP 3468 digital multimeter.

The calibration process began at room temperature. The temperature of the digital readout was recorded, as was the approximately stable voltage output of the thin-film thermocouple. The oven temperature was then increased about 5-10 degrees, and allowed about 5 minutes to reach equilibrium. The steady state of the 5 ½ -digit voltage reading was difficult to determine due to the thin-film thermocouple sensitivity, so an estimated average was taken in each instance. This procedure was repeated until the maximum range of the epoxy was reached and the silver paint broke loose, around 290 °C. After all the data was taken, it was entered into a computer program which calculated the average sensitivity for a nickel-copper thermocouple in microvolts per °C (Figure 41 on page 114). From the samples tested, the average sensitivity was found to be in the range of 21-25 μV/ °C. Looking at the data in Figure 42 on page 115, Figure 43 on page 116, and Figure 44 on page 118, one can see that the calibration results of the thin-film copper-nickel thermocouple are very repeatable. A calibration curve, emf output versus temperature, was drawn from each data set and was found to follow the curve predicted using bulk temperature theory (Figure 45 on page 119). Any inconsistencies between the curves may be due to a more accurate oven control system used in the latter calibration.

```
**   THIS PROGRAM READS ALL OF THE THERMOCOUPLE CALIBRATION DATA,
**    EMF AND TEMPERATURE OUTPUT, AND CALCULATES THE AVERAGE
**    SENSITIVITY OF THE SENSOR.
**   DATA FILE MUST BE TWO COLUMNS, EMF AND TEMPERATURE.


     REAL SUM,EMF(100),TEMP(100),EDIFF(100),TDIFF(100)
     REAL AVGS,SENS(100)


      WRITE(8,*) 'THIS IS THE DATA FOR THE CALIBRATION OF A THIN FILM
    CTHERMOCOUPLE'
      WRITE(8,*) 'DATE:'
      WRITE(8,*) 'MATERIAL: COPPER/NICKEL WITH ALUMINUM NITRIDE'
      WRITE(8,*) 'SUBSTRATE: GLASS'
      WRITE(8,*) 'ZERO POINT REFERENCE'
      WRITE(8,*) 'LINE THICKNESS:'
      WRITE(8,*) 'METAL FILM THICKNESS:'

      SUM = 0.0

      DO 10 I = 1,100
      READ(3,*) EMF(I),TEMP(I)
      IF(EMF(I).EQ.0.0) GOTO 20
10    CONTINUE
20    DO 30 J = 2,100
       IF(EMF(J).EQ.0.0) GOTO 40
        EDIFF(J) = EMF(J)-EMF(J-1)
        TDIFF(J) = TEMP(J)-TEMP(J-1)
        SENS(J) = (EDIFF(J)/TDIFF(J))*1000.0
        SUM = SUM + SENS(J)
30    CONTINUE
40     AVGS = SUM/(J-2)
      WRITE(8,*) '    '
      WRITE(8,*) '  TEMPERATURE          EMF              SENSIT
    CIVITY'
      WRITE(8,*) '(DEGREES CELSIUS)   (MILLIVOLTS)  (MICROVOLTS PER
    C DEGREE CELSIUS)'
      WRITE(8,*) '                '
     DO 50 I = 1,100
       SENS(1) = 0.0
     IF(EMF(I).EQ.0.0) GOTO 58
      WRITE(8,55) TEMP(I),EMF(I),SENS(I)
55     FORMAT(6X,F6.2,11X,F7.3,18X,F6.2)
50    CONTINUE
58     WRITE(8,60) AVGS
60     FORMAT(/,'THE AVERAGE SENSITIVITY IS',F6.2,2X,'MICROVOLTS PER
    CDEGREE C.')
      STOP
      END
```

Figure 41. Thermocouple Calibration Program

THIS IS THE DATA FOR THE CALIBRATION OF A THIN FILM THERMOCOUPLE
DATE:
MATERIAL: COPPER/NICKEL WITH ALUMINUM NITRIDE
SUBSTRATE: GLASS
ZERO POINT REFERENCE
LINE THICKNESS:
METAL FILM THICKNESS:

TEMPERATURE (DEGREES CELSIUS)	EMF (MILLIVOLTS)	SENSITIVITY (MICROVOLTS PER DEGREE CELSIUS)
23.00	0.463	0.00
28.00	0.567	20.80
56.00	1.166	21.39
51.00	1.056	22.00
46.00	0.942	22.80
41.00	0.847	19.00
37.00	0.767	20.00
60.00	1.256	21.26
45.00	0.919	22.47
49.00	1.023	26.00
67.00	1.410	21.50
24.00	0.471	21.84
76.00	1.620	22.10
80.00	1.682	15.50
97.00	2.135	26.65
117.00	2.603	23.40
119.00	2.653	25.00
135.00	3.069	26.00
147.00	3.370	25.08
171.00	4.034	27.67

THE AVERAGE SENSITIVITY IS 22.66 MICROVOLTS PER DEGREE C.

Figure 42. Thermocouple Calibration Data (9/2/88)

THIS IS THE DATA FOR THE CALIBRATION OF A THIN FILM THERMOCOUPLE
DATE:
MATERIAL: COPPER/NICKEL WITH ALUMINUM NITRIDE
SUBSTRATE: GLASS
ZERO POINT REFERENCE
LINE THICKNESS:
METAL FILM THICKNESS:

TEMPERATURE (DEGREES CELSIUS)	EMF (MILLIVOLTS)	SENSITIVITY (MICROVOLTS PER DEGREE CELSIUS)
20.00	0.380	0.00
30.00	0.602	22.20
35.00	0.702	20.00
40.00	0.810	21.60
45.00	0.934	24.80
50.00	1.028	18.80
55.00	1.132	20.80
60.00	1.236	20.80
65.00	1.355	23.80
70.00	1.461	21.20
75.00	1.578	23.40
80.00	1.688	22.00
85.00	1.808	24.00
90.00	1.920	22.40
95.00	2.046	25.20
100.00	2.165	23.80
105.00	2.288	24.60
110.00	2.410	24.40
115.00	2.535	25.00
120.00	2.651	23.20
125.00	2.786	27.00
130.00	2.904	23.60
135.00	3.032	25.60
140.00	3.220	37.60
145.00	3.310	18.00
150.00	3.427	23.40
155.00	3.562	27.00
160.00	3.698	27.20
165.00	3.831	26.60
170.00	3.969	27.60
175.00	4.109	28.00
180.00	4.252	28.60
185.00	4.390	27.60
190.00	4.535	29.00
195.00	4.682	29.40
200.00	4.807	25.00
205.00	4.960	30.60
210.00	5.113	30.60
220.00	5.378	26.50

Figure 43. Thermocouple Calibration Data (9/12/88)

232.00	5.720	28.50
240.00	5.940	27.50
251.00	6.245	27.73
259.00	6.455	26.25
270.00	6.744	26.27
285.00	7.138	26.27

THE AVERAGE SENSITIVITY IS 25.30 MICROVOLTS PER DEGREE C.

THIS IS THE DATA FOR THE CALIBRATION OF A THIN FILM THERMOCOUPLE
DATE:120
MATERIAL: COPPER/NICKEL WITH ALUMINUM NITRIDE
SUBSTRATE: GLASS
ZERO POINT REFERENCE
LINE THICKNESS:
METAL FILM THICKNESS:

TEMPERATURE (DEGREES CELSIUS)	EMF (MILLIVOLTS)	SENSITIVITY (MICROVOLTS PER DEGREE CELSIUS)
26.30	0.523	0.00
38.20	0.746	18.74
50.40	0.982	19.34
62.50	1.253	22.40
73.50	1.501	22.55
86.80	1.797	22.26
98.50	2.070	23.33
110.00	2.337	23.22
122.70	2.606	21.18
134.20	2.898	25.39
146.70	3.219	25.68
159.70	3.533	24.15
174.00	3.895	25.31
188.00	4.257	25.86
196.00	4.449	24.00

THE AVERAGE SENSITIVITY IS 23.10 MICROVOLTS PER DEGREE C.

Figure 44. Thermocouple Calibration Data (1/20/89)

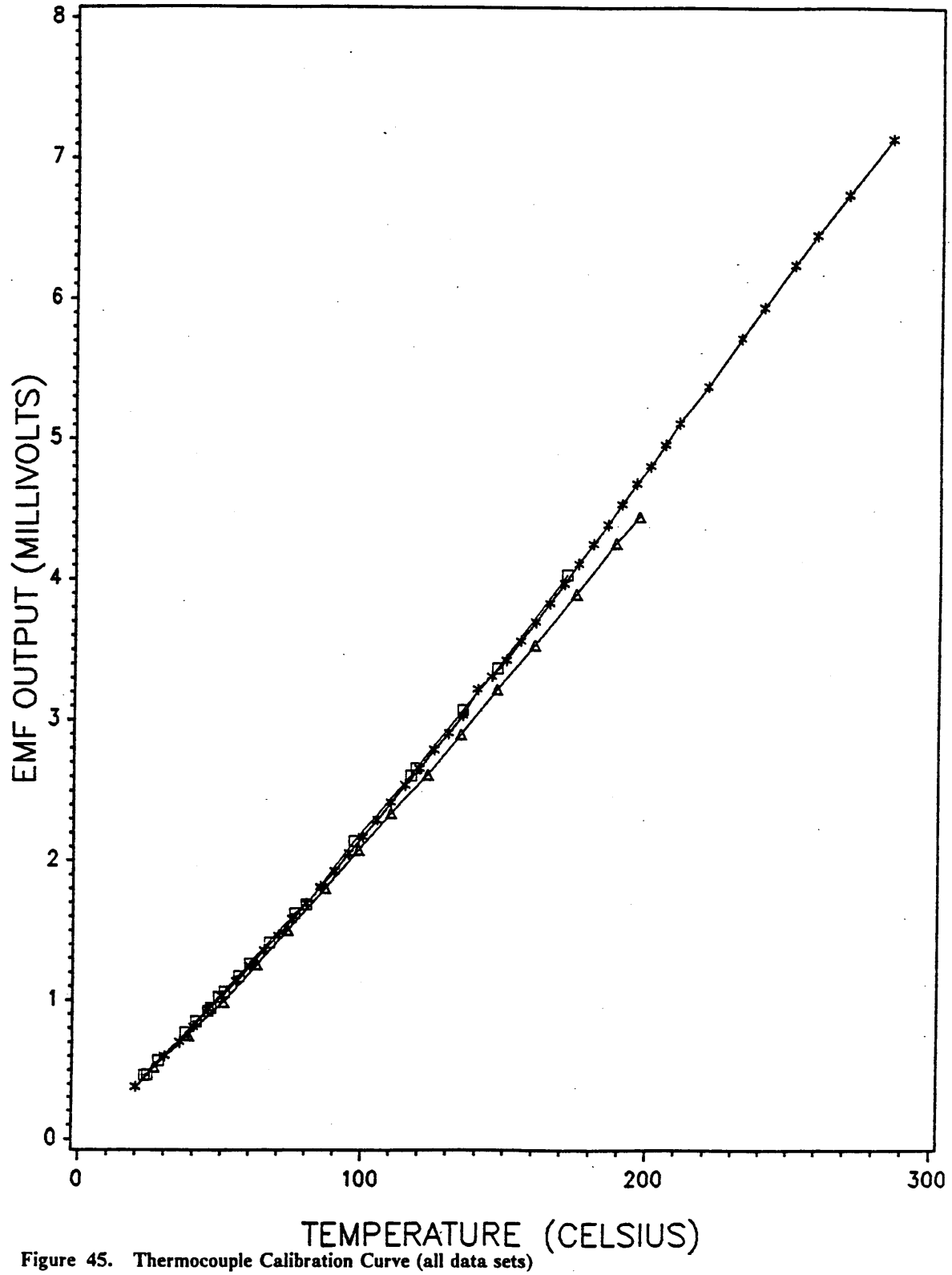

Figure 45. Thermocouple Calibration Curve (all data sets)

Appendix F. Automation of the Calibration Plate

One of the techniques used for the calibration of the microcircuit heat flux gage was a steady state convection apparatus. This apparatus was originally developed in 1983 by Borell and Diller for convective calibration of Gardon type heat flux sensors. It was later used by Campbell in 1985 for calibration of resistance film wafer gages. By comparing known values of heat flux to emf output of the gage, a steady-state calibration can be obtained resulting in a gage sensitivity.

The original calibration environment was created by using a square free jet of air striking a vertical heated plate in stagnation position(Figure 46 on page 122). The vertical plate was encased in an insulated box which consisted of a 6″×6″ calibration plate at the center and 4 8″×2″ guard plates on the outside edge. A shield with a 10″ × 10″ aperture was placed over the front, and a crank was used to transverse the gage across the flow field *window* . This was done to assure the uniformity of h . By 1985, the temperature of each of the five plates was automatically controlled by Eurotherm temperature controllers driving Watlow silicon rubber resistance heaters. Thermocouples imbedded in each of the plates acted both as temperature monitors and feedback to the controllers. During calibration the heat flux gage is mounted in the center of the calibration plate, which is kept isothermal to within 1 °C. The guard plates are maintained within 0.2 degrees of this value. Upon achieving equilibrium for the setpoint temperature, the voltage output of both the gage and the voltage required by the controller to maintain the setpoint temperature are re-

corded. This is done with the aid of a HP-3468 digital multimeter connected through a HP-IL interface to a HP-44CV calculator which averages a number of readings over a period of time in order to reduce the uncertainty involved in individual estimated readings. This data acquisition is done using 2 different programs in the calculator. One is for recording the DC voltage of the gage and the other is for the AC voltage of the controller (Figure 47 on page 123) The temperature of the calibration plate is determined by averaging the thermocouple temperatures using a Doric 410A thermocouple readout, calibrated to 0.1 degree Celsius accuracy, along with a channel selecting junction box. This is sufficient information to enter into a computer program which both reduces the data and calculates the corrected calibration coefficient along with its accuracy (Figure 48 on page 124 and Figure 49 on page 128)

After using the apparatus a number of times, it was found to be very time consuming to obtain enough data for a reliable calibration. Three variables have to be varied independently; gage position, plate temperature and air flow. It was determined that the multiple variations necessary could be done by a computer if the apparatus were automated. In addition to automation, there was a need for increased heat flux, durability and interchangeability so that the apparatus could be used for the heat flux microsensor research. The increased heat flux was achieved by a combination of two changes. The first was to purchase lower resistance heaters which produced a watt density of 23,250 watts/m^2, 3 times more than the previous heaters. The second was to reduce the jet size to a 1 inch diameter tube which increased the local heat flux. This combination enabled an increased range of heat flux values attainable starting at around 1200 watts/m^2 up to about 15,000 watts/m^2 as compared to the previous maximum value of 5000. To increase the durability, the apparatus was rebuilt out of aluminum angle and thicker higher-quality wood along with increased capacity insulation. The replacement of the armaflex insulation by a high density fiberglass insulation was necessary due to the service temperature restriction of the armaflex. To protect the entire unit, the shield was designed to fully enclose all parts. Finally there was a need for interchangeability so that the apparatus could be used for different gage designs. For a metal substrate microsensor, a different center plate design was needed for mounting purposes. This meant that the outer shield had

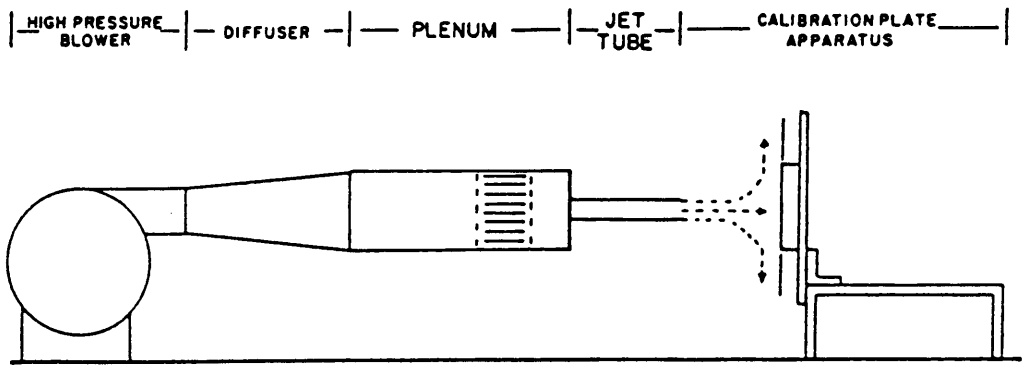

SIDE VIEW

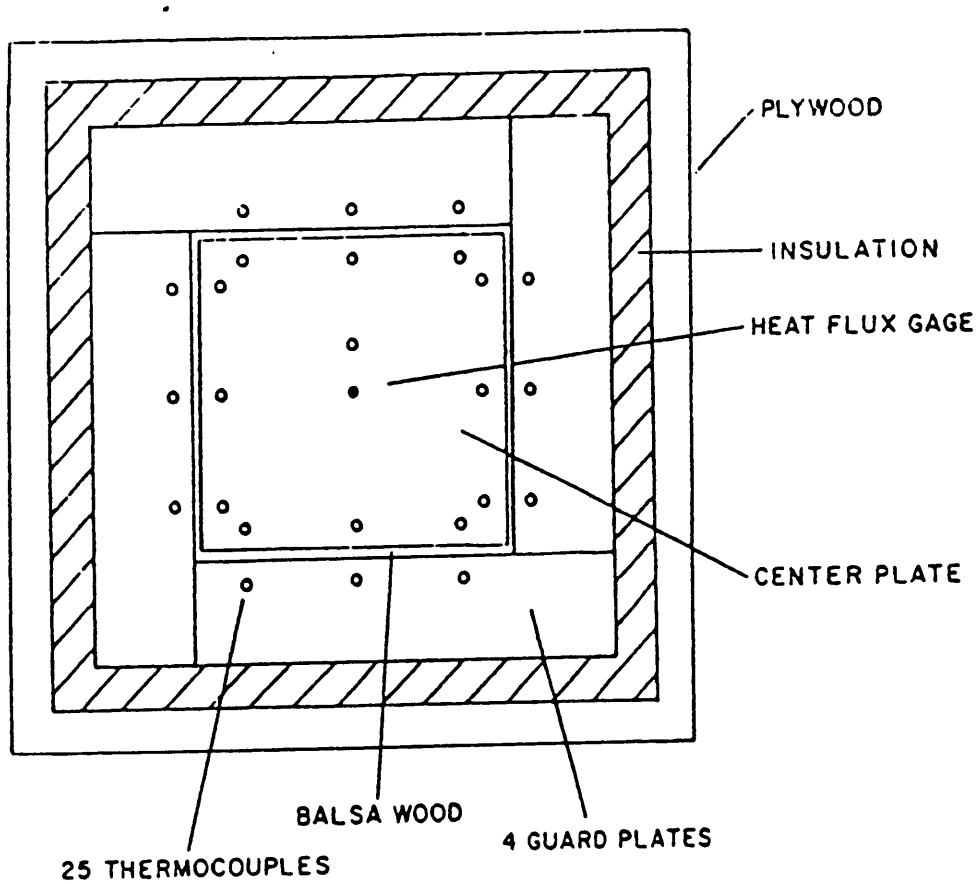

Figure 46. Original Convective Calibration Apparatus

	DC Voltage		AC Voltage
01	LBL T GAGE	01	LBL T CONT
02	T GAGE DC VOLTS	02	T CONT AC VOLTS
03	AVIEW	03	AVIEW
04	PSE	04	PSE
05	PSE	05	PSE
06	T N-READINGS?	06	T N-READINGS?
07	PROMPT	07	PROMPT
08	1000	08	1000
09	/	09	/
10	1.0E-5	10	1.0E-5
11	+	11	+
12	STO 05	12	STO 05
13	&SUM. REG 11	13	&SUM. REG 11
14	CL &SUM.	14	CL &SUM.
15	AUTOIO	15	AUTOIO
16	REMOTE	16	REMOTE
17	F1R1RA	17	F2R4
18	OUTA	18	OUTA
19	LBL 02	19	LBL 02
20	ISG 05	20	ISG 05
21	GTO 03	21	GTO 03
22	GTO 04	22	GTO 04
23	LBL 03	23	LBL 03
24	IND	24	IND
25	&SUM.+	25	&SUM.+
26	GTO 02	26	GTO 02
27	LBL 04	27	LBL 04
28	MEAN	28	MEAN
29	1000	29	T VOLTS
30	/	30	PSE
31	T MILLIVOLTS	31	T AVG AC VOLT =
32	PSE	32	ARCL&BULLET.X
33	T AVG DC VOLT =	33	AVIEW
34	ARCL&BULLET.X	34	BEEP
35	AVIEW	35	END
36	BEEP		
37	END		

AC readings are taken by pressing shift - key in user mode
AC readings are taken by pressing shift + key in user mode
STD can be found by pressing shift 8 key in user mode

Figure 47. HP Data Acquisition Programs

```
C   PROGRAM CALCULATES THE HEAT FLUX, HEAT TRANSFER COEFFICIENT,
C   AND GAGE SENSITIVITY USING THE BORELL-DILLER CONVECTION
C   CALIBRATION APPARATUS.
C-------------------------------
C   DATA FILE MUST BE CREATED
C    FILENAME DCAL3.DAT
C    TAG,N,OHMS,AMPS
C    VOLTS,TPLATE,TAIR,OUTPUT,DELP,TINF
C    ..................
C   FIRST EXECUTE CALAA.FOR FOLLOWED BY FITER.FOR
C-------------------------------
C    TAG   = GAGE IDENTIFICATION (MAX. 6 CHARACTERS)
C    N     = NUMBER OF TRIALS
C    OHMS  = RESISTANCE OF CENTER HEATER
C    AMPS  = AMPLIFICATION OF OUTPUT
C    VOLTS = INPUT TO TEMPERATURE CONTROLLER (VOLTS)
C    TPLATE= CENTER PLATE TEMPERATURE (C)
C    TAIR  = AIR FLOW TEMPERATURE (C)
C    OUTPUT= GAGE OUTPUT (MILLIVOLTS)
C    DELP  = DELTA H ON MANOMETER (INCHES)
C    TINF  = AMBIENT TEMPERATURE (C)
C-------------------------------

     REAL OHMS,AMPS
     REAL VOLTS(20),TPLATE(20),TAIR(20),OUTPUT(20)
     REAL DELP(20),TINF(20),F1(20),TPOUT(20),TAOUT(20)
     REAL QGSI(20),QGEN(20),OUTP(20),QDSI(20),QDEN(20),OUTD(20)
     REAL VEL(20),FLOWR(20)
     CHARACTER*6 TAG
     DIMENSION ITEST(20)
     ISTART = 1
       READ(7,6) TAG,N,OHMS,AMPS
 6     FORMAT(A6,I4,F6.2,F6.2)
     DO 5 I = 1,N
       READ(7,*) VOLTS(I),TPLATE(I),TAIR(I),OUTPUT(I),DELP(I),TINF(I)
       TPOUT(I) = TPLATE(I)
       TAOUT(I) = TAIR(I)
 5   CONTINUE
     WRITE(6,1)
 1   FORMAT(///1X,'TEST',3X,'INPUT POWER',9X,'H',6X,'DELTA T',5X,
    $ 'HEAT FLUX',6X,'OUTPUT',8X,'F',8X,'OUTPUT/DELTA T',3X,'QGAGE/DELT
    $A T')
C  **********AREAS**********
C     AGAGE = .165**2*3.14159/4.*.0254**2
     AGAGE = 4.0E-7
     APLATE = 36.*.0254**2-AGAGE
     ATOTAL = APLATE + AGAGE
```

Figure 48. Calibration Data Reduction Program

```
C  ***************EMISSIVITIES*****************
      EGAGE = .92
      EPLATE = .20
      SIGMA = 5.67E-08
      DO 100 I = 1,N
      ITEST(I) = ISTART + I-1
C  **************FLOW RATE EXITING IMPINGED JET***********
      VEL(I) = ((13.6*9806*DELP(I)*0.0254)*2*(1/1.177))**0.5
      FLOWR(I) = VEL(I)*(0.102**2)
      QTOTAL = (VOLTS(I)**2)/OHMS
      EA = EPLATE*APLATE + EGAGE*AGAGE
      TP4 = (TPLATE(I) + 273.2)**4
      TA4 = (TINF(I) + 273.2)**4
      DELTAT = TPLATE(I)-TAIR(I)
      H1 = (QTOTAL-SIGMA*EA*(TP4-TA4))/(ATOTAL*DELTAT)
C  **************CONDUCTIVE ANALYSIS****************
   20 QBACK = (.00322 + 43.1/H1)/49.8
      CALL QSIDE(H1,TPLATE(I),TAIR(I),QSIDES)
      QREAL = (1.-QBACK)*QTOTAL-QSIDES
C  **************CONVECTIVE ANALYSIS****************
      H2 = (QREAL-SIGMA*EA*(TP4-TA4))/(ATOTAL*DELTAT)
      CHECK = H2-H1
      IF(ABS(CHECK) .LT. .1) GO TO 10
      H1 = H2
      GO TO 20
   10 QGAGE = H2*DELTAT + EGAGE*SIGMA*(TP4-TA4)
      QGSI(I) = QGAGE
      QGEN(I) = QGAGE*(1/2.3901E-05)
      OUT = OUTPUT(I)/AMPS
      F = OUT/QGAGE
      F1(I) = F
      OUTDEL = OUT/DELTAT
      QDELT = QGAGE/DELTAT
      QDSI(I) = QDELT
      QDEN(I) = QDELT*(1/2.3901E-05)
      OUTP(I) = OUT
      OUTD(I) = OUTDEL

C  **********************OUTPUT**************************
      WRITE(6,2) ITEST(I),QREAL,H2,DELTAT,QGAGE,OUT,F,OUTDEL,QDELT
    2 FORMAT(1X,I3,3X,F10.2,4X,F10.2,4X,F5.2,4X,E10.4,4X,F10.6,4X,E10.4,
     $ 5X,E10.4,5X,E10.4)
  100 CONTINUE
      WRITE(6,3)
    3 FORMAT(///1X,'INPUT POWER IN                    WATTS'
     $/1X,'H IN                          WATTS/SQ. METER K'
     $/1X,'DELTA T IN                       DEGREES C'
     $/1X,'HEAT FLUX IN                       WATTS/SQ. METER'
     $/1X,'GAGE OUTPUT IN                        MILLIVOLTS'
     $/1X,'F IN                          MV/WATTS/SQ.METER'///)

      WRITE(9,198) TAG
  198 FORMAT(15X,'CALIBRATION DATA FOR THERMOGAGE ',A6)
      WRITE(9,200)
  200 FORMAT(//10X,'QG/AG',16X,'E',12X,'QG/AG/DELT',13X,'E/DELT')
```

```
      WRITE(9,210)
  210 FORMAT(/5X,'W/M2',6X,'CAL/CM2-S',5X,'MILIV',7X,
     $'W/M2-C',3X,'CAL/CM2-S-C',5X,'MILIV/C')
      WRITE(9,212)
  212 FORMAT('-------------------------------------------------------
     $----------')
      DO 215 I=1,N
      WRITE(9,220) QGSI(I),QGEN(I),OUTP(I),QDSI(I),QDEN(I),OUTD(I)
  220 FORMAT(/1X,E11.5,2X,E11.5,3X,F8.6,3X,F8.3,3X,E11.5,3X,E11.5)
  215 CONTINUE
C     ********CREATE DATA FILE FOR FITER3A.FOR*****************
      WRITE(8,231) TAG,N,AMPS
  231 FORMAT(A6,I4,F6.2)
      DO 230 I=1,N
      WRITE(8,235) TPOUT(I),TAOUT(I),OUTPUT(I),TINF(I),F1(I)
  235 FORMAT(F5.1,1X,F5.1,1X,E11.5,1X,F5.1,1X,E11.5)
  230 CONTINUE
      STOP

      END

C     ************CONDUCTION ANALYSIS SUBROUTINE***************
      SUBROUTINE QSIDE(H,TP,TA,Q)
      DIMENSION TNEW(36),TOLD(36)
      REAL K
      K=.00055
      TA=TA+273.2
      TP=TP+273.2
      DELX=.0794
      DELY=.0794
      PERIM=60.96
      N=0
      DO 10 I=1,36
      TNEW(I)=TP
   10 TOLD(I)=TP
   15 N=N+1
      DO 20 I=11,17
   20 TNEW(I)=(TOLD(I-1)+TOLD(I+1)+TOLD(I+9)+TOLD(I-9))/4.
      DO 30 I=20,26
   30 TNEW(I)=(TOLD(I-1)+TOLD(I+1)+TOLD(I-9)+TOLD(I+9))/4.
      DO 40 I=29,35
   40 TNEW(I)=(TOLD(I-1)/2.+TOLD(I+1)/2.+TOLD(I-9))/2.
      I=10
   50 TNEW(I)=(K*(TOLD(I-9)+2.*TOLD(I+1)+TOLD(I+9))+2.*H/10000.*DELX*TA)
     $ /(2.*(2.*K+H/10000.*DELX))
      IF(I .EQ. 19) GO TO 60
      I=19
      GO TO 50
   60 TNEW(28)=(K*(TOLD(18)+TOLD(29))+H/10000.*DELX*TA)/(H/10000.*DELX
     $ +2.*K)
```

```
      DO 70 I = 1,36
      DIFF = TNEW(I)-TOLD(I)
      IF(ABS(DIFF) .LT. .1) GO TO 70
      DO 80 J = 1,36
80    TOLD(J) = TNEW(J)
      IF(N .GT. 50) GO TO 99
      GO TO 15
70    CONTINUE
      GO TO 100
99    WRITE(6,1)
1     FORMAT(1X,'DID NOT CONVERGE')
100   Q = H*DELX*PERIM*((TNEW(1)-TA)/2. + TNEW(10)-TA + TNEW(19)-TA + (TNEW(28)
     $ TA)/2.)/10000.
      RETURN
      END
```

```
C    PROGRAM CORRECTS THE GAGE SENSITIVITY FOR EFFECTS
C    DUE TO CONVECTION
C-------------------------
C    DATA FILE CREATED IN CALAA FORTRAN
C     FILENAME FITER DATA
C-------------------------
C    TP    =CENTER PLATE TEMPERATURE (C)
C    TINF  =AMBIENT TEMPERATURE (C)
C    TA    =AIR FLOW TEMPERATURE (C)
C    OUTPUT=GAGE OUTPUT (MILLIVOLTS)
C    HM    =MEAN HEAT TRANSFER COEFFICIENT (WATTS/M2 C)
C    FCOR  =CORRECTED GAGE SENSITIVITY
C    F1    =UNCORRECTED GAGE  SENSITIVITY
C    AMPS  =AMPLIFICATION OF OUTPUT
C    DELTA =ERROR FROM MEAN
C    STD   =STANDARD DEVIATION
C    NFC   =95% CONFIDENCE INTERVAL
C-------------------------

     REAL TP(20),TINF(20),TA(20),OUTPUT(20),HM(20),FCOR(20),F1(20)
     REAL AMPS,DELTA,STD,NFC
     CHARACTER*6 TAG
     DELTA=0.0
     READ(5,3) TAG,N,AMPS
   3 FORMAT(A6,I4,F6.2)
     DO 4 I=1,N
      READ(5,*) TP(I),TA(I),OUTPUT(I),TINF(I),F1(I)
   4 CONTINUE
     ITER=0
     F=.9000E-04
   5 ITER=ITER+1
     SUM=0.0
     DO 10 I=1,N
     TP4=(TP(I)+273.2)**4
     TI4=(TINF(I)+273.2)**4
     HM(I)=(OUTPUT(I)/(F*AMPS)-.82*5.67E-08*(TP4-TI4))/(TP(I)-TA(I))
     CORR=1./(1.-0.75*F*HM(I)/.042)
     FCOR(I)=F1(I)*CORR
  10 SUM=SUM+FCOR(I)
     FAVE=SUM/FLOAT(N)
     CHECK=FAVE-F
     IF(ABS(CHECK) .LT. .01E-05) GO TO 20
     F=FAVE
     IF(ITER .GT. 60) GO TO 100
     GO TO 5
  20 WRITE(6,12) TAG
```

Figure 49. Calibration Coefficient Program

```
12  FORMAT(/,8X,'CORRECTED SENSITIVITIES FOR ',A6,/)
    WRITE(6,1)
 1  FORMAT(1X,'TEST',7X,' H MEASURED',7X,'F CORRECTED')
    DO 30 I = 1,N
    NTEST = I
    WRITE(6,2) NTEST,HM(I),FCOR(I)
2   FORMAT(1X,I3,8X,E11.5,7X,E11.5)
30  CONTINUE
    WRITE(6,40) FAVE
40  FORMAT(/,1X,'THE AVERAGE OF ALL THE F VALUES IS:',E11.5)
    DO 85 I = 1,N
    DELTA = DELTA + (FCOR(I)-FAVE)**2
85  CONTINUE
    STD = (DELTA/(N-1))**0.5
    WRITE(6,45) STD
45  FORMAT(/,1X,'THE RESULTING STANDARD DEVIATION IS:',E12.5)
    NFC = 1.96 * STD
    WRITE(6,55) NFC
55  FORMAT(/,1X,'THE 95% CONFIDENCE INTERVAL IS: ',E11.5)

100 STOP
    END
```

to be easily removed to access the insulated box in order to change the center plate. Instead of running into the difficulty involved in trying to re-feed thermocouple and gage wires, a second insulated box was made. To interchange boxes simply requires loosening 4 press screws on the aluminum frame and replacing the box. The additional advantage of the removable box is that any gage refitting can be done on a bench top which was not previously possible.

The plan for automation had to be incorporated in the new design (Figure 50 on page 131). The aluminum frame was used to mount the roller bearing pillow blocks which ride on horizontal transversing shafts mounted independent of the insulated box. This enabled easy removal of the box. The transversing shafts were mounted to the backboard at their endpoints. The bearing blocks allowed for easy travel of the box across the flow field with the aid of a stepping motor driving a lead screw mounted to the base of the frame. All of this was easily encased within the shield for compactness. The stepping motor can position the gage horizontally in any position within the flow field by computer software through an A/D converter. The A/D converter also junctions to a 16 channel multiplexor readout card. A Doric 410A thermocouple readout can be connected to a number of channels so that any temperature can be monitored and stored. The output of the gage can be recorded by amplifying the output signal to fall in the ± 4.0 volt input range of the card using Thermogage DC low noise amplifier. Though not done yet, the input to the temperature controllers will in the future be interfaced with the computer through the HP multimeter. The data acquisition software uses a communication program to read each individual channel in sequence, or send commands to the stepping motor. The stepping motor routine in the data acquisition program (Figure 51 on page 132). is able to move the gage to a particular position with a maximum resolution of 2200 steps per inch across the 10 inch flow field. The code then allows a set amount of time for the system to come to equilibrium before reading the temperatures and the voltages from the remaining channels. The time delay, number of channels to be read, and plate positions are each set by the user through an interactive program that precedes data acquisition. All of the necessary data is then saved in a data file for recall at the completion of the calibration.

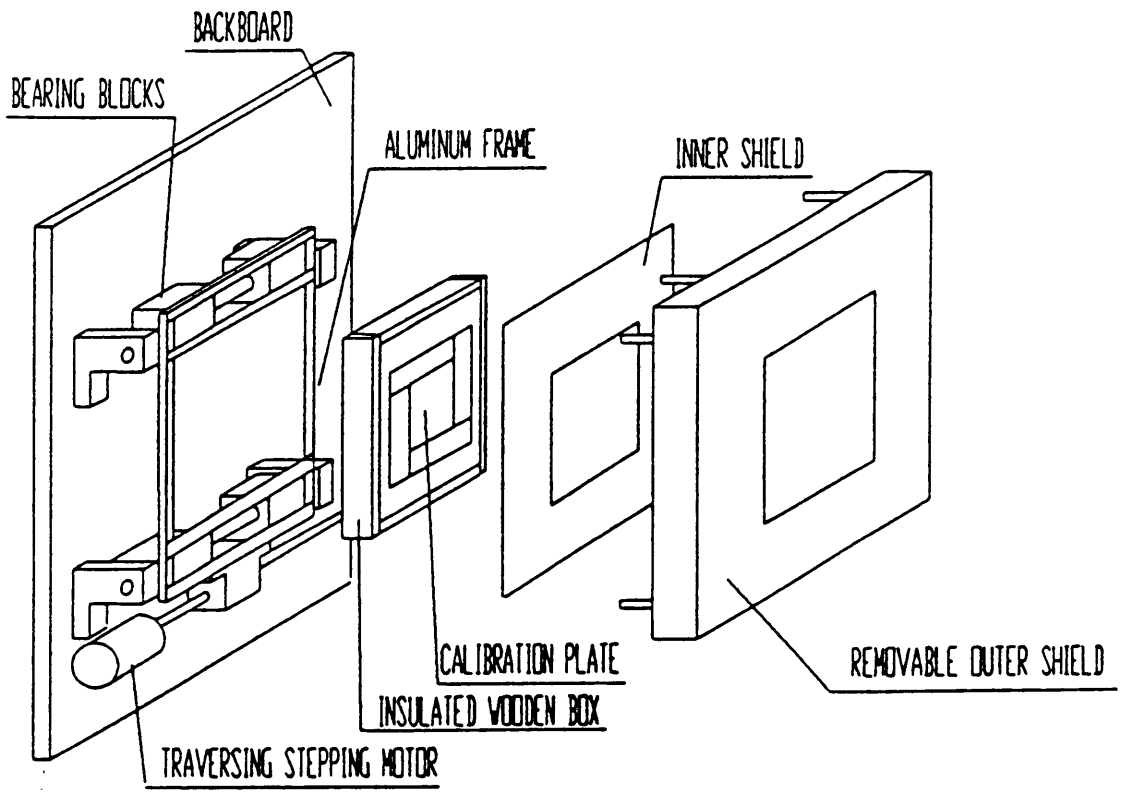

Figure 50. Redesigned Convective Calibration Apparatus

```
2 KEY OFF: CLS
9 '
60 CLS: INPUT "input name of data file ";NAM$
70 CLS: INPUT "enter # of Channels (1-16)";CHN
80 CLS: INPUT "ENTER RUN #";R1
81 INPUT "NPTS(10?)";NPTS
83 INPUT "FLOW TEMP";TF
84 INPUT "AMB TEMP";TA
85 INPUT "BAR PR";BAR
86 INPUT "GAIN";GANE
87 INPUT "MICROGAIN";GANE2
90 OPEN "B:" + NAM$ FOR OUTPUT AS #2
100 CLS
120 LOCATE 1,1
130 NP = 25
140 WRITE #2,DAT1$
150 WRITE #2, R1,NPTS,TF,TA,BAR,GANE,GANE2
160 K = 1
170 FOR L = 1 TO 8125: NEXT
180 FOR J = 0 TO CHN-1
190 SUM(J) = 0!
200 S2(J) = 0!
210 NEXT J
215 '
220 FOR I = 1 TO NP
230 FOR CH% = 0 TO CHN-1
240 GOSUB 420
250 IF CH% = 0 THEN GOSUB 420 ELSE 290
260 GOSUB 420
262 GOSUB 420
264 GOSUB 420
266 GOSUB 420
268 GOSUB 420
270 GOSUB 420
290 IF CH% = 1 THEN GOSUB 420 ELSE 295
295 NEXT CH%
300 NEXT I
305 '
306 SUM(0) = SUM(0)/200
307 S2(0) = SQR(ABS(S2(0)-200*SUM(0)¢2)/200)
308 SUM(1) = SUM(1)/200
309 S2(1) = SQR(ABS(S2(1)-200*SUM(1)¢2)/200)
312 WRITE #2, K,SUM(0),S2(0),SUM(1),S2(1)
314 FOR IJ = 2 TO CHN-1
320 SUM(IJ) = SUM(IJ)/NP
330 S2(IJ) = SQR(ABS(S2(IJ)-NP*SUM(IJ)¢2)/NP)
```

Figure 51. Data Acquisition Program

```
340 WRITE #2, K,SUM(IJ),S2(IJ)
350 NEXT IJ
360 K = K + 1
370 IF K > NPTS THEN GOTO 410
380 'GOTO 390
410 END
412 '
415 'DATA ACQUISITION SUBROUTINE
420     OUT &H310,&H80 + CH%
430     OUT &H310,CH%
440     HB% = INP(&H310)
450     IF (HB% AND 32) = 0 THEN 440
460     SON% = HB% AND 128
470     HB% = HB% AND 15
480     LB% = INP(&H311)
490     D = 256*HB% + LB%
500     IF SON% = 0 THEN D = D*-1
510 SUM(CH%) = D! + SUM(CH%)
520 S2(CH%) = D!¢2 + S2(CH%)
530 LOCATE CH% + 1,1
540 PRINT NPTS,K,I,CH%,D!;"
9550 RETURN
```

The automation of the calibration system to this point reduces the time that a person must monitor the calibration but does not fully automate the system. The additional requirements for full automation which are being pursued are to be able to control the jet speed and to be able to control the temperature controllers. Control of the jet speed is intended to be done using a stepping motor driven set of louvers at the blower inlet. To computer control the Eurotherm units would require considerable circuit additions or a new controller, designed for this application, could be purchased. A fully automated system would enable a full calibration to be completed over night. The acquired data could be automatically uploaded to data reduction programs on the IBM mainframe where the gage sensitivity can be calculated. Another program could be accessed which would produce the calibration curve and tabulate the necessary output data. The results would be available the following morning in both tabular and graphical form.

The vita has been removed from the scanned document